EINDHOVEN UNIVERSITY OF TECHNOLOGY

Patient specific prediction of bone failure using microstructure-enhanced continuum finite element models

Citation for published version (APA):
Hazrati Marangalou, J. (2013). *Patient specific prediction of bone failure using microstructure-enhanced continuum finite element models*. [Phd Thesis 1 (Research TU/e / Graduation TU/e), Biomedical Engineering]. Technische Universiteit Eindhoven. https://doi.org/10.6100/IR759548

DOI:
10.6100/IR759548

Document status and date:
Published: 01/01/2013

Document Version:
Publisher's PDF, also known as Version of Record (includes final page, issue and volume numbers)

Please check the document version of this publication:

• A submitted manuscript is the version of the article upon submission and before peer-review. There can be important differences between the submitted version and the official published version of record. People interested in the research are advised to contact the author for the final version of the publication, or visit the DOI to the publisher's website.
• The final author version and the galley proof are versions of the publication after peer review.
• The final published version features the final layout of the paper including the volume, issue and page numbers.

Link to publication

General rights
Copyright and moral rights for the publications made accessible in the public portal are retained by the authors and/or other copyright owners and it is a condition of accessing publications that users recognise and abide by the legal requirements associated with these rights.

• Users may download and print one copy of any publication from the public portal for the purpose of private study or research.
• You may not further distribute the material or use it for any profit-making activity or commercial gain
• You may freely distribute the URL identifying the publication in the public portal.

If the publication is distributed under the terms of Article 25fa of the Dutch Copyright Act, indicated by the "Taverne" license above, please follow below link for the End User Agreement:

www.tue.nl/taverne

Take down policy
If you believe that this document breaches copyright please contact us at:

openaccess@tue.nl

providing details and we will investigate your claim.

Download date: 17. Nov. 2023

Patient Specific Prediction of Bone Failure Using Microstructure-enhanced Continuum Finite Element Models

Javad Hazrati Marangalou

Patient Specific Prediction of Bone Failure Using Microstructure-enhanced Continuum Finite Element Models Javad Hazrati Marangalou

Patient Specific Prediction of Bone Failure Using Microstructure-enhanced Continuum Finite Element Models

Javad Hazrati Marangalou

Printed by University Press Facilities, Eindhoven, The Netherlands.

A catalogue record is available from the Eindhoven University of Technology Library.

ISBN: 978-90-386-3464-7

Copyright © 2013 by Javad Hazrati Marangalou

All rights reserved. No part of this book may be reproduced, stored in a database or retrieval system, or published, in any form or in any way, electronically, mechanically, by print, photo print, microfilm or any other means without prior written permission of the author.

Funding from the European Union for the Osteoporotic Virtual Physiological Human Project (VPHOP FP7-ICT2008-223865) is gratefully acknowledged.

The printing costs of this thesis were partially supported by SCANCO MEDICAL, Switzerland.

VPHOP
OSTEOPOROTIC
VIRTUAL
PHYSIOLOGICAL
HUMAN

SCANCO MEDICAL

Patient Specific Prediction of Bone Failure Using Microstructure-enhanced Continuum Finite Element Models

PROEFSCHRIFT

ter verkrijging van de graad van doctor aan de
Technische Universiteit Eindhoven, op gezag van de
rector magnificus, prof.dr.ir. C.J. van Duijn, voor een
commissie aangewezen door het College voor
Promoties in het openbaar te verdedigen
op maandag 21 oktober 2013 om 16.00 uur

door

Javad Hazrati Marangalou

geboren te Urmia, Iran

Dit proefschrift is goedgekeurd door de promotor:

prof.dr. K. Ito

Copromotor:

dr.ir. B. van Rietbergen

To my parents,

for their endless love, support and encouragement.

Contents

BONE **1**

BONE 2
BONE BIOMECHANICS 4
MECHANICAL PROPERTIES OF BONE 5
PATIENT SPECIFIC FE MODELS 7
AIM AND THESIS OUTLINE 8

A NEW APPROACH TO DETERMINE THE ACCURACY OF MORPHOLOGY-ELASTICITY RELATIONSHIPS IN CONTINUUM FE ANALYSES OF HUMAN PROXIMAL FEMUR **11**

ABSTRACT 12
INTRODUCTION 13
MATERIALS AND METHODS 15
RESULTS 18
DISCUSSION 22

A NOVEL APPROACH TO ESTIMATE TRABECULAR BONE ANISOTROPY FROM STRESS TENSORS **27**

ABSTRACT 28
INTRODUCTION 29
MATERIALS AND METHODS 30
RESULTS 34
DISCUSSION 38

A NOVEL APPROACH TO ESTIMATE TRABECULAR BONE ANISOTROPY USING A DATABASE APPROACH **41**

ABSTRACT 42
INTRODUCTION 43
MATERIAL AND METHODS 44
RESULTS 49
DISCUSSION 52

INTER-INDIVIDUAL VARIABILITY OF BONE DENSITY AND MORPHOLOGY DISTRIBUTION IN THE PROXIMAL FEMUR AND T12 VERTEBRA **57**

ABSTRACT 58
INTRODUCTION 59
MATERIALS AND METHODS 60
RESULTS 63
DISCUSSION 69

VERTEBRAL STRENGTH CAN BE ACCURATELY PREDICTED FROM BONE MICROSTRUCTURAL PARAMETERS **73**

ABSTRACT 74
INTRODUCTION 75
MATERIAL AND METHODS 76

RESULTS 79
DISCUSSION 84
GENERAL DISCUSSION 89
SUMMARY 95
REFERENCES 98
ACKNOWLEDGEMENTS 113
CURRICULUM VITAE 114

Chapter 1

Bone

Bone

According to the Merriam-Webster dictionary (2013), bone is "the hard largely calcareous connective tissue of which the adult skeleton of most vertebrates is chiefly composed". This, however, is only a formal definition, that does not give right to all the functions of bone tissue. These functions include: to provide structural support and protection of vital organs such as heart and brain, to provide attachment sites for muscles facilitating locomotion, to act as a reservoir for ions particularly for calcium and phosphorus and to act as a trap for some dangerous materials such as lead. Although bone thus serves many different functions, its main one is a mechanical one. For this reason, bones are highly optimized to this mechanical task, and this makes bone an ultimate biomaterial: a strong yet lightweight material that can adapt to the mechanical demands and can repair itself.

Based on their shapes, bones are roughly categorized as flat, long, short or irregular. The flat bones are generally associated with protection, e.g. the sternum, whereas the long bones, e.g. the femur and tibia are the main supporting structures for loads as they occur during daily activities. The short bones often have a smaller range of motion and are essential in structural support and stability. Vertebrae, tarsals in the foot and carpals in the hand are examples of short bones.

From a material point of view, bone tissue can be considered a porous material with a varying degree of porosity. At the center of long bones, it usually forms a tube-like structure of high-density bone (cortical bone), whereas near the joints and in short bones, most of the space is occupied by the porous type of bone (trabecular bone). One level lower, at the level of the extracellular space, bone tissue is a composite material, made up of organic and inorganic components. Organic components include collagen, proteoglycans, cytokine and growth factors. Inorganic components include calcium hydroxyapatite, osteocalcium phosphate and non-collagenous proteins. Whereas the composition of the bone tissue at the extracellular level is rather constant, its porosity can vary widely and can be changed and adapted depending on loading conditions, making it a dynamic tissue.

This dynamic behavior unfortunately also makes it susceptible to certain affections and diseases. Osteoporosis, osteopenia, osteogenesis imperfecta and bone cancer are the more common bone disorders. Most of these disorders affect the bone mechanical properties and make them more susceptible to fractures. Among these, osteoporosis is the most epidemic bone disease in elderly populations (Johnell and Kanis, 2005). It is characterized by low bone mass, deterioration of bone micro-architecture (Figure 1) and compromised bone strength, leading to bone fragility and increased risk of fracture under low loads. Osteoporosis is a disease of enormous socioeconomic impact (Gullberg et al., 1997; Johnell, 1997); according to the International Osteoporosis Foundation (IOF), 1 out of 3 women and 1 out of 5 men are

at risk of an osteoporotic fracture during their lifetime worldwide. In fact, an osteoporotic fracture is estimated to occur every 3 seconds. These fractures most commonly occur in the spine, lower forearm and hip. Forearm and hip fractures are commonly associated with falls (Grisso et al., 1991; Hedlund and Lindgren, 1987), whereas spine fractures are usually the results of normal activities for which the vertebrae can no longer withstand the forces. Among these fractures, hip fractures are the most dramatic, they are usually associated with profound disability and mortality (Farahmand et al., 2005; Forsén et al., 1999; Johnell et al., 2004). Given the dramatic consequences of these fractures, their prevention is the best strategy (Gass and Dawson-Hughes, 2006). Such prevention, however, relies on an accurate diagnosis. The current clinical diagnosis of osteoporosis as defined by the World Health Organization (WHO) is based on the site specific measurement of bone mineral density (BMD) by dual energy X-ray absorptiometry (DXA) techniques: Osteoporosis is a value of BMD > 2.5 SD below the young adult average value (Kanis, 1994). However, it has been demonstrated that the clinical diagnostic standard approach based on site specific BMD measurements using DXA is not a very good predictor of osteoporotic fractures (Eckstein et al., 2004; Lochmüller et al., 2001; Lochmüller et al., 2000; Prentice et al., 1994; Svendsen et al., 1995), and more than 50% of these fractures occur in patients that would not have been diagnosed as osteoporotic according to this WHO definition (Kanis et al., 2005; Siris Es and et al., 2004). It has been stated that this poor performance could be related to the fact that DXA provides an averaged density measure, and that it does not provide any information about the bone micro-architecture which plays an important role in bone strength (Dalle Carbonare and Giannini, 2004; Kanis, 2002; Lochmüller et al., 2003). In concordance with this, it has been stated that a first requirement for a more accurate assessment of bone fracture risk is an accurate assessment of bone strength, as it relates not only to its density, but also to its micro-architecture and loading conditions. This requires a thorough understanding of bone biomechanics.

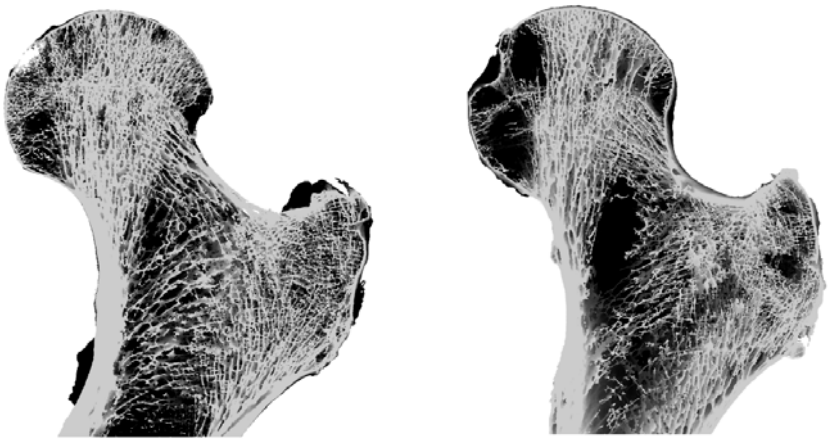

Figure 1. Healthy (left) and osteoporotic (right) femurs (adapted from (Van Rietbergen et al., 2003).

Bone biomechanics

The present knowledge of bone biomechanics stems from three different aspects developed during the present and last century: bone as a structure, as a biological system and as a material (Roesler, 1987).

The definition of bone as a structure can be traced back to the 17th century when the attempts were to express biological phenomena within the framework of the fundamental concepts of mechanics (Nagel, 1951). It was only much later however, that it was discovered that the architecture of trabecular bone is not only there to withstand the forces, but that this structure is also formed in response to these forces. In 1867, when von Meyer presented his observations of the trabecular architecture in the human proximal femur, Culmann, a structural engineer, noticed that von Meyer's trabecular drawings bore a striking resemblance to the principal stress directions that can be expected in the femur for typical loading conditions. Von Meyer published this phenomenon in a paper entitled "Die Architectur der Spongiosa" (Meyer, 1867). Later based on these observations, Wolff (Wolff, 1892) formulated a functional adaptation theory now generally known as “Wolff’s law” which states that the bone micro-architecture is adapted to coincide with principal stress trajectories that result from functional use. This theory will be further discussed in the third chapter of this thesis.

In addition to Wolff’s theory, structure and geometrical shape of bones have been approached from biological perspective (bone as a biological system) as well. Roux (Roux, 1881) was the first to propose a “quantitative self-regulating mechanism” to describe bone structural and geometrical adaptation. Present ideas about bone remodeling as a cellular process originate from his idea that bone cells respond to local loading conditions and that this process can explain the evolution of such typical irregular shapes and structures (Roesler, 1987).

“To measure is to know” (Lord Kelvin). Bone as a material was first explored by Rauber (Rauber, 1876) who investigated failure behavior of whole bones such as the skull, mandible, femur, radius, pelvis etc. under tension, compression, bending and torsion loading. Since then, a large number of papers were published on the mechanical properties of bone, often listing very different values for these mechanical properties. However, “a great deal of variation in bone mechanical properties found in the literature, which is the real variation and is not caused by sloppy experimental work” (Currey, 2002). It is believed that this variation in mechanical properties originates from the variation in bone hierarchical microstructure between species, individuals and sites.

Despite the large variation found in mechanical properties of bone, in the last few decades, “we are now in a position to start to understand bone” (Currey, 2009). This is due to new techniques that have become available over the last 20 years. In particular, increasing

precision of the actual physical and mechanical tests, the application of new methods such as finite element (FE) analysis, a better understanding of factors that can affect the measurements, such as size effects, and the characterization of bone as a hierarchical structure (Rho et al., 1998) were key factors to develop a better understanding of bone mechanical behavior (Currey, 2009). Among these, the finite element method, an advanced computer technique of structural stress analysis plays a special role since it is a computational rather than an experimental technique. It was introduced to orthopaedic biomechanics in 1972 to evaluate stresses in human bones (Brekelmans et al., 1972; Huiskes and Chao, 1983). Traditional biomechanical methods including analytical and experimental approaches (Biewener, 1992; Huiskes et al., 1981) provide at best only an approximation of how structures respond under the applied loads. Although strains can be measured using strain gauges, there are limits to where these can be placed and they can measure the strains only at the bone surface (Richmond et al., 2005). Analytical tools may work fine in case the geometry can be simplified (such as for the shaft region of long bones), but are rather useless for complex structures such as complete long bones and vertebrae with their complicated shape and presence of cancellous bone with different material properties at each location (Currey, 2002). The FE method, however, can provide an (approximate) pattern of the strain distribution throughout the whole bone by subdividing the complex geometry into a finite number of elements of simple geometry with distinct material properties. For this reason, FE modeling now plays an eminent role in bone biomechanics.

Mechanical properties of bone

In order to understand the mechanical properties of bone tissue, it is important to understand its hierarchical structure (Currey, 2012; Nair et al., 2013; Rho et al., 1998). At the lowest level (1-10 nm), bone consists of hydroxyapatite (HA) crystals; Ca10(PO4)6(OH)2, collagen fibers and non-collagenous proteins. At the second level (0.5-1 μm), HA crystals occur within the discrete spaces inside the collagen fibrils to form mineralized collagen fibrils. At the third level, the level of the extracellular matrix (1-10 μm), these mineralized fibrils are stacked in thin sheets to form lamellae (about 7 μm thick) in which unidirectional fibrils are arranged in alternating angles between layers. At the fourth level, the microstructural level (10-500 μm), lamellae of mineralized collagen fibers wrap in concentric layers (3–8 lamellae) around a central canal to form what is known as an osteon or a Haversian system. The osteon looks like a cylinder about 200–250 μm in diameter running roughly parallel to the long axis of the bone. At the highest or macro-structural level, there are two types of bone: cancellous and cortical bone. Cancellous bone, also called trabecular bone, is a cellular solid that consists of a connected network of rods and plates about 100 to 300 μm thick. Its volume fraction ranges anywhere from 5% to 40%. Cortical bone, on the other hand, is much denser and its volume fraction is greater than about 70%. Because the mechanical properties of in particular

cancellous bone are largely determined by its structure at the macro level, in this thesis, the focus will be on bone mechanical properties at the macro-structural level.

Reflecting the anisotropy of its microstructure, the elastic and strength properties of human cortical bone are anisotropic (Keaveny et al., 2009). Cortical bone is both stronger and stiffer along the diaphyseal axis than in the radial directions (Lotz et al., 1991; Reilly and Burstein, 1975; Wirtz et al., 2000). Anisotropic properties of human cortical bone have been investigated extensively using different experimental techniques such as (micro)tensile/compression tests (Lotz et al., 1991; Rho et al., 1993), ultrasonic techniques (Pithioux et al., 2002; Yoon and Lawrence Katz, 1976) and nanoindentation tests (Hengsberger et al., 2002; Rho et al., 2002; Xu et al., 2003).

Cancellous bone is highly anisotropic and inhomogeneous; its anisotropic material behavior is largely determined by its trabecular architecture. Complete identification of its anisotropic elastic and failure properties requires multiple tests on the same specimen which is almost impossible. Therefore, other non-destructive techniques such as ultrasound wave propagation techniques (Ashman and Jae Young, 1988; Haïat et al., 2006; Haïat et al., 2009; Malandrino et al., 2012) or image based micro-FEM (Gross et al., 2013; Van Rietbergen et al., 1996; Yang et al., 1998) are nowadays used to quantify all elastic constants of trabecular bone. It should be noted that cancellous bone is nonlinearly elastic even at small strains (Morgan et al., 2001), however, for virtual all applications, it can be considered as linearly elastic until yielding (Keaveny et al., 2009).

Given that the mechanical properties of cancellous bone are so much dependent on its micro-architecture, many different empirical relationships have been described in the literature to relate bone morphological parameters to its elastic and strength properties. Some of these empirical relationships are based on bone density as quantified by Hounsfield units in clinical CT images only, and can provide only the stiffness in the anatomical loading direction (Carter and Hayes, 1977; Helgason et al., 2008; Keller, 1994; Lotz et al., 1991; Wirtz et al., 2000; Zannoni et al., 1999). More recent empirical relationships also take bone anisotropy that results from its micro-architecture into account. In such models, the microstructure is usually quantified by a so-called fabric tensor that provides the principal directions of the trabeculae (Harrigan and Mann, 1984; Odgaard, 1997). Mathematical relationships then are used to relate the anisotropic bone stiffness to the fabric tensor and its density. Using such relationships, it was shown, e.g. that trabecular bone elastic properties are best described as orthotropic (Kabel et al., 1999b; Odgaard et al., 1997; Pahr and Zysset, 2009; Turner et al., 1990).

Patient specific FE models

At the organ level, finite element (FE) models have become a standard pre-clinical tool to study mechanical behavior of bone and bone-implant configurations (Figure 2). In these models, bone geometry as well as its material properties is based on clinical CT images. Since even standard clinical CT scanners can achieve a sub-millimeter resolution, the geometry of such models usually is highly accurate. The implementation of bone material properties, however, is less accurate. Finite element models usually implement elastic and strength properties that are based on the local bone density as quantified by Hounsfield units in clinical CT images (Keyak, 2001; Liebschner et al., 2003; Taddei et al., 2007; Yosibash et al., 2007). Empirical power-law relationships are then used to derive the elastic and strength properties (Carter and Hayes, 1977; Helgason et al., 2008; Keller, 1994; Lotz et al., 1991; Wirtz et al., 2000; Zannoni et al., 1999). In virtually all studies done so far, material properties assigned to the bone elements are chosen as isotropic based on the bone density distribution only, even though, as mentioned earlier, experimental and numerical studies have shown that elastic and strength properties of bone are well described as orthotropic. However, the application of anisotropic relationships require the measurement of a fabric tensor, which is not currently possible from clinical CT images since the resolution of such images is not good enough to resolve the trabecular architecture. Although recent developments in high resolution in-vivo imaging make it possible to measure fabric tensors for peripheral regions such as distal radius and tibia (MacNeil and Boyd, 2008; Van Lenthe and Muller, 2008; Varga et al., 2011), presently no such resolutions can be achieved for the most interesting sites: the hip and spine.

To overcome this problem, and thus to enable the use of sophisticated anisotropic material models, in this thesis we developed alternative approaches to obtain bone microstructural information, which can be used even with clinical CT images (Chapters 3 & 4).

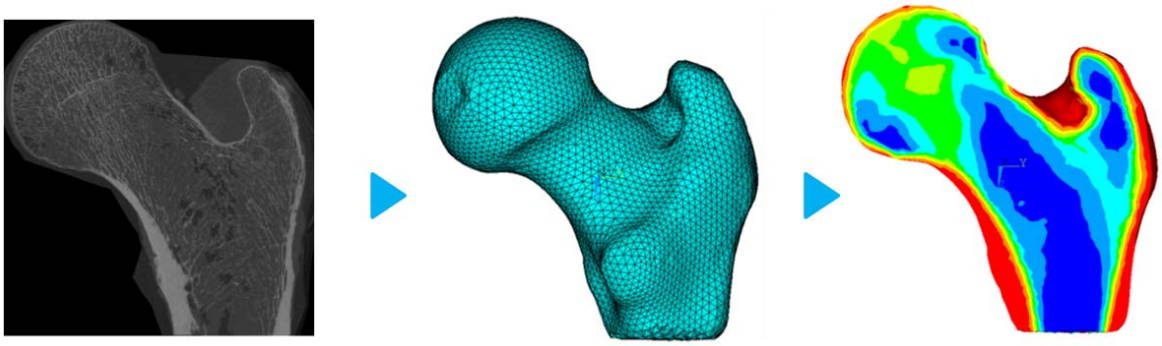

Figure 2. Continuum-level FE model of a human proximal femur generated from CT images.

Aim and thesis outline

The research project presented in this thesis focuses on patient specific prediction of bone strength using microstructure-enhanced continuum FE models.

In order to do so, the first question we posed was: what material model should we use, and what morphological parameter(s) should it account for? To answer this first question, we developed a new approach to identify the accuracy of continuum-level material models (Chapter 2). The current standard approach is to use experimental tests to validate results of FE analysis. However, as mentioned before, measurements using strain gauges are limited to the bone surface and thus cannot be used to validate the stress or strain distribution within the cancellous bone region, which is expected the region that could benefit most from a more accurate anisotropic material model. In a first study, we therefore introduce a novel computational approach that uses results of micro-FE models, which can represent the bone trabecular architecture in detail, as a reference. By comparing the homogenized micro-FE stress results to stress results obtained from continuum FE models, it is possible to identify the errors related to the use of empirical relationships that translate bone density and microstructure to stiffness.

The material model we then select required the measurement of bone fabric. The next questions then were: how can we obtain bone fabric information, which is needed for such anisotropic fabric-elasticity relationships, if we are not able to measure this from clinical CT scans? And also: are the results of models enhanced in this way really better than those of isotropic models?

Two approaches for the determination of bone fabric were proposed and tested. The first approach (Chapter 3) is based on the notion that the bone micro-architecture is adapted to the continuum-level stress state. As a result of this adaptation, the principal directions of the fabric and stress tensors will align. We explored this concept in the inverse way: to derive the fabric tensor from the stress tensor as obtained from continuum FE analyses under physiological loading conditions. The second approach is presented in chapter 4, this method uses a database of high-resolution bone models to derive the fabric information that is missing in clinical images. Databases of human proximal femurs and vertebrae were generated from micro-CT scans and continuum FE models were generated from these images using a pre-defined mesh template and an iso-anatomic mesh morphing procedure which ensures that each element within the mesh template is at a specific anatomical location. This makes it possible to map microstructural parameters that cannot be measured for patients from a best matching model in the database. By combining the patient-specific density information measured from the CT scan with fabric information from the database, the microstructure-

enhanced anisotropic material models can be used for non-linear failure analysis of a patient's bone.

By using the database approach as described above, it became clear that considerable inter-individual variation on bone density and morphology can exist. This led us to formulate a new question: what is the inter-individual variation between subjects and how do these depend on location? To answer this additional question, we created maps of the average density and other bone morphological parameters for each element in the mesh template, as well as of the inter-individual variability in these parameters. These maps clearly revealed locations where inter-individual variation was high (Chapter 5), and this begged a second additional question: would it be possible to predict bone strength from bone density or other parameters measured locally at a very specific 'critical site' directly, by using a statistical model? To investigate the latter additional question, we correlated bone density and structural parameters as determined for each element in the mesh template to whole bone strength data obtained from compression tests performed on the same bones.

Chapter 2

A New Approach to Determine the Accuracy of Morphology-Elasticity Relationships in Continuum FE Analyses of Human Proximal Femur

The concepts of this chapter are based on: Javad Hazrati Marangalou, Keita Ito and Bert van Rietbergen. A New Approach to Determine the Accuracy of Morphology-Elasticity Relationships in Continuum FE Analyses of Human Proximal Femur. Journal of Biomechanics, 45(16): 2884-2892.

A New Approach to Determine the Accuracy of Morphology-Elasticity Relationships in Continuum FE Analyses of Human Proximal Femur

Javad Hazrati Marangalou, Keita Ito, Bert van Rietbergen

Orthopaedic Biomechanics, Biomedical Engineering Department, Eindhoven University of Technology, Eindhoven, The Netherlands

Abstract

Continuum finite element (FE) models of bones are commonly generated based on CT scans. Element material properties in such models are usually derived from bone density values using some empirical relationship. However, many different empirical relationships have been proposed. Most of these will provide isotropic material properties but relationships that can provide a full orthotropic elastic stiffness tensor have been proposed as well. Presently it is not clear which of these relationships best describes the material behavior of bone in continuum models, nor is it clear to what extent anisotropic models can improve upon isotropic models. The best way to determine the accuracy of such relationships for continuum analyses would be by quantifying the accuracy of the calculated stress/strain distribution, but this requires an accurate reference distribution that is not depended on such empirical relationships. In the present study, we propose a novel approach to generate such a reference stress distribution. With this approach, stress results obtained from a micro-FE model of a whole bone, that can represent the bone trabecular architecture in detail, are homogenized and the homogenized stresses then are used as a reference for stress results obtained from continuum models. The goal of the present study was to demonstrate this new approach and to provide examples of comparing continuum models with anisotropic vs. isotropic material properties.

Continuum models that implemented isotropic and orthotropic material definitions were generated for two proximal femurs for which micro-FE results were available as well, one representing a healthy, the other an osteoporotic femur. It was found that the continuum FE stress distributions calculated for the healthy femur compared well to the homogenized results of the micro-FE although slightly better for the orthotropic model (r=0.83) than for the isotropic model (r=0.79). For the osteoporotic bone, the orthotropic model also did better (r=0.83) than the isotropic model (r=0.77). We propose that this approach will enable a more relevant and accurate validation of different material models than experimental methods used so far.

Introduction

Continuum finite element (FE) analysis has become a standard computational tool for the analysis of bone mechanical behavior in orthopaedic biomechanics. It is commonly used to evaluate bone loading conditions, e.g. after the placement of implants (Huiskes, 1993; Huiskes and Chao, 1983; Pettersen et al., 2009; Weinans et al., 2000) and to evaluate bone strength e.g. in case of osteoporosis or drug treatments (Chevalier et al., 2010; Guo and Kim, 2002; Tawara et al., 2010; Verhulp et al., 2008). Patient-specific finite element models are usually generated based on clinical CT scans. From such scans, the geometry as well as the bone density distribution can be easily derived. Empirical relationships are then needed to calculate bone material parameters from the measured density distribution.

Many different empirical relationships have been described in the literature. With the more simple ones, bone is modeled as isotropic and a power law relationship is used to calculate the isotropic Young's modulus from the bone density (Carter and Hayes, 1976; Keller, 1994; Keyak et al., 1994; Keyak et al., 1997; Morgan et al., 2003; Rice et al., 1988). It is known, however, that cancellous bone can be highly anisotropic. More advanced relationships that can describe the full anisotropic elastic behavior of cancellous bone have been developed as well. With such relationships, bone elastic behavior is usually described as orthotropic with the principal orthotropic axes determined by the underlying micro-architecture and some power law to calculate the values of the orthotropic elastic constants. In this case also, several different orthotropic relationships have been developed (Cowin, 1985; Cowin and Turner, 1992; Kabel et al., 1999b; Turner et al., 1990; Yang et al., 1998; Zysset and Curnier, 1995). In these relationships, the orientation of the trabeculae is usually quantified by a second rank fabric tensor which represents the average trabecular orientation (Harrigan and Mann, 1984; Odgaard, 1997). Since this can be difficult or impossible to measure from clinical CT scans, it has been proposed as well to base the trabecular orientation on the anatomical site (Yang et al., 1998).

It presently is unclear which relationship would provide the best results for continuum FE analyses of whole bones. Moreover, it is even unclear to what extent the use of such more advanced anisotropic relationships would improve the accuracy of the finite element calculations over more simple isotropic models.

In order to test the accuracy of different isotropic or anisotropic relationships for modeling material properties in continuum FE analyses, a 'gold standard' is required relative to which the results of the analyses can be tested. So far, experimental test on whole bones have been used as a reference (Chevalier et al., 2008; Keyak et al., 1993; Pahr and Zysset, 2009; Taddei et al., 2006; Trabelsi et al., 2011). For whole bones, however, experimental results are usually limited to surface strain measurements and to measurement of the stiffness of the whole bone.

Based on such measurements, it is not possible to validate the stress or strain distribution within the cancellous bone tissue, which is the most important region for implant fixation. Also, the surface strains and total bone stiffness obtained from FE models might not be very sensitive for the choice of the empirical constants, as long as the cortical bone stiffness is well represented, nor for the choice of an isotropic versus an anisotropic model for the cancellous bone.

In the present study, we propose another approach to test the accuracy of different empirical material laws for continuum FE analyses of bone. With this approach, results obtained from a micro-FE model of a whole bone that can represent the bone trabecular architecture in detail are used as a reference (Figure 1). Such micro-FE models thus account for the effect of the bone density and anisotropy that result from the bone micro-architecture without the need for any empirical relationships. The stresses and strains obtained from such models are those at the level of the bone tissue, but after homogenization of these stresses and strains they can be directly compared to those obtained from continuum FE models. The difference between the standard approach to calculate the continuum level stress distribution and the approach that we take here to generate a 'gold standard' is depicted in Figure 1. With the standard approach, the bone micro-architecture is homogenized to a density and fabric value, and a continuum FE model is created with material properties based on these homogenized values. With the approach that we take here, a micro-FE model is used to calculate bone tissue level stresses and strains and the results are homogenized.

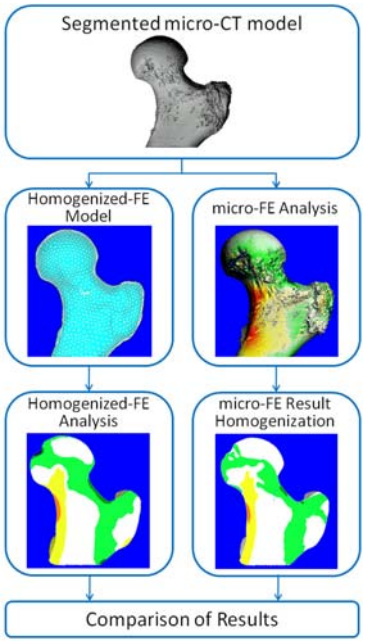

Figure 1. Design of the study; results of a continuum-level FE model that incorporates the material law to be tested (left) are compared to homogenized micro-FE results that are taken as the gold standard (right).

The goal of the present study was to demonstrate this new approach by comparing the calculated stress distributions in a continuum model of a healthy and an osteoporotic femur, implementing isotropic and anisotropic material properties, with homogenized micro-FE results of the same bones.

Materials and Methods

Samples

Two human proximal femurs, a healthy femur and a severely osteoporotic femur collected for an earlier study (Van Rietbergen et al., 2003) were used. These femurs were scanned using a micro-CT scanner (micro-CT80; Scanco, Brüttisellen, Switzerland) at a resolution of 80 microns covering a length of approximately 92 mm of each femur. After scanning, a thresholding algorithm was applied to separate the bone from the marrow phase. More information about the samples and scanning procedure can be found in van Rietbergen, et al. (2003).

Creation of continuum-FE meshes

Continuum finite element models of proximal femurs were generated based on contours of the bone periosteal surface that were generated semi-automatically using software provided with the micro-CT scanner. Using a marching cubes algorithm on the volume comprised by these contours, a triangularisation of the bone surface was obtained. This surface was converted to STL format and imported into ANSYS 12.1 (Ansys, Inc., United States) for volumetric meshing. Meshing was done using tetrahedron elements with a typical size of 2 mm.

Calculation of homogenized material properties

In order to calculate anisotropic material properties, an element density and fabric tensor were calculated for each element. This was done using a semi-automatic mapping algorithm. In the first step; the femur was separated into two compartments: a cortical and a cancellous one using software provided with the micro-CT scanner (IPL, Scanco Brüttisellen, Switzerland). A minimum of 1 mm cortical thickness was assumed near bone external surfaces. Using an in-house developed algorithm, the type (cortical or cancellous) and number of voxels within each element were determined. For each element, fully or partially within the cancellous compartment, a spherical VOI around the element center with a radius of 2 mm was defined. For each VOI, bone volume fraction (BV/TV) and mean intercept length (MIL) based fabric tensor were determined and assigned to the element, considering only the region in the cancellous compartment. For elements fully or partly in the cortical compartment, a cortical volume fraction was defined considering only the region within the cortical compartment and an identity tensor was specified as the fabric tensor. As an example, a contour band plot of the

calculated bone volume fraction (ρ) and a vector plot of the fabric main direction (largest eigenvalue after normalization) for the osteoporotic and healthy femurs are shown in Figure 2.

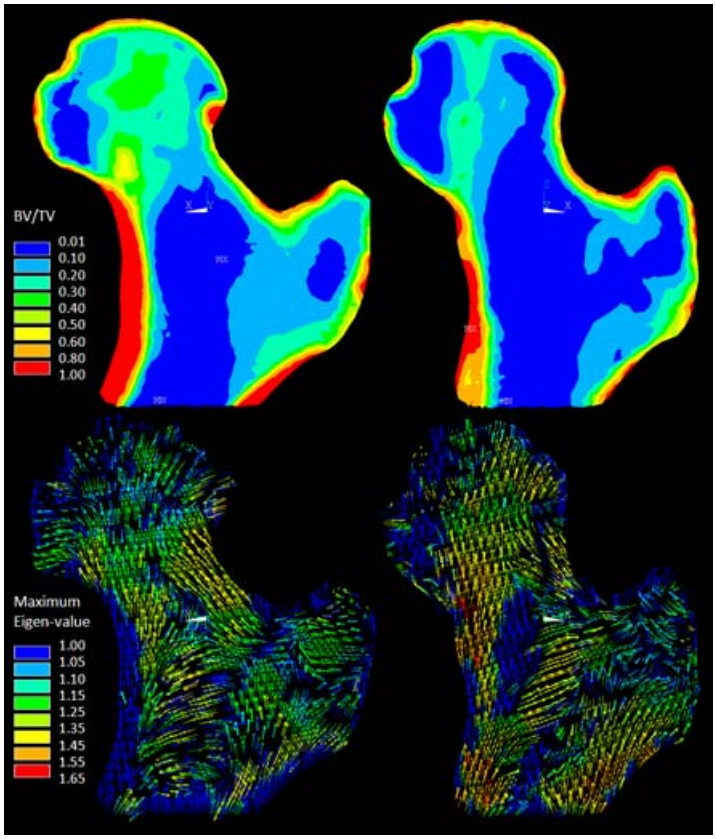

*Figure 2. Bone morphological parameters; bone volume fraction and main direction (eigenvalues normalized to have Tr(**M**)=3, where M is the fabric tensor) for healthy (left) and osteoporotic (right) femurs.*

Based on the element density ρ and fabric tensor **M**, the element compliance tensor was calculated using the fabric-elasticity relationship of Zysset and Curnier (Zysset, 2003; Zysset and Curnier, 1995):

$$\mathbb{C}=\sum_{i=1}^{3}\frac{1}{\varepsilon_0\rho^k m_i^{2l}}\mathrm{M}_i\otimes\mathrm{M}_i-\sum_{i,j=1;i\neq j}^{3}\frac{\nu_0}{\varepsilon_0\rho^k m_i^l m_j^l}\mathrm{M}_i\otimes\mathrm{M}_j+\sum_{i,j=1;i\neq j}^{3}\frac{1}{2G_0\rho^k m_i^l m_j^l}\mathrm{M}_i\overline{\underline{\otimes}}\mathrm{M}_j \quad (1)$$

$\varepsilon_0, \nu_0, G_0$ are elastic constants, m_i the normalized eigenvalues and $\mathbf{M}_i$ the dyadic product of the eigenvectors of fabric tensor $\mathbf{M}$:

$$\mathbf{M}=\sum_{i=1}^{3}m_i\mathrm{M}_\mathrm{i}=\sum_{i=1}^{3}m_i(\mathrm{m}_\mathrm{i}\otimes\mathrm{m}_\mathrm{i}),\quad Tr(\mathbf{M})=3\,, \quad (2)$$

In the case of modeling isotropic material properties, the fabric tensor is simply replaced by the identity tensor. The elastic constants (Table 1) were scaled to be in agreement with the

Young's moduli used for micro-FE analyses (Verhulp et al., 2006). For elements that cover both compartments, a mixture rule was used to calculate a stiffness tensor that is a mixture of the cancellous and cortical stiffness tensor, using the element cancellous and cortical bone fraction as scaling factors.

Table 1. Constants used in the Zysset-Curnier relationship.

ε_0 *[GPa]*	ν_0	G_0 *[GPa]*	k	l
22.5	0.3	8.65	1.914	1

Homogenization of micro-FE results

As mentioned earlier, micro-FE results obtained for the same femurs (Verhulp et al., 2008) were taken as the gold standard. Using the same meshes as used for the continuum model, an averaging technique was used to homogenize the bone tissue stress tensors over the element volumes. This averaging should be performed over the total element volume, V_{tot}, comprising both the voxels that represent bone tissue and those that represent the marrow region. In the micro-FE model, however, stress and strain values were calculated only for the voxels representing bone tissue V_{tissue}. Since the stresses in the other voxels (representing bone marrow) are zero anyway, the homogenized stress $\bar{\boldsymbol{\sigma}}$ could be calculated by integrating the tissue stress tensors $\boldsymbol{\sigma}$ over the bone tissue volume only:

$$\bar{\boldsymbol{\sigma}} = \frac{1}{V_{tot}} \int \boldsymbol{\sigma} \; dV_{tot} = \frac{1}{V_{tot}} \int \boldsymbol{\sigma} \; dV_{tissue} \tag{3}$$

After calculating the homogenized stress tensor for each element, the homogenized principal stress values were calculated

Boundary conditions

The boundary conditions applied were chosen to be the same in the continuum and micro-FE model and represented loading conditions typically applied in an experimental setting to simulate a fall-on-the-side situation (Cheng et al., 1997a; Courtney et al., 1994, 1995). In this setup the angle between the vertical and the shaft axis was 10 degrees and the femur was internally rotated by 15 degrees. The load magnitude was 1 kN, distributed over the femoral head. The individual nodal forces were directed towards the center of the femoral head to represent loading conditions expected when a frictionless cartilage layer is present. The nodes on the surface of the trochanter, in a 5 mm layer perpendicular to the resultant hip force, were fixed in the vertical direction and the nodes on the distal end of the femur were constrained in the horizontal direction (Figure 3).

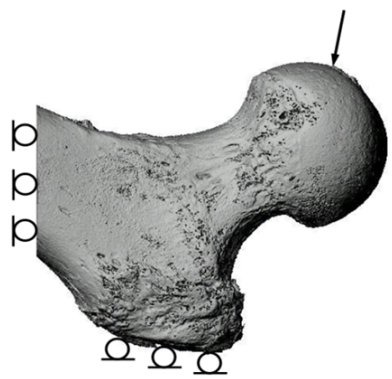

Figure 3. Applied boundary conditions to FE models, the arrow represent resultant hip force.

Comparison of results

Contour and vector plots of the largest principal stress component were made for a qualitative comparison of the stress distribution obtained from the continuum model and from the homogenized micro-FE results. For a quantitative comparison, the homogenized micro-FE principal stress values for elements in the neck region were correlated with those of the continuum models and a Pearson's linear correlation coefficient was calculated based on an element by element value comparison. Only elements in the femoral neck were selected since this is the most critical region for loading condition as applied here and since it is far enough away from the regions where boundary conditions were applied, thus avoiding errors due to the close proximity of external constraints.

Furthermore, the whole bone stiffness was calculated and compared for all models. Since in all models the applied load was distributed over a large number of nodes, it was not possible to define a meaningful deflection of the bone when loaded. Instead, an energy-equivalent deflection *d* was calculated from the energy equation:

$$\frac{1}{2}F\ d = \int U\ dV \tag{4}$$

with *F* the applied force and *U* the strain energy density. Using this deflection d, the stiffness k then was calculated as:

$$k = \frac{F}{d} = \frac{F^2}{2\int U\ dV} \tag{5}$$

Results

Contour plots of the homogenized principal stress values are shown in Figure 4. These plots serve as the gold standard relative to which the results of the continuum FE will be compared.

Contour plots of the largest principal stress component in the healthy and osteoporotic femur as obtained from the continuum models are depicted in Figure 5.

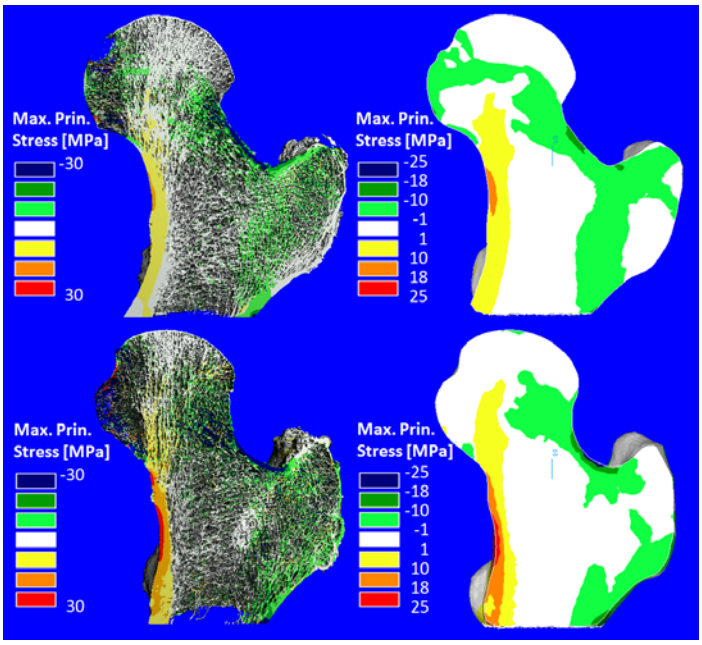

Figure 4. micro-FE results and homogenized micro-FE results; maximum principal stress [MPa] distributions in the micro-FE models (Verhulp et al., 2008) and homogenized distributions in the continuum-FE models for the healthy (top) and osteoporotic (bottom) femurs.

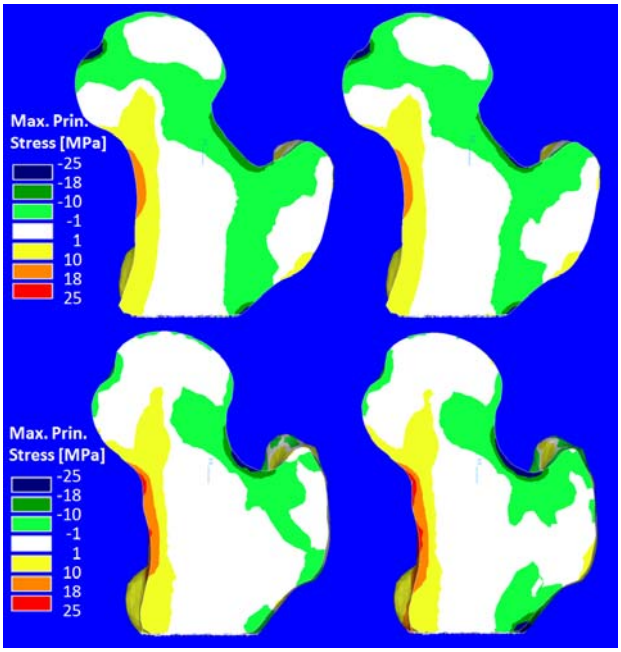

Figure 5. Top: maximal principal stress [MPa] distribution for the healthy femur, calculated using the orthotropic continuum model (left) and the isotropic continuum model (right).Bottom: the same for the osteoporotic femur.

It can be seen that the stress distribution obtained from the continuum models are both qualitatively and quantitatively very similar to those obtained from the micro-FE results. The most notable difference is the somewhat higher stress values at the distal side of the femoral neck and the proximal side of the femoral head in the continuum models. The latter likely is an effect of the applied boundary conditions. For the isotropic models a comparison of the stress distribution in the continuum FE and homogenized micro-FE models resulted in a correlation coefficient of r=0.798 for the healthy model and of r=0.773 for the osteoporotic model. For the orthotropic models, a correlation coefficient of r=0.831 was found for the healthy femur and of r=0.830 for the osteoporotic one (Figure 6).

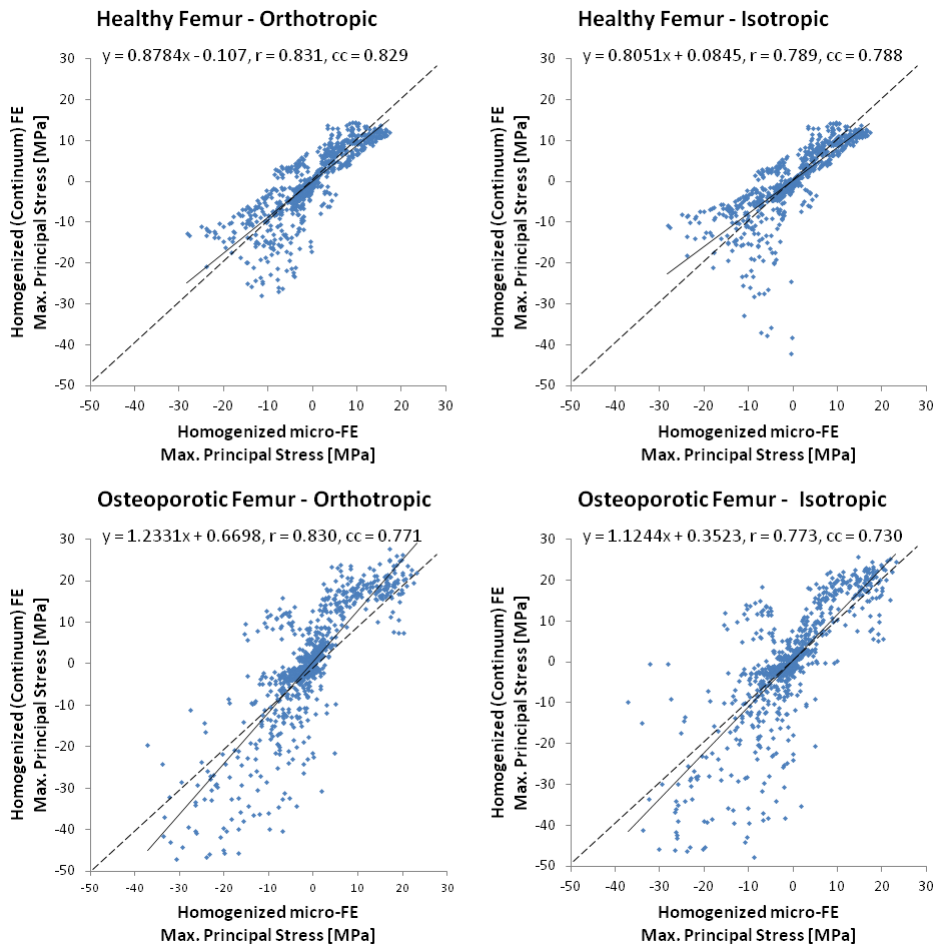

Figure 6. Regression of micro-FE and continuum-FE predicted results based on isotropic and orthotropic material properties for the healthy (upper panels) and osteoporotic (bottom panels) bone (r: linear correlation coefficient and cc: concordance correlation coefficient).

Contour plots of the strain energy density distribution (Figure 7) showed very similar results as the maximum principal stress plots. In particular for the osteoporotic femur, the orthotropic model better compared to the micro-FE results than the isotropic model.

To get a better insight in the differences between the results of continuum and homogenized micro-FE stresses, we also plotted the relative error in the maximum principal stress calculation obtained from the isotropic model when compared to the gold standard for the healthy femur versus the bone volume fraction (Figure 8). From this result, it is clear that the larger errors are found in regions with low bone volume fraction.

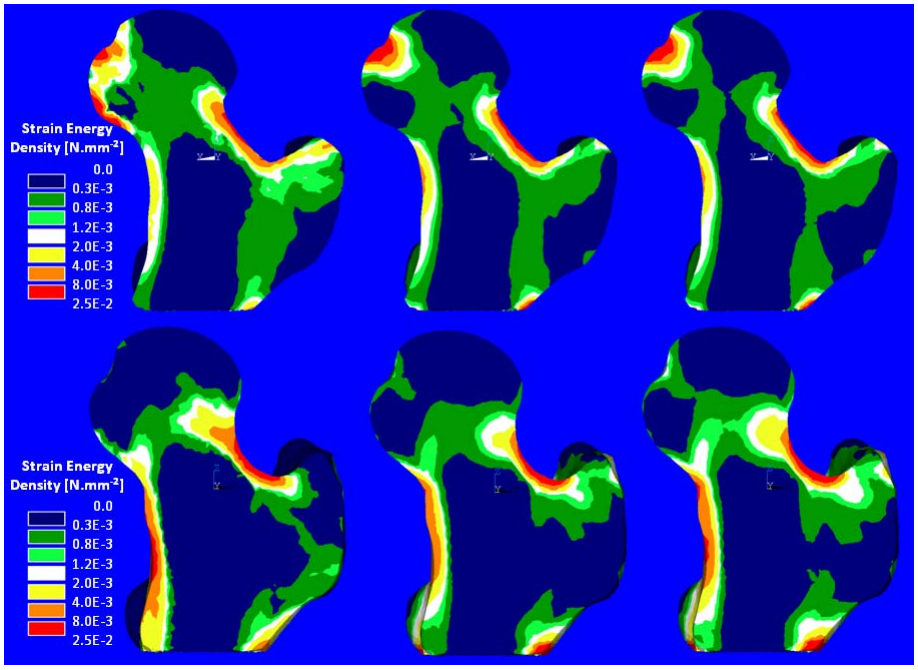

Figure 7. Strain energy density (SED) plots for homogenized micro-FE (left), orthotropic (middle) and isotropic (right) models within healthy femur (top) and osteoporotic femur (bottom).

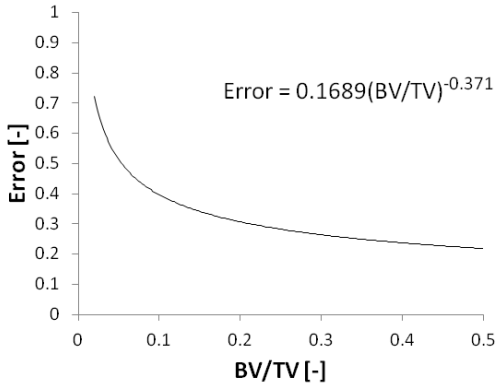

Figure 8. Relative error in the maximum principal stress magnitude in the isotropic model for the healthy femur.

In order to visualize the correspondence in the directions of the maximum principal stress component, vector plots of the maximum principal stress are shown in Figure 9. The vector

plots from continuum models compare qualitatively well with the ones from micro-FE models. In particular for the osteoporotic femur it can be seen that at some locations (notably Ward's triangle) the agreement is less favorable.

Figure 9. Maximum principal stress vector plots for micro-FE (left), orthotropic (middle) and isotropic (right) models for the healthy femur (top) and osteoporotic one (bottom).

The results for the whole bone stiffness are shown in Table 2 from these results it can be seen that the continuum models tend to overestimate the stiffness, in particular when using isotropic material properties. For the healthy femur, this overestimation was 10% for the orthotropic model and 14% for the isotropic model. For the osteoporotic femur, the same overestimation was found for orthotropic model, but for the isotropic model the stiffness was overestimated by as much as 52%.

Table 2. The stiffness calculated for the different models [N/mm].

	micro-FE	Orthotropic	Isotropic
Healthy	3865.967	4263.505 (+10%)	4406.971 (+14%)
Osteoporotic	2643.209	2915.581 (+10%)	4025.246 (+52%)

Discussion

The goal of this study was to demonstrate a new approach to evaluate the accuracy of the stress distributions calculated from continuum FE models that implement different material

models. The material model used in this study was either an isotropic one based on the density distribution or an orthotropic one, based on bone density and fabric using a relationship proposed in the literature (Zysset and Curnier, 1995). This new approach uses homogenized micro-FE stress distributions as the gold standard relative to which the results of the continuum models can be compared.

We found good agreement between results obtained from the homogenized micro-FE models and those of the continuum models. This indicates that bone density, or a combination of bone density and fabric, in combination with the material models chosen well represents the mechanical properties of cancellous bone. For the two bones investigated here, the orthotropic models provided slightly more accurate results than isotropic models. These results are in accordance with earlier studies where orthotropic models improved the predictions of vertebral body apparent stiffness with respect to isotropic models (Pahr and Zysset, 2009). The osteoporotic bone benefited more from an orthotropic material description than the healthy bone model. However, a thorough comparison between the accuracy of isotropic and orthotropic models is not possible due the limitations in the number of the samples used in this study.

In the present study we could use micro-CT images of the bones for the measurement of the element fabric tensor. When only clinical CT data is available, this is not possible since the resolution of such images is not good enough to resolve the trabecular architecture required to measure fabric. Nevertheless, methods have been developed to obtain at least some indication of the bone fabric even from clinical CT images (Tabor, 2007). Recently developed high resolution flat-panel CT scanning techniques might even provide a resolution that is good enough to determine fabric of trabecular bone in-vivo (Bredella et al., 2008; Cheung et al., 2009; Gupta et al., 2006; Walsh et al.). Although in most of these studies only bone in the peripheral skeleton was considered, applications to the spine and femur have been reported as well (Mulder et al.). In case no patient-specific information about the fabric can be obtained, using a generalized fabric direction might be a possible solution as well.

The present study only focused on the accuracy of the stress distribution. The accuracy of the strain distribution was not investigated. The reason for this is that for the homogenization of the micro-FE calculated strains also the strains in the marrow region are needed. Unlike for the stresses, the strains in these regions are not zero and eq. [3] cannot be used for strains. Since the marrow region was not meshed in the micro-FE models, it was not possible to apply a proper homogenization of the micro-FE calculated strains. It is possible though, to compare the strains for the continuum models that implement isotropic and anisotropic material properties. Figure 10 shows the maximum principal strain distribution for all continuum models. It can be seen that the strain distributions in the isotropic and orthotropic models are

very similar, although strains in the isotropic model are slightly higher than those in the anisotropic model.

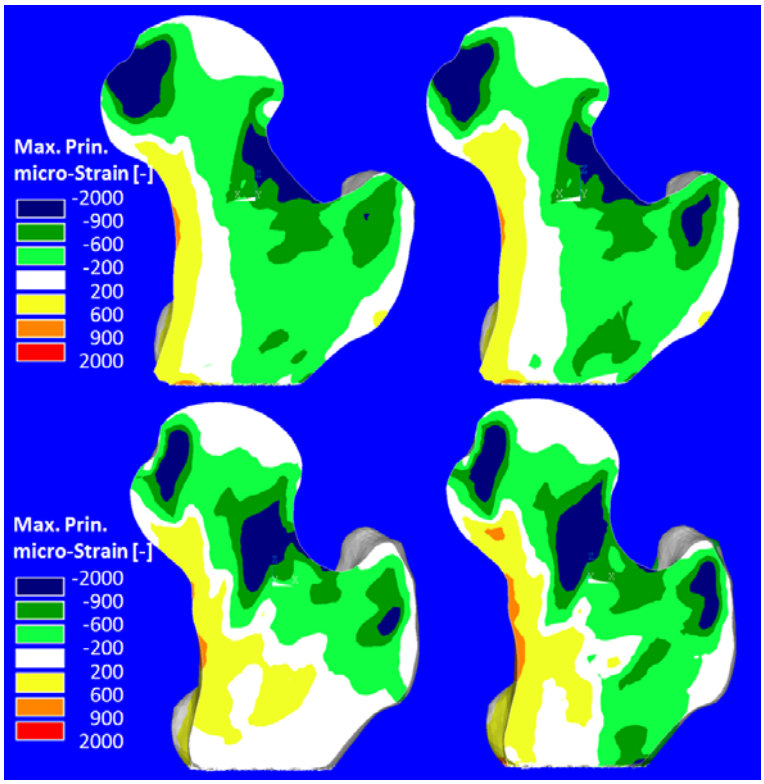

Figure 10. Top: maximal principal strain [-] distribution for the healthy femur, calculated from the orthotropic continuum model (left) and the isotropic continuum model (right). Bottom: the same for the osteoporotic femur.

Although in this study we have compared the whole-bone stiffness, we did not compare the elastic properties of the elements in the continuum models to the elastic stiffness of the corresponding regions in the micro-FE models. The reason for this is twofold. First, most bone morphology-stiffness relationships have already been well validated by comparing elastic properties calculated from the morphology parameters with those measured in experiments or from micro-FE analyses of the same specimens (Matsuura et al., 2008; Rincon-Kohli and Zysset, 2009). Second, although it would theoretically be possible to calculate the stiffness of the spherical region around each element based on micro-FE results, this would be extremely expensive and was out-of the scope of the present study.

Some other limitations of this study must be mentioned as well. First, we only analyzed 2 femurs and only two material models. However, our main goal was to test the new approach, and the results provided here should be considered merely as a demonstration. Second, we applied only one set of loading conditions. We selected loading conditions representing a fall because we expected that stresses and strains during non-physiological loading conditions

might be more sensitive for the material model used than those during physiological loading conditions. The reason for this expectation is that, if bone is adapted to physiological loading conditions, the highest stress and strain values are expected in the principal anisotropic direction. In that case only the stiffness in that principal direction is of importance, whereas the stiffness in the transversal directions hardly plays a role. During non-physiological loading, however, high stresses and strains are expected also in transversal directions.

It should be noted as well that the exact way, in which the bone density and fabric (from which the elastic properties in the continuum model were derived) are determined, could also have an effect on the results. In the present study we defined a spherical volume with a radius of 2 mm around the element centroid for calculation of the element density and fabric. This choice was based on the notion that, in order to define valid continuum level properties, measurements over a length scale on the order of 4 mm is required (Harrigan et al., 1988). Setting this radius to a larger or smaller value will slightly change the results, and thus the material properties in the continuum model. To test the sensitivity of the results to the radius size, we performed a pilot study in which the radius was varied from 2 mm to 8 mm. The results showed that the actual chosen size has a very small effect on the calculated bone volume fraction, fabric tensor and degree of anisotropy. Our choice of the fabric tensor used (MIL) was based on the fact that this was the tensor that was used when the orthotropic material models were defined. Selecting other fabric tensors, however, will likely not affect the results much (Kabel et al., 1999a).

In conclusion, we have demonstrated that a micro-FE stress/strain homogenization procedure can be used as a reference relative to which results of continuum models can be compared to evaluate the accuracy of the models. We propose that this approach will enable a more relevant and accurate validation of different material models than experimental methods used so far.

Acknowledgments

Funding from the European Union for the osteoporotic virtual physiological human project (VPHOP FP7-ICT2008-223865) is gratefully acknowledged.

Conflict of interest statement

Bert van Rietbergen is a consultant for Scanco Medical AG.

Chapter 3

A Novel Approach to Estimate Trabecular Bone Anisotropy from Stress Tensors

The concepts of this chapter are based on: Javad Hazrati Marangalou, Keita Ito and Bert van Rietbergen. A Novel Approach to Estimate Trabecular Bone Anisotropy from Continuum-level Stress Tensors. Submitted

A Novel Approach to Estimate Trabecular Bone Anisotropy from Stress Tensors

Javad Hazrati Marangalou, Keita Ito, Bert van Rietbergen

Orthopaedic Biomechanics, Biomedical Engineering Department, Eindhoven University of Technology, Eindhoven, The Netherlands

Abstract

Continuum finite element (FE) models of bones and bone-implant configurations are usually based on clinical CT scans. In virtually all of these models, material properties assigned to the bone elements are chosen as isotropic. It has been shown, however, that cancellous bone can be highly anisotropic and that its elastic behavior is best described as orthotropic. Material models have been proposed to derive the orthotropic elastic constants from measurements of density and a fabric tensor. The use of such relationships in FE models derived from CT scans, however, is hampered by the fact that the measurement of such a fabric tensor is not possible from clinical CT images since the resolution of such images is not good enough to resolve the trabecular micro-architecture.

In this study, we explore an alternative approach that is based on the paradigm that bone adapts its micro-architecture to the loading conditions, hence, that fabric and stress tensors should be aligned and correlated. With this approach the eigenvectors and eigenvalues of the element continuum-level stress tensor are used as an estimate of the element fabric tensor, from which the orthotropic material properties then are derived. Using an iterative procedure, element orthotropic material properties and fabric tensors are updated until a converged situation is reached. The goals of this study were to investigate the feasibility and accuracy of such an iterative approach to derive orthotropic material properties for a human proximal femur, and to investigate if models derived in this way can provide more accurate results than isotropic models. Results were compared to those obtained from models of the same femurs for which the fabric was measured from micro-CT scans.

It was found that the iterative approach could well estimate the orientation of the fabric principal directions (average error = 12%). When comparing the stress/damage values in the models with material properties based on estimated and measured fabric tensors, the differences were not significant suggesting that the material properties based on the estimated fabric tensor well reflected those based on the measured fabric tensor. Errors were less than those obtained when using isotropic models.

It is concluded that this novel approach can provide a reasonable estimate of anisotropic material properties of cancellous bone. We expect that this approach can lead to more accurate results in particular for models used to study implants, which are usually anchored in highly anisotropic cancellous bone regions.

Introduction

Continuum level finite element (FE) models of bones are often used for pre-clinical evaluation of implants and orthopaedic interventions. Such FE models are commonly generated from CT scans, such that a patient-specific geometry and density distribution can be assigned. The bone material properties are then derived by using some sort of empirical power law that relates the measured density to local bone stiffness and strength (Carter and Hayes, 1976; Keyak, 2001; Morgan et al., 2003; Rice et al., 1988; Taddei et al., 2007). In such studies, stiffness and strength properties are usually modeled as isotropic. In particular in cancellous regions, however, bone can be highly anisotropic due to its structural organization of trabeculae in preferred directions, as commonly quantified by a so called fabric tensor (Cowin, 1985; Harrigan and Mann, 1984; Odgaard, 1997; Zysset et al., 1998). Since the resolution of clinical CT imaging techniques is not sufficient to capture this organization, it is not possible to account for this anisotropic behavior in continuum FE models.

In an earlier study, we introduced an approach that makes use of a database of high-resolution micro-CT scans from which the fabric can be obtained, which is then mapped to a patient model. In this way it is possible to create FE-models with patient-specific geometry and density and database-derived anisotropy. In that study we also demonstrated that such models better reproduce the stress and damage distribution as well as bone stiffness and strength than isotropic models (Hazrati Marangalou et al., 2013). A disadvantage of this approach, however, is that it can be used only for sites for which such databases are available.

In the present study, we explore a more versatile alternative approach that does not require a database for deriving anisotropic material properties in continuum models of bone. This alternative approach is based on the commonly accepted paradigm that bone adapts its micro-architecture to the loading conditions. The fact that elastic properties of cancellous bone are best described as orthotropic (Pahr and Zysset, 2009; Yang et al., 1998) has been explained by the fact that its underlying micro-architecture is adapted to a second-rank continuum-level stress tensor (Odgaard et al., 1997; Turner, 1992). With this adaptation, a bone micro-architecture is formed in which most trabeculae are oriented in the direction where, on average, the magnitude of the principal stress is maximal, and less trabeculae are oriented in the direction where, on average, the magnitude of the principal stress is minimal (Fyhrie and Carter, 1986; Vander Sloten and Van der Perre, 1989). As a result of this adaptive process, the orientation of the orthotropic axes will thus coincide with the principal stress directions

whereas the degree of anisotropy relates to the degree of anisotropy of the principal stress magnitudes (Turner, 1992). This suggests that it would be possible to derive the fabric tensor from measurements of the principal stress orientation and magnitudes, such as can be obtained from continuum FE-analyses. This, however, would be possible only if the correct anisotropic material properties are specified in the FE-model, which is not known beforehand. A solution to this problem that is investigated in this study is to use an iterative approach that starts with isotropic material properties to calculate the principal stresses from which orthotropic material properties are calculated. Using these updated orthotropic material properties, the principal stresses are re-evaluated and the material properties updated accordingly. This procedure can be repeated until no more changes are found.

The first goal of this study was to investigate the feasibility and accuracy of such an iterative approach to calculate the fabric tensor from the stress tensor. In order to investigate the accuracy, the approach was applied using continuum FE models of 10 femurs that were generated from micro-CT images, which made it possible to compare the estimated fabric tensors from stress tensors with the ones measured from the bone micro-architecture. The data set used was the same as the one used in the earlier study where we tested the database approach to derive anisotropic properties (Hazrati Marangalou et al., 2013). By comparing our present results with results obtained in that study, our second goal was to investigate if this alternative approach can provide more accurate results than models generated by a database approach or isotropic models which account only for the density distribution.

Materials and methods

Materials

Ten human cadaver femurs (mean age: 71.9 ± 8.55 years) obtained from three female and seven male donors were used for this study. The femurs were selected from a database of 33 femurs used in earlier studies. The selected femurs are the same as the ones used in an earlier study that uses a database approach to derive anisotropic properties, in order to facilitate an easy comparison between results of that earlier approach and the present approach. Imaging and processing of these femurs was described earlier (Hazrati Marangalou et al., 2013). In summary: micro-CT scans (XtremeCT, Scanco Medical AG, Brüttisellen, Switzerland) of the most proximal part (9 to 12 cm in length) were made with a nominal isotropic resolution of 82 μm. Images were filtered and processed according to the protocol recommended by the manufacturer. Compartments of cortical and cancellous bone were identified using masks obtained from a filtering procedure, while also all bone within 1 mm from the periosteal surface was identified as part of the cortical compartment.

Continuum finite element models of the proximal femurs were generated based on contours of the bone periosteal surface as obtained using software provided with the micro-CT scanner

(IPL V5.16, Scanco Medical AG, Brüttisellen, Switzerland). Using a marching cube algorithm, a triangularisation of the bone surface was made and exported in STL format to ANSYS finite element software (Ansys Inc., US) for volumetric meshing. Meshing was done using second order tetrahedron elements with a typical size of 2 mm, the number of elements on the proximal femur models varied from approximately 80,000 to 90,000 depending on the scan length. For all elements at the cortical/cancellous region, we calculated a bone volume fraction BV/TV and fabric tensor **M** as described earlier (Hazrati Marangalou et al., 2013). In summary for the elements that were at least partly within the cancellous bone, a spherical region around the element centroid with a diameter of 4 mm was defined (Harrigan et al., 1988) and the mean intercept length (MIL)-based fabric tensor was calculated for that spherical volume of interest using the image processing software provided by micro-CT system.

Fabric estimation algorithm

Two load cases were applied to the model, representing walking and stair climbing. These were selected because walking is the most dominant loading mode, while stair climbing represents a common loading mode for which the forces act in rather different directions. The magnitudes and the number of cycles for each load case in a daily life were taken from previous studies (Bergmann G. et al., 2010; Heller et al., 2005).

Linear-elastic analyses were performed for each individual load case and the stress tensors for each load case and each element were stored. The time-averaged element stress tensor $\overline{\boldsymbol{\sigma}}$ then was calculated from the stress tensors stored for the two load cases $\boldsymbol{\sigma}_i$:

$$\overline{\boldsymbol{\sigma}} = \sum_{i=1}^{2} \frac{n_{cycles,i}}{n_{cylcles,tot}} \boldsymbol{\sigma}_i \tag{1}$$

where $n_{cycles,i}$ relates to the number of cycles for that load case and $n_{cycles,tot}$ to the total number of cycles for all load cases. Eigenvectors of the averaged stress tensor were calculated and used as an estimate of the fabric tensor. The eigenvalues of the average stress tensor were used to calculate the eigenvalues of the fabric tensor (Turner, 1992). The eigenvalues of the stress tensor, however, were first scaled to be in agreement with the relationship between the normalized fabric tensor eigenvalues (m_i), the bone volume fraction (ρ) and the elastic modulus in the direction of the fabric tensor eigenvectors as proposed by (Zysset and Curnier, 1995):

$$E_i = 8237.1 \rho^{2.5} m_i^{3.76} \tag{2}$$

This relationship involves a power of 3.76 for the relationship between fabric eigenvalues and Young's modulus. We assumed a similar relationship holds for the relationship between the eigenvalues of the stresses and fabric, and that the power can be rounded to 4:

$$\sigma_{principal,i} = c\, m_i^4 \tag{3}$$

with c a constant. The eigenvalues of the fabric tensor then can be calculated from the inverse relationship. Since the fabric tensor is scaled such that $\det(\mathbf{M}) = 1;\ (\mathbf{M} = m_i(e_i \otimes e_i),\ e_i : eigenvectors)$ the constant c can be eliminated and the following relationship is obtained:

$$m_i = \frac{1}{(\sigma_{principal,1}^{1/4} \cdot \sigma_{principal,2}^{1/4} \cdot \sigma_{principal,3}^{1/4})^{1/3}} \sigma_{principal,i}^{1/4} \tag{4}$$

Figure 1 shows an overview of the iterative procedure. For the first iteration, no fabric estimate was available and the fabric tensor was set to the identity tensor, thus specifying isotropic material properties based only on the BV/TV distribution. The two load cases then were applied to the FE models and the fabric tensor calculated. In the following increments, orthotropic compliance tensors (Eq. 5) were assigned based on the fabric tensor calculated in the previous increment (Zysset and Curnier, 1995):

$$\mathbb{C} = \sum_{i=1}^{3} \frac{1}{\varepsilon_0 \rho^k m_i^{2l}} \mathrm{M}_i \otimes \mathrm{M}_i - \sum_{i,j=1;i\neq j}^{3} \frac{\nu_0}{\varepsilon_0 \rho^k m_i^l m_j^l} \mathrm{M}_i \otimes \mathrm{M}_j + \sum_{i,j=1;i\neq j}^{3} \frac{1}{2G_0 \rho^k m_i^l m_j^l} \mathrm{M}_i \underline{\overline{\otimes}} \mathrm{M}_j \tag{5}$$

with ε_0, ν_0 and G_0 elastic constants, m_i the normalized eigenvalues and M_i the dyadic product of the eigenvectors of fabric tensor **M**. FE analyses were repeated and a new estimate of the fabric tensor was calculated. Iterations continued until no further reduction was found in calculated average stress tensor.

Accuracy check

Statistical analysis: For the elements within the cancellous region, an element-wise Hotelling's T^2 test is used for the comparison of the eigenvalues and the eigenvectors of estimated and measured fabric tensors for the 10 samples used in this study (Schwartzman et al., 2010). This method is commonly used for group comparison of the eigenvalues and the eigenvectors of the diffusion tensors in magnetic resonance imaging (Lepore et al., 2008; Whitcher et al., 2007).

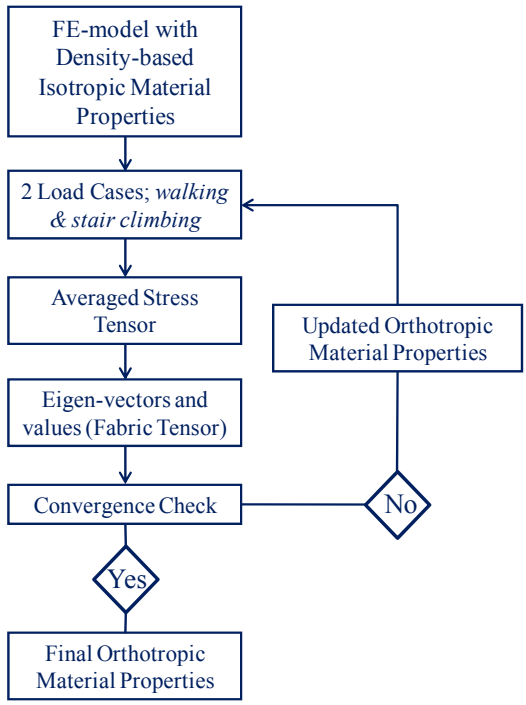

Figure 1. Overview of fabric estimation procedure.

To test the differences in the eigenvalues and the eigenvectors of measured and estimated fabric tensors, two likelihood ratio tests (LRT) are calculated (Schwartzman et al., 2010). Cumulative distribution functions (CDF) of the eigenvalue and the eigenvector LRT values are approximated as the distribution of a scaled chi-squared variable and the p-value is computed as 1-F(LRT), where F is the cumulative distribution function of LRT values. Another cumulative distribution function is calculated for the p-values (F(p-value)) which describes the probability of finding a p-value less than a specific value. Low values of the CDF at low p-values indicates that the probability of getting a significant difference between measured and estimated fabric tensors is low, hence that the regions where significant differences are found are small. In contrast, a high values of CDF for low p-values indicates that differences between the measured and estimated fabric tensors are likely significant for large regions. Finally, contour plots of the p-value distribution for eigenvalues and eigenvectors are made.

For further interpretation of the results, the angular deviation between the estimated major fabric direction and the measured one was calculated as a measure of eigenvector agreement. The agreement between the eigenvalues of the estimated and the measured fabric tensors was also quantified by the tensor norm error (Eq. 6).

$$err = \frac{\| M_{measured} - M_{estimated} \|}{\| M_{measured} \|} \tag{6}$$

Finite element analyses: In order to further test the effect of the estimated fabric tensor on the calculated mechanical properties, the results of models with material properties based on these estimated fabric tensors were compared to those of models generated in an earlier study (Hazrati Marangalou et al., 2013). In that earlier study, a reference model was generated for each bone in which orthotropic material properties were defined for elements within the cancellous region based on the actually measured fabric tensors and isotropic material properties were defined for the elements within cortical region while a rule of mixture was used for elements covering both compartments. As in that previous study, this model will serve as the gold standard relative to which the results of the model with estimated fabric are compared. The second reference model was an isotropic one with material properties based only on the density distribution. In the present study, we will also compare the results of the model with estimated fabric to those of these isotropic models.

For all models, elastic plastic damage constitutive behavior in local form (Charlebois et al., 2010) was used to simulate failure and post-failure behavior of the 10 femurs. Loading conditions represented a fall to the side configuration (Courtney et al., 1995; Verhulp et al., 2008). Whole bone stiffness, maximum load and stress distribution of the orthotropic models based on estimated fabric were compared to the gold standard and isotropic models of the previous study. Differences were quantified by calculating root-mean-square errors (RMSE), determination coefficients and concordance correlation coefficients. One-way ANOVA was used to test the significance of differences ($p < 0.05$).

Results

The iterative procedure was continued until the norm error between sequential averaged stress tensors is below one percent (Figure 2).

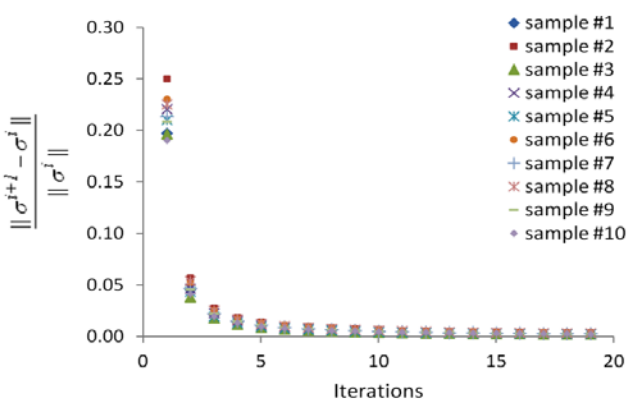

Figure 2. Convergence checks between to sequential iterations.

From the vector plot of the major fabric direction, it can be seen that the estimated fabric major directions generally agree well with those based on micro-CT measurements (Figure 3). In some regions, however, large deviations between estimated and measured vectors were

found particularly in Ward's triangle region and the shaft region, which are low-density regions. When averaged over all elements within the cancellous region, the angular deviation between the estimated major fabric direction and the measured one was 30° (28°-32°).

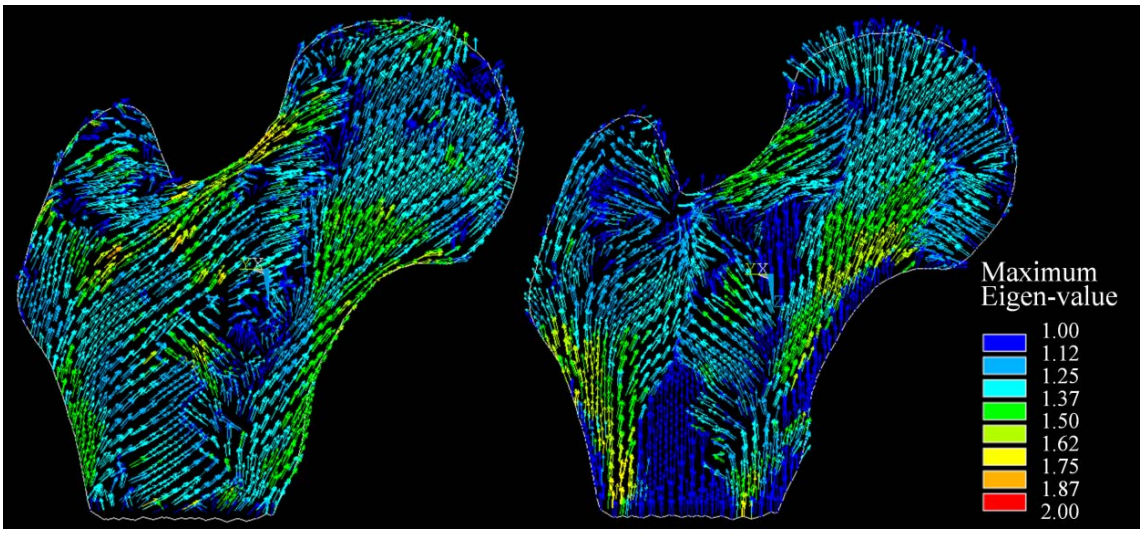

Figure 3. Vector plot of the estimated (left) and measured (right) major fabric direction, vector colors show the maximum eigenvalue of fabric tensor.

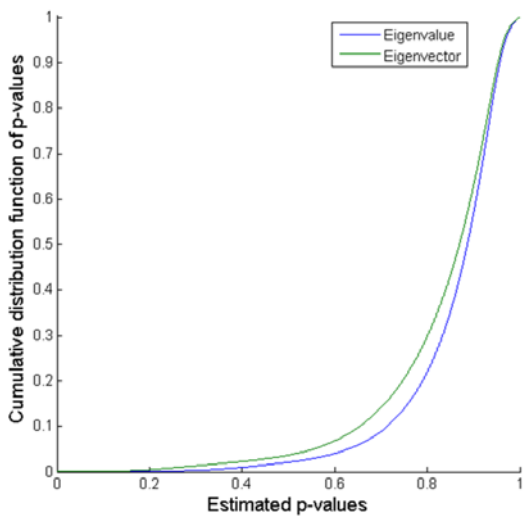

Figure 4. Cumulative distribution function of estimated p-values from eigenvalue and eigenvector tests (n=10).

Figure 4 shows the distribution of the estimated p-values for the eigenvalue and eigenvector tests. For most elements, the p-values calculated for the eigenvalues and eigenvectors was larger than 0.05, indicating that no significant differences could be detected between the estimated and measured fabric distribution. Contour plots of p-value distributions shows that high p-values usually occur in the cancellous region while lower p-values are in the cortical regions (Figure 5). The latter is due to the fact that for cortical bone an isotropic fabric tensor

was defined in the measured model, leading to an arbitrary orientation of the eigenvectors whereas the three eigenvalues per element now are equal. Furthermore, significant differences in the eigenvalues and the eigenvectors are found at the location where the external forces were applied. At these locations, relatively large deformations are found, resulting in some element distortion, which in turn leads to disagreement in the eigenvalues and the eigenvectors.

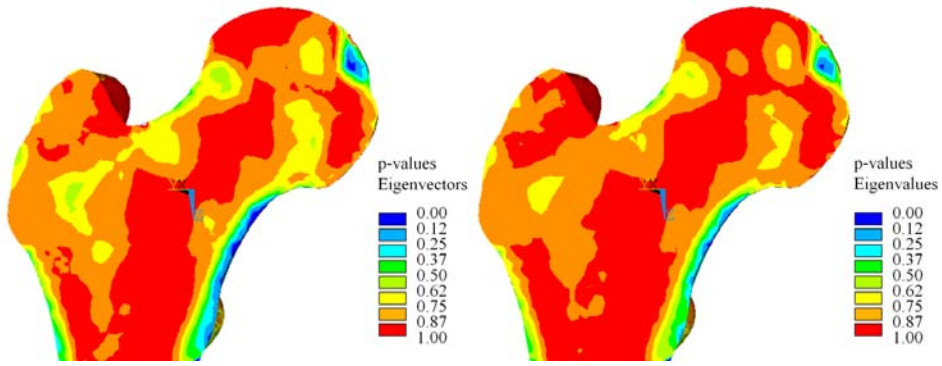

Figure 5. Contour plots of p-value distribution for eignvectors (left) and eigenvalues (right).

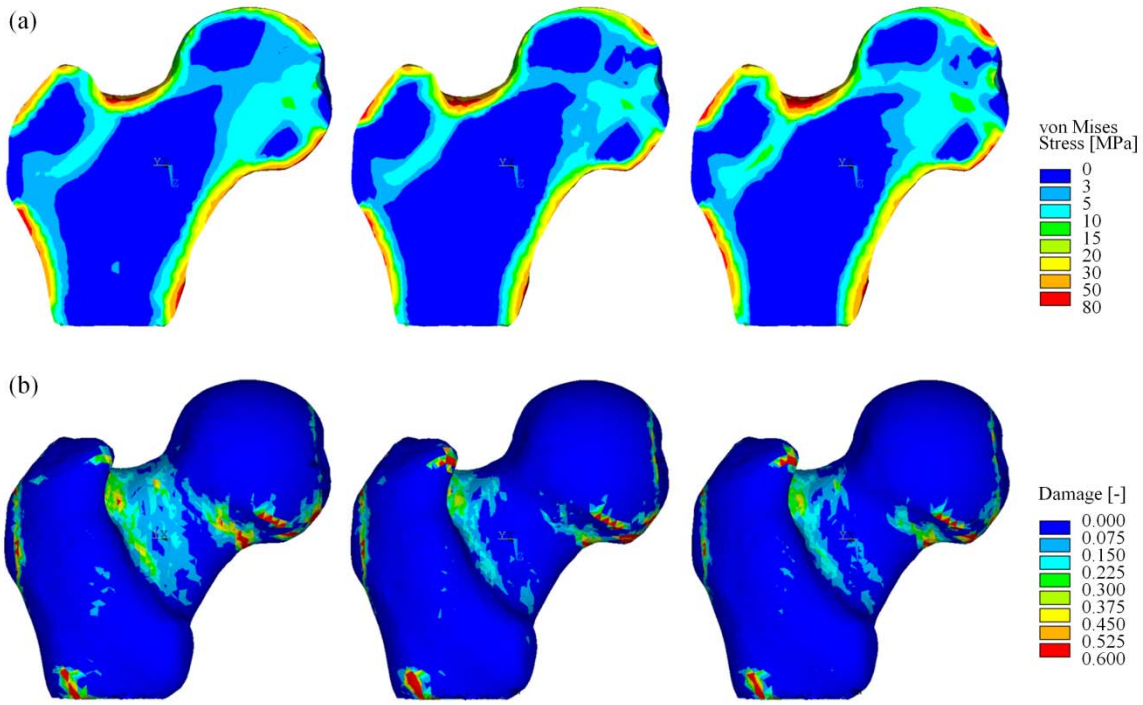

Figure 6. (a) von-Mises stress and (b) damage parameter distribution in the gold standard (left), isotropic (middle) and orthotropic model with estimated fabric (right). Results for the gold standard model and the isotropic model are reproduced from an earlier publication (Hazrati Marangalou et al., 2013)

The averaged norm difference between the actual and the estimated fabric tensors varied between 9.4%-28% for the ten samples (mean=12%, n=10). However, when comparing the degree of anisotropy, only a very low correlation was found between the estimated and measured values, with an average coefficient of determination of R^2=0.11.

Contour plots of the von-Mises stress and the damage distribution are shown in Figure 6. For comparison, results of the gold standard model and the isotropic model as presented in an earlier publication are reproduced in this figure as well. The results show that the orthotropic model with estimated fabric tensors tends to slightly overestimate the stresses (Hazrati Marangalou et al., 2013). Although there are differences in the stress magnitude between the models, the distributions of the stresses in all models are rather similar. When plotting the amount of damage, the orthotropic models with estimated fabric tensors underestimate the amount of damage at the femoral neck and produce a distribution that is more similar to that of the isotropic model.

Whole-bone force displacement curves show that the orthotropic model with estimated fabric tensors can well replicate the force-displacement curves found for the gold standard and behaves better than the isotropic model that underestimates both the stiffness and strength (Figure 7).

For the orthotropic model with estimated fabric the root mean square error (RMSE) for whole-bone stiffness, taking the gold standard as the reference, was 11.8%, which is less than the error found earlier for the isotropic model (26.3%). A good correlation was found for whole bone stiffness with determination coefficient of 89.2% and concordance correlation (CC) of 87%. For the ultimate load an RMSE of 8.4% was found for orthotropic models with estimated fabric, when compared to the gold standard, which again was less than the error found earlier for the isotropic model (14.5%). Similar to the stiffness, good correlations were found with an R^2=97.2% and CC=92.6% (Figure 8).

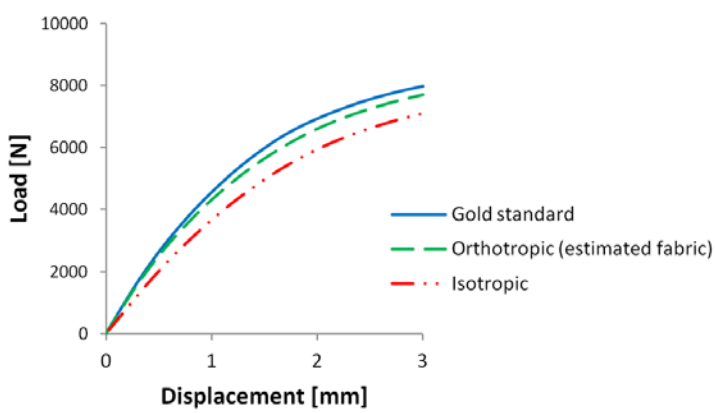

Figure 7. Typical force-displacement curves obtained from different orthotropic and isotropic models (adapted and extended from Hazrati Marangalou et al., 2013).

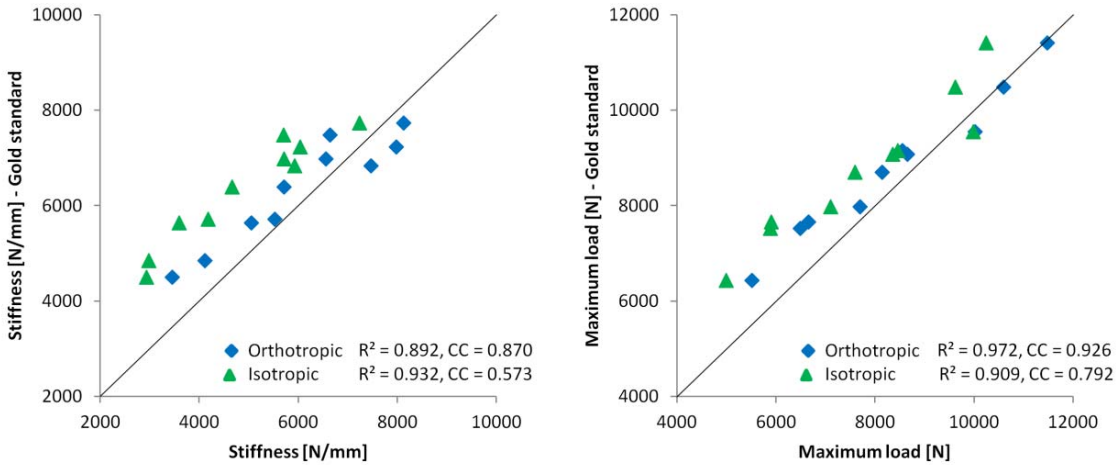

Figure 8. Correlation of results with those obtained for the gold standard for whole bone stiffness (left) and ultimate load (right) (adapted from Hazrati Marangalou et al., 2013) when implementing isotropic material properties or anisotropic properties based on an estimated fabric tensor. Results for the isotropic and gold standard model are reproduced from Hazrati Marangalou et al., 2013.

Results of the ANOVA test revealed that no significant differences exist between the results of the orthotropic models with estimated fabric and the gold standard, neither for whole bone properties nor for the stress/damage distributions.

Discussion

The first goal of this study was to investigate the feasibility and accuracy of an iterative approach to calculate the fabric tensor from the principal stress distribution. We found that, indeed, this approach can lead to reasonable estimates of the fabric tensor orientation. On average, the difference in norm between estimated fabric tensors and the fabric tensors measured from the bone micro-architecture was less than 12%. However, the degree of anisotropy of the estimated and the measured fabric tensors did not compare well and at some locations the orientations of the estimated fabric tensor deviated much from that of the measured ones. In spite of these differences, the stress calculation of the model with its anisotropy based on estimated fabric compared very well to that of a model with its anisotropy based on measured fabric. This suggests that in those regions where the correspondence was not very good, the stresses are either low or the material anisotropy is not very pronounced.

The second goal of this study was to investigate if such microstructural enhanced orthotropic models based on estimated fabric can provide more accurate results than a database approach introduced earlier or than using isotropic models. In that earlier study, we found that, compared to the gold standard, using a database-derived models resulted in a RMS error of 4.9% and 3.1% for the stiffness and ultimate load respectively. In the present study, using the

estimated fabric, these errors were 11.8% and 8.4% respectively, indicating that the approach tested in the present study is less accurate than the database approach. For the standard isotropic model investigated in that earlier study (named isotropic-I), these errors were 26.3% and 14.5% respectively, demonstrating that the orthotropic models based on estimated fabric as tested here can produce more accurate results than the isotropic model. As was indicated in the earlier study, significant differences were found for bone stiffness, the stress and damage distribution, when comparing results obtained from the isotropic model with the gold standard, whereas no significant differences were found for results obtained from the orthotropic model based on estimated fabric as tested here. It should be noted though, that differences between the isotropic model and the gold standard, though significant, are generally small.

It would be possible to scale the elastic constants of the isotropic model to make the whole bone stiffness or strength in better agreement with those of the gold standard model. Such a scaling to reach correct whole bone stiffness was also performed in the earlier database study (Hazrati Marangalou et al., 2013) but did not lead to much improvement in the whole bone maximum load prediction. Scaling also does not much affect the stress distribution.

It is possible that the accuracy of the present approach can be further improved by analyzing more load cases to better represent the state of loading towards which the bones are adapted. In the present study only 2 generic load cases were analyzed. Since no information about the donors' history was available, it is possible that this loading history does not represent that of the donor very well. This could lead to differences between the estimated and measured fabric directions. A possible solution to this could be the use of a load estimation algorithm to define the loading history to which the bones are adapted (Campoli et al., 2012; Christen et al., 2012). This could also make the approach developed here suitable for bones at different sites for which no information about the loading history is available. Nevertheless, it is promising that even when using only a few generic load cases as done in the present study, good results were obtained.

The results demonstrate that only a few iterations are needed to reach a converged state and that further iterations will not further improve the results. The fact that the angular deviation between estimated and measured major fabric direction is very large (~ 90°) in some regions (Figure 3) is probably due to the fact that, in particular for near isotropic stress states, the principal directions can change order. In such cases a small change in magnitude can result in a 90 degrees change in the principal directions.

Some limitations of this study must be mentioned as well. First, only a limited number of bones were tested, and since these were obtained from an elderly population it is not known if similar results would be obtained for younger subjects. Nevertheless, the age group

investigated here is relevant for one of the main applications of the tested approach, being improving pre-clinical testing of bone-implant configurations. Second, to be able to create a gold standard model with measured fabric, we used micro-CT images for the generation of the continuum FE models. For clinical application, however, clinical CT will need to be used. Nevertheless, since bone geometry and density can be measured accurately from clinical CT scans, we expect that similar accurate results can be obtained when using such scans. Third, in this study the cortical bone was always assumed isotropic. Although it would be possible to define orthotropic properties for the cortical bone as well, we expect that this will not affect the results too much since for typical loading configurations the cortical bone is merely loaded in the longitudinal direction (by bending or compression), such that only the stiffness in that direction is relevant.

In conclusion, we have demonstrated that this novel approach can be used to estimate the fabric tensor of the proximal femur with some fair accuracy. This procedure could lead to the generation of FE-models that can account for bone anisotropic material properties. Although the results were slightly less accurate than those of a database approach developed earlier, a major advantage of the present approach is that it does not require such a database, and can be applied to any bone for which reasonable estimates of the loading history are available. We expect that this approach can lead to more accurate results in particular for models used to study implants, which are usually anchored in highly anisotropic cancellous bone regions.

Acknowledgements

Funding from the European Union for the osteoporotic virtual physiological human project (VPHOP FP7-ICT2008-223865) is gratefully acknowledged.

Conflict of interest statement

Bert van Rietbergen is a consultant for Scanco Medical AG.

Chapter 4

A Novel Approach to Estimate Trabecular Bone Anisotropy Using a Database Approach

The concepts of this chapter are based on: Javad Hazrati Marangalou, Keita Ito, Matteo Cataldi, Fulvia Taddei and Bert van Rietbergen. A Novel Approach to Estimate Trabecular Bone Anisotropy Using a Database Approach. Journal of Biomechanics, in press.

A Novel Approach to Estimate Trabecular Bone Anisotropy Using a Database Approach

[a]*Javad Hazrati Marangalou,* [a]*Keita Ito,* [b]*Matteo Cataldi,* [b]*Fulvia Taddei,* [a]*Bert van Rietbergen*

[a]*Orthopaedic Biomechanics, Biomedical Engineering Department, Eindhoven University of Technology, Eindhoven, The Netherlands*

[b]*Laboratorio di Tecnologia Medica, Istituti Ortopedici Rizzoli, Bologna, Italy*

Abstract

Continuum finite element (FE) models of bones have become a standard pre-clinical tool to estimate bone strength. These models are usually based on clinical CT scans and material properties assigned are chosen as isotropic based only on the density distribution. It has been shown, however, that trabecular bone elastic behavior is best described as orthotropic. Unfortunately, the use of orthotropic models in FE analysis derived from CT scans is hampered by the fact that the measurement of a trabecular orientation (fabric) is not possible from clinical CT images due to the low resolution of such images. In this study, we explore the concept of using a database (DB) of high-resolution bone models to derive the fabric information that is missing in clinical images. The goal of this study was to investigate if models with fabric derived from such a small database can already produce more accurate results than isotropic models.

A DB of 33 human proximal femurs was generated from micro-CT scans with a nominal isotropic resolution of 82 µm. Continuum FE models were generated from the images using a pre-defined mesh template in combination with an iso-anatomic mesh morphing tool. Each element within the mesh template is at a specific anatomical location. For each element within the cancellous bone, a spherical region around the element centroid with a radius of 2 mm was defined. Bone volume fraction and the mean-intercept-length fabric tensor were analyzed for that region. Ten femurs were used as test cases. For each test femur, four different models were generated: (1) an orthotropic model based on micro-CT fabric measurements (gold standard), (2) an orthotropic model based on the fabric derived from the best-matched database model, (3) an isotropic-I model in which the fabric tensor was set to the identity tensor, and (4) a second isotropic-II model with fitted total bone stiffness on the gold standard. An elastic-plastic damage model was used to simulate failure and post failure behavior during a fall to the side.

The results show that all models produce a similar stress distribution. However, compared to the gold standard, both isotropic-I and II models underestimated the stress/damage

distributions significantly. We found no significant difference between DB-derived and gold standard models. Compared to the gold standard, the isotropic-I models further underestimated whole bone stiffness by 26.3% and ultimate load by 14.5%, while these differences for the DB-derived orthotropic models were only 4.9% and 3.1% respectively.

The results indicate that the concept of using a DB to estimate patient-specific anisotropic material properties can considerably improve the results. We expect that this approach can lead to more accurate results in particular for cases where bone anisotropy plays an important role, such as in osteoporotic patients and around implants.

Introduction

Patient specific continuum finite element (FE) models have become a standard pre-clinical tool to study mechanical behavior of bone alone or with implants. Such models usually implement material properties with elastic and strength properties that are based on the local bone density as quantified by Hounsfield units in clinical CT images (Keyak, 2001; Liebschner et al., 2003; Taddei et al., 2007; Yosibash et al., 2007). Empirical power-law relationships are then used to derive the elastic and strength properties (Carter and Hayes, 1977; Helgason et al., 2008; Keller, 1994; Lotz et al., 1991; Wirtz et al., 2000; Zannoni et al., 1999). In virtually all studies done so far, material properties assigned to the bone elements are chosen as isotropic based on bone density distribution only. Experimental and computational studies, however, have shown that bone can be highly anisotropic, particularly in cancellous bone regions, and that its elastic behavior is best described as orthotropic. In most cases, the experimentally derived power-law relationships are determined only after aligning the measurement direction with the anatomical direction. As such these power-laws may well represent the stiffness and strength in the principal load carrying direction, but will likely overestimate these values in other directions. It was demonstrated that models that account for this anisotropic behavior better predict whole bone stiffness and stress distributions than isotropic models (Hazrati Marangalou et al., 2012; Kabel et al., 1999b; Pahr and Zysset, 2009; Turner et al., 1990). The anisotropy of cancellous bone is largely determined by its microstructural organization. Theoretical and experimental studies demonstrated that the orthotropic principal directions and the anisotropic stiffness tensor can be well predicted from a second rank fabric tensor that describes the average orientation of this trabecular microarchitecture (Cowin, 1985; Cowin and Mehrabadi, 1989; Gross et al., 2013; Harrigan and Mann, 1984; Kabel et al., 1999b; Odgaard et al., 1997; Zysset, 2003; Zysset et al., 1998). Measurement of such fabric tensors, however, requires images with a resolution that is good enough to resolve the trabecular architecture. For bone in-vivo, this presently is possible only for the peripheral skeleton (Boutroy et al., 2005; Burghardt et al., 2011; Burrows et al., 2010; Liu et al., 2010; MacNeil and Boyd, 2008). Although recent studies have introduced approaches to calculate such micro-structural properties from clinical

CT (Saha and Wehrli, 2004; Tabor et al., 2013; Tabor and Rokita, 2007) and high-resolution flat-panel CT systems (Bredella et al., 2008; Mulder et al., 2012), the accuracy of such measurements still has to be established.

In this study, we explore a different approach to derive patient-specific fabric information: by using a database of high-resolution bone models. By combining the density information measured from a patient CT scan with fabric information from the database, patient-specific anisotropic properties can be defined. Presently, only a rather limited number (n=33) of bones are available for this database. The goal of this study therefore was to investigate if models with fabric derived from such a limited database can already produce more accurate results than isotropic models. To investigate this, we compared the stress and damage distribution as well as the whole bone stiffness and strength for FE models with fabric derived from the actual bone with those of model with fabric mapped from the database or isotropic mechanical properties.

Material and methods

Material

A database (DB) of thirty-three human cadaver femurs (mean age: 77.8±10.0 year) obtained from 17 female and 16 male donors was generated for all these bones. Micro-CT scans (XtremeCT, Scanco Medical AG, Brüttisellen, Switzerland) of the most proximal part (9 to 12 cm in length) were made with a nominal isotropic resolution of 82 µm. Images were filtered and processed according to the protocol recommended by the manufacturer. Compartments of cortical and cancellous bone were identified using masks. A first mask comprising the whole bone was made based on the periosteal contour. In order to find the cortical shell, original images were filtered using a strong Gauss filter (sigma=5, support=5 voxels) and segmented using a threshold of 15% of the maximum gray-value, leaving only the cortical bone. This image was used to identify the cortical shell in the original mask. In addition, the most periosteal 1 mm region of the original mask was identified as part of the (sub)cortical compartment. The remainder of the mask was considered the cancellous compartment.

Creation of FE models

Continuum finite element models of the thirty-three proximal femurs were generated based on contours of the bone periosteal surface as obtained using software provided with the micro-CT scanner (IPL V5.16, Scanco Medical AG, Brüttisellen, Switzerland). Isotopological models were generated for each bone segment using a pre-defined mesh template based on a generalized femur geometry that contained approximately 300 thousand second order tetrahedron elements with a typical edge length of 2mm. This mesh template was morphed onto the bone surface extracted from the micro-CT scan by identifying a minimum of 8

anatomical landmarks. After morphing, each element number identifies an element that, with good approximation, is at the same specific anatomical location in all samples (Grassi et al., 2011). Since the mesh template comprises the whole femur while the micro-CT scans only covered the most proximal part of these, the number of elements on the proximal femur models was less and varied from approximately 80,000 to 90,000 depending on the scan length.

To each element a volume fraction and morphological properties were assigned using a homogenization technique described earlier (Hazrati Marangalou et al., 2012). In summary: first, we determined whether the element was in the cortical or cancellous compartment. If an element was at the cortical/cancellous interface, we calculated what fraction of its volume was in each of both compartments. For each element that was at least partly within the cancellous bone, a spherical volume of interest around the element centroid with a diameter of 4 mm was defined (Harrigan et al., 1988). Trabecular bone architectural parameters, including bone volume fraction (BV/TV) and the mean intercept length (MIL)-based fabric tensor, were analyzed for the volume of interest as far as it was within the cancellous compartment using the image processing software provided by the micro-CT system. Measured morphological parameters were then assigned to the elements. For elements in the cortical compartment, only a volume fraction for the volume comprised by the element itself was defined whereas a rule of mixture was used for elements that cover both compartments based on the portion of the element volume within the cortical/cancellous compartments. Figure 1 depicts mesh generation and bone morphology analysis procedures.

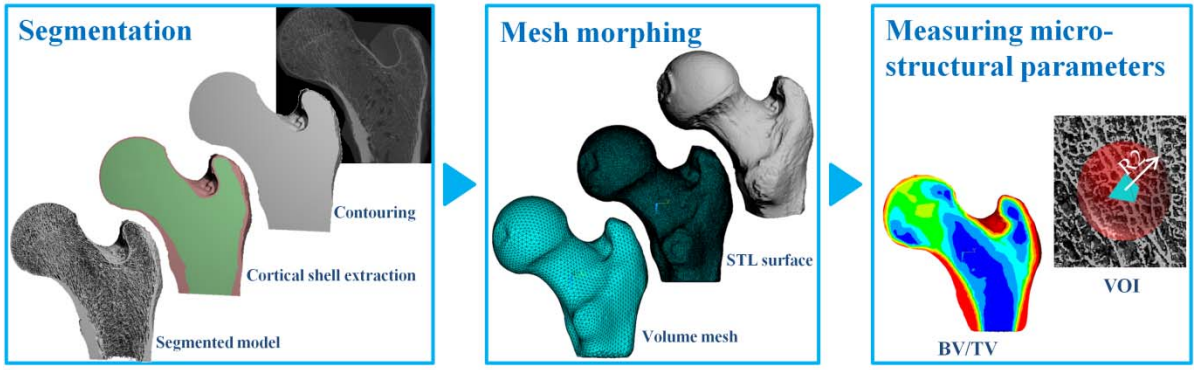

Figure 1. FE models creation procedure for proximal femur models.

Ten femurs were randomly taken from the database as test cases. For each test case, three different FE models were generated. In the first model, orthotropic material properties were specified based on the actual fabric and density measurements of that bone. In the second FE model, orthotropic material properties were specified based on the actual density measurement and fabric derived from a corresponding DB model. To do so, the DB model with a density distribution most similar to that of the test bone was selected and its fabric was

mapped to the test model. The test model itself was excluded from the database during the selection process. In the third FE model, isotropic material properties were specified based on the actual density measurements only (Figure 2).

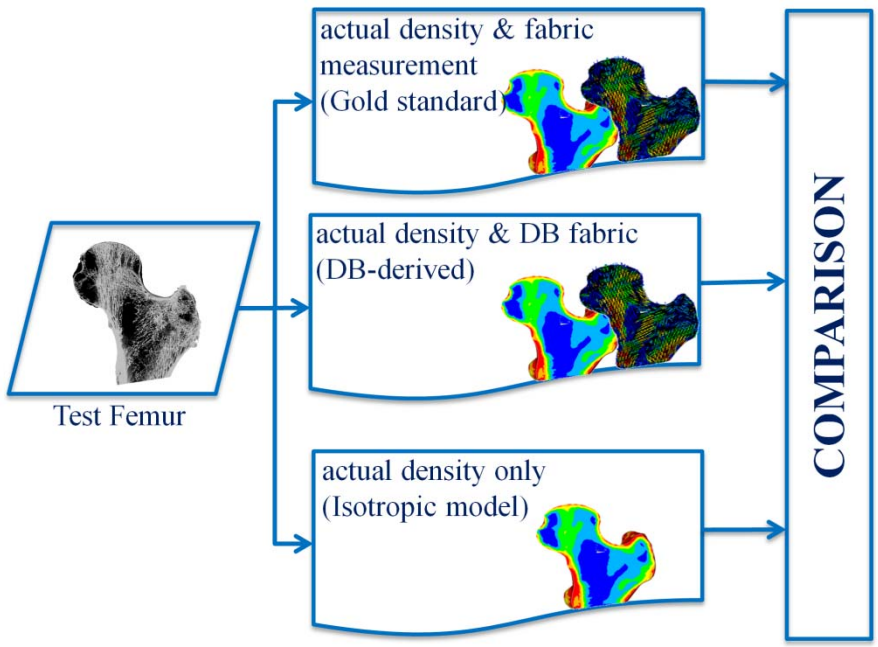

Figure 2. Study design.

To select a DB model j with a density distribution most similar to that of the test bone i, we selected the DB model that minimized the root-mean-square error:

$$Err_i = \min_{j=1}^{32} \left(\sqrt{\frac{\sum_{k=1}^{Nelements} (\rho_{i,k} - \rho_{j,k})^2}{Nelements}} \right) \quad (1)$$

with $N_{elements}$ the number of elements and $\rho_{i,k}$ the density of element k of model i.

Whereas the use of the template enables an easy mapping and comparison of scalar properties between models, the mapping of tensor properties, such as fabric tensor is not straightforward. For these properties the principal directions must be also updated to account for differences in element orientation (Figure 3a). The procedure proposed here to account for this is to define a local orthonormal coordinate system $\{\vec{e_1}, \vec{e_2}, \vec{e_3}\}$ for each element in the model. This coordinate system is based on the vectors $\vec{v_1}$ and $\vec{v_2}$ that are defined by the nodes of the tetrahedron element (Figure 3b) using:

$$\vec{e}_1 = \frac{\vec{v}_1}{|\vec{v}_1|}$$
$$\vec{e}_2 = \frac{(\vec{v}_1 \times \vec{v}_2) \times \vec{v}_1}{|(\vec{v}_1 \times \vec{v}_2) \times \vec{v}_1|} \qquad (2)$$
$$\vec{e}_3 = \frac{\vec{v}_1 \times \vec{v}_2}{|\vec{v}_1 \times \vec{v}_2|}$$

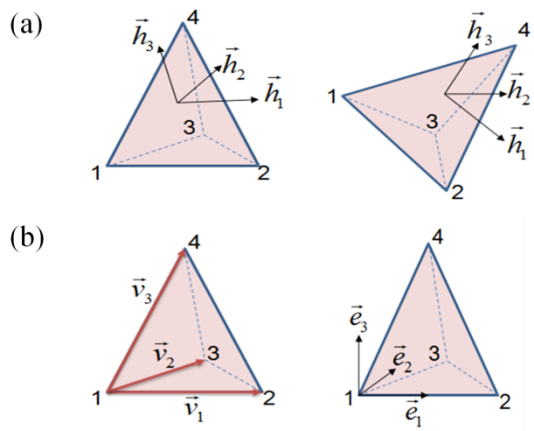

Figure 3. (a) When the orientation of corresponding elements is not the same, the fabric principal directions must be rotated accordingly, (b) Definition of the element local coordinate system based on vectors defined by its nodal points.

For all elements a compliance tensor $\mathbb{C}$ was derived from the element density ρ and fabric tensor **M** using the Zysset-Curnier relationship (Zysset and Curnier, 1995):

$$\mathbb{C} = \sum_{i=1}^{3} \frac{1}{\varepsilon_0 \rho^k m_i^{2l}} \mathrm{M}_i \otimes \mathrm{M}_i - \sum_{i,j=1;i\neq j}^{3} \frac{\nu_0}{\varepsilon_0 \rho^k m_i^l m_j^l} \mathrm{M}_i \otimes \mathrm{M}_j + \sum_{i,j=1;i\neq j}^{3} \frac{1}{2G_0 \rho^k m_i^l m_j^l} \mathrm{M}_i \underline{\overline{\otimes}} \mathrm{M}_j \qquad (3)$$

with ε_0, ν_0 and G_0 elastic constants, m_i the normalized eigenvalues and M_i the dyadic product of the eigenvectors of fabric tensor **M**, det(**M**)=1.

For the isotropic models, the fabric tensor was replaced by a scaled identity tensor. Different choices, however, can be made for the scaling. In a first model (isotropic-I), the identity tensor was taken as the fabric tensor. As a consequence of this scaling the isotropic models will have a lower stiffness than the orthotropic model in the dominant principal direction (Figure 4). For that reason, a second isotropic model was generated by scaling the fabric tensor (**M**=α.**I**, α > 1). The value of α was determined from a set of initial linear elastic analyses, in such a way that the stiffness of the scaled isotropic model is the same as that of the gold-standard model.

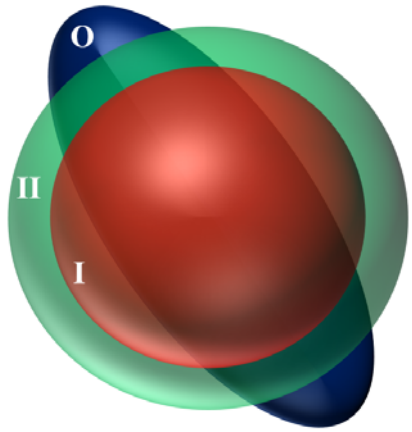

Figure 4. Fabric tensor representation for orthotropic (O) and isotropic (I and II) models; models O and I were normalized such that det(M)=1, model II was scaled such that the total bone stiffness of models II and O is the same.

Elastic plastic damage constitutive behavior in the local form (Charlebois et al., 2010) was used to simulate failure and post-failure behavior of test femurs. This material model contains a damage variable D (ranging from D=0: no damage to D=1: fully damaged) to account for the reduction of stiffness due to propagation of voids and cracks, and due to breakage of individual trabeculae. Loading conditions applied to the models represented a fall to the side configuration (Courtney et al., 1995; Verhulp et al., 2008). The nodes on the surface of the greater trochanter, in a 3 mm layer were fixed in medio-lateral direction and the nodes at the distal end were fixed except for medio-lateral movements. The nodes at the femoral head medial side were fixed in all direction while a displacement in the lateral direction was applied to mimic fall to the side condition. A total compressive displacement of 3 mm was applied in 100 load increments, and for each step the total reaction force was calculated. The force displacement curve maximum was taken as the femur ultimate load.

Table 1. Constants used in the material model (constants were taken from (Charlebois et al., 2010)).

E_0	ν_0	k	l	σ^{0+}	σ^{0-}	χ^{0+}	χ^{0-}	p	q	σ^{H}	s	D_c	a
8237.1	0.18	2.5	1.88	57.4	132.4	-0.748	0.340	2.5	0.86	6.0	37.5	0.6	22.5

At the first load increment, the whole-bone stiffness was calculated from the reaction force and the applied displacement. At the last loading increment (3mm displacement) the ultimate load was calculated from the reaction force. In addition, contour plots of the Von Mises stress and the damage variable D were created.

Whole bone stiffness, ultimate load and the von Mises stress, damage and strain energy density distributions of the orthotropic models based on DB-derived fabric and the two

isotropic models were compared to those of the orthotropic models based on actual fabric measurements, which were taken as the gold standard. Differences were quantified by calculating determination coefficients and relative root-mean-square errors (RRMSE):

$$RRMSE = \sqrt{\frac{\sum_{i=1}^{n}\left(\frac{x_i' - x_i}{x_i'}\right)^2}{n}} \tag{4}$$

x_i' are the values obtained from the gold standard models and x_i are the values obtained from the isotropic or DB-derived models (n=10).

One-way ANOVA was used to test the significance of differences ($p<0.05$) between isotropic, DB-derived models and the gold standard in predictions of whole bone properties as well as damage/stress distributions.

Results

The major fabric value and its direction for a representative femur as obtained from direct measurement (left) and from the database mapping procedure (right) for a typical case are shown in Figure 5. Overall, the fabric directions and values of the mapped model corresponded well with the measured one. Differences are most notable in the most distal end (due to an effect of the boundary) and in the region of Ward's triangle, which is due to the low volume fraction in that region that makes the fabric measurement unreliable.

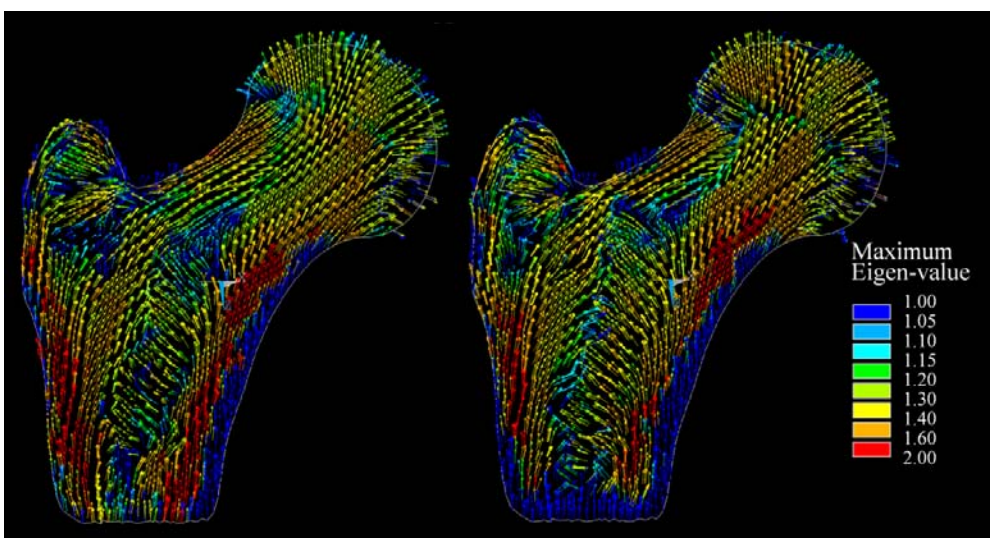

Figure 5. Major fabric direction as obtained from the direct measurement (left) and from the database mapping procedure (right).

Contour plots of the von-Mises stress (Figure 6a) show that the isotropic model-I slightly underestimates the stresses, which is due to the fact that its stiffness in the anatomical

directions is less. In contrast, the isotropic-II model overestimates the stresses. The DB-derived orthotropic model tends to slightly overestimate the stresses as well. In all cases, however, a good qualitative agreement with the gold-standard was obtained.

More pronounced differences were found when looking at the predicted damage distribution (Figure 6b). The isotropic models underestimates the amount of damage in the neck regions, in particular for the isotropic-I model, whereas the DB-derived model well represents the distribution found for the gold-standard (Figure 6b). Similar to the Damage and von Mises stress, DB-derived models slightly overestimated strain energy density (SED) values with respect to the gold standard in the femoral neck while the isotropic-I and isotropic-II models slightly underestimated SED values in particular near the femoral head (Figure 6c).

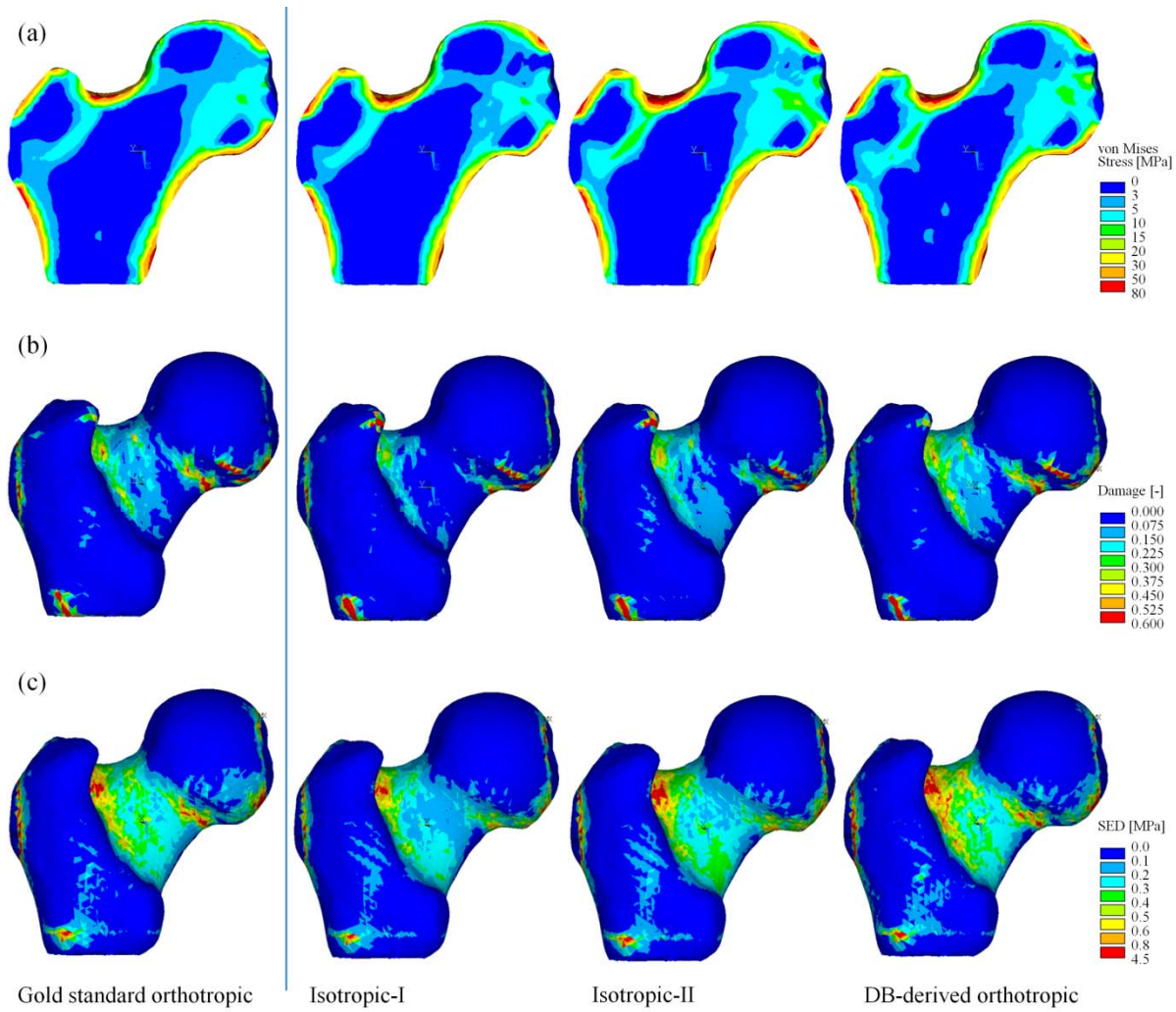

Figure 6. (a) von-Mises stress, (b) damage parameter and (c) strain energy density (SED) distribution in the gold standard, isotropic-I, isotropic-II and DB-derived orthotropic models respectively from left to the right.

Whole-bone force displacement curves shows that the DB-derived orthotropic model can accurately replicate the force-displacement curves found for the gold standard while the isotropic-I model underestimates both the stiffness and ultimate load (Figure 7). The isotropic-II model with adjusted stiffness, on the other hand, clearly overestimates ultimate load (Figure 7).

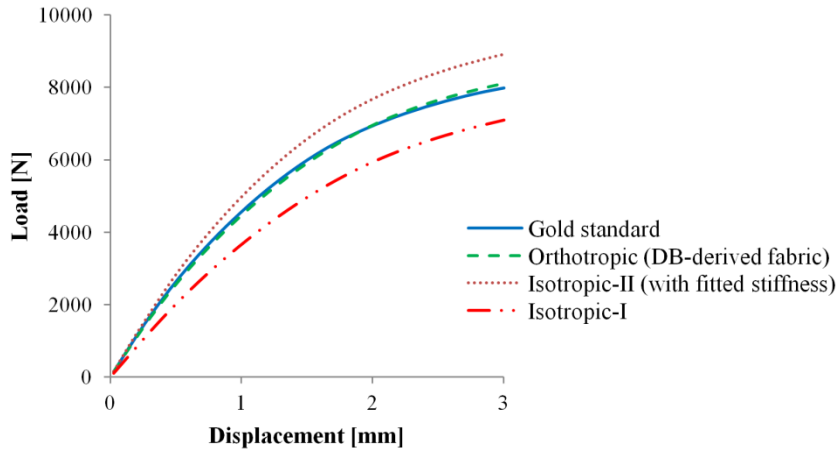

Figure 7. Typical force-displacement curves obtained from different orthotropic and isotropic models for a femur model under fall to the side condition.

Compared to the gold standard, the relative root mean square error (RRMSE) for whole-bone stiffness was 4.9% for the DB-derived model and 26.3% for the isotropic-I model. For all ten femurs analyzed, the isotropic-I model underestimated whole bone stiffness. Nevertheless, the correlation between predicted and gold-standard values was very good, with a coefficient of determination R^2=93.2% for the Isotropic-I model (Figure 8). In this case also, a very good correlation was found for the DB-derived model with an R^2=90.9%. We found a high one-to-one correlation for the DB-derived orthotropic model with the gold standard (CC=94.5%) while a low concordance correlation was found (CC=57.3%) for the isotropic-I models.

The isotropic-I models also underestimate the ultimate load with an RRMSE of 14.5% while the isotropic-II model overestimated the ultimate load with an RRMSE of 7.92%. For the DB-derived orthotropic model this error was 3.1%. In this case also, predicted and gold-standard values for the ultimate load correlated well for all cases, with a coefficient of determination R^2=90.9% for the isotropic-I model, R^2=85.6% for the isotropic-II model and R^2=96.3% for the DB-derived model (Figure 8). Compared to the gold standard, there is a low concordance correlation between isotropic-I and the gold standard (CC=79.2%) and for the isotropic-II model (CC=88.9%) while this value for the DB-derived models is CC=97.6%.

One-way ANOVA revealed that there is a significant difference between isotropic-I models and the gold standard for whole bone stiffness (p=0.039) however no significant differences were found for failure load, neither for the isotropic-I model (p=0.324) nor for the isotropic-II

model (p=0.683). Significant differences were found for the stress and damage distributions for both isotropic models and the gold standard. For the DB-derived models, neither the whole bone properties (stiffness/failure load) nor stress/damage distributions were significantly different from the gold standard.

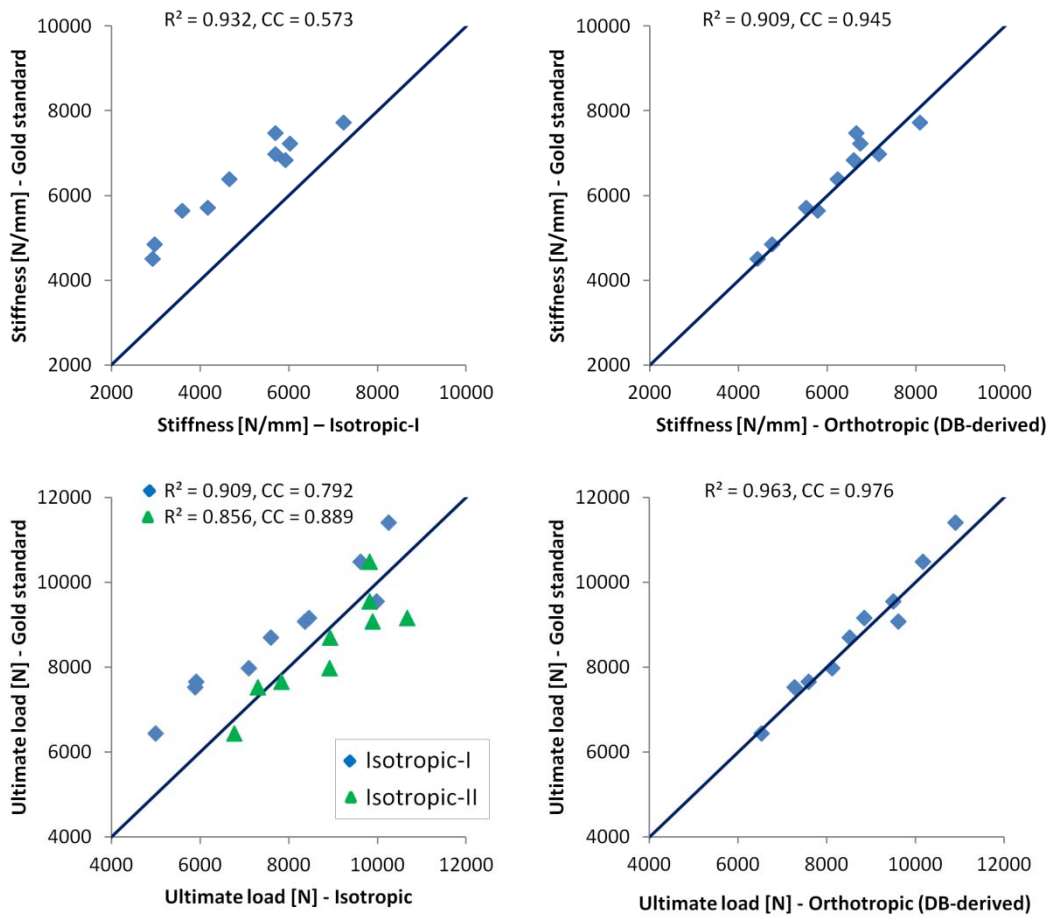

Figure 8. Correlation of isotropic and DB-derived orthotropic models with the gold standard in whole bone stiffness (upper row) and ultimate load (bottom row) predictions; (solid line: 45° line, CC: concordance correlation).

Discussion

The goal of this study was to investigate if models with fabric derived from a limited database can produce more accurate results than isotropic models. We found that indeed this is the case. Whole bone properties (stiffness and failure load) and stress and damage distributions were better predicted by the DB-derived orthotropic model than by the isotropic model. In fact, no significant differences were found in all these properties, whereas significant differences were found for the isotropic models tested here for whole bone stiffness, stress distribution and damage distribution.

As different approaches exist to make an isotropic model from an existing anisotropic one, we tested two different approaches. With the first one, the fabric tensor was made isotropic and normalized such that its determinant remained the same as in the orthotropic case, with the other approach the fabric tensor was scaled such that the whole bone stiffness would be the same as that of the orthotropic model. Other choices would have been possible as well. For example, in many studies isotropic models are used with material properties based on laws that relate the stiffness in the anatomical direction to the bone density (such as the Carter-Hayes (Carter and Hayes, 1977) and Ashman et. al. (Ashman et al., 1989) relationships). In such studies, the highest modulus is assigned in all directions. In our study, this would correspond to scaling the fabric tensor such that it value equals the largest value of the orthotropic model. Clearly, this would result in an overprediction of bone stiffness and ultimate load. Since the isotropic-II models used in our study here already led to an overprediction of stresses and strength, we did not further consider this option.

In our study we used fall-to-the-side boundary conditions because we expected that effects of anisotropy for this non-habitual loading case would be more pronounced than for physiological loading conditions. During physiological loading conditions, the bone will be loaded in its principal fabric direction. In that situation, the use of experimentally-derived relationships that relate the stiffness in the anatomical direction to the bone density might produce more accurate results than in ours study. Nevertheless, this load case is commonly used for analyses of bone strength. Also: implants will also lead to non-habitual loading conditions of bone, at least locally. We thus think the results here are relevant for many situations.

In this study, we did not explicitly investigate the sensitivity of the database approach for errors in the mesh morphing and mapping procedure, however this error was addressed implicitly. Since the mesh morphing tool was used 33 times to generate the femur database in this study, large deviations from the intended anatomical position would lead to larger RRMS errors in density distribution. However the results show that for the ten test cases used in this study, good correlations were found. On average the correlation between the density of a test bone and its selected DB entry was R=91% (89-92%) while on average the RMSE was 0.11 (0.10-0.12), demonstrating that in all cases a bone was found in the DB that has a very similar density distribution. In clinical practice, however, the patient image would be obtained from a clinical CT scanner rather than from the same micro-CT scanner as in our study. It is possible that this will lead to a less favorable fit. Nevertheless, since reliable density information can be obtained from clinical CT scanners as well, we expect that in that case also the same database model would be selected.

Some limitations of this study must be mentioned as well. First the database generated in this study contained only thirty-three femurs. Although this was large enough to improve results

in this study, it might not cover enough cases needed when used for larger populations. Increasing the number of database entries, however, is trivial and would increase the accuracy in database selection procedure and would result in more accurate prediction of bone orthotropic material properties.

Second, we use only one parameter (BV/TV) in our selection model to choose the models which best matches the patient model. In particular, we did not consider the size or shape of the bone. Adding more parameters such as shape parameters (e.g. femoral neck angle or other anthropometric parameters or results from modal analyses (Cheng et al., 1997a; Taylor et al., 2002) or other parameters such as age in addition to the density distribution might result in more accurate results. In this study, however adding more selection criteria is not feasible due to limited number of database entries.

Third, mesh quality is a crucial factor in the fabric mapping procedure. Since a local element-based coordinate system is used to map the fabric tensor from best matched database model to patient model, severe deformities of elements (e.g. tetrahedrons with high aspect ratios) would introduce inaccuracies in the procedure. We found that in some regions the fabric orientation can be inaccurate due to element distortion. However, apparently such errors do not much affect the whole bone and stress distribution results.

Fourth, the mesh template geometry did not distinguish explicitly between the cancellous and cortical compartments, such that elements can be in both compartments. To make sure a clear cortical regions exists, we assumed a minimum thickness of 1 mm for the cortical region, although previous studies have shown that the cortical shell thickness can be less than 1 mm at some locations (Treece et al., 2010; Yan et al., 2003). We do not expect this assumption would affect our results much though, since, with our approach a cortical thickness of less than 1 mm would also results in a lower density of the cortical element and thus would be accounted for. Furthermore, we only quantified morphological parameters in the cancellous bone region, not for the cortical region. The determination of cortical morphological parameters, such as cortical thickness and cortical porosity from micro-CT scans is possible as well. However, cortical thickness cannot be assigned per element since at most locations the thickness is larger than the element size, whereas cortical porosity is similar to the density that is calculated for the cortical elements. A more accurate representation of the cortical and cancellous compartments would require that separate templates for cortical and cancellous bone are needed. Since this would considerably complicate the meshing and mapping procedure, we decided to cover both compartments with one mesh template.

Finally, we used a local formulation of the constitutive law of Charlebois et al. whereas non-local formulations are available as well. However, since a typical length scale for cancellous

bone would be round 1 mm, and since our elements also are about the same in size, we expect that a local and non-local formulation would provide very similar results.

In conclusion, the approach presented here can be used to create patient-specific anisotropic finite element models of bones even in cases where the bone fabric cannot be measured in-vivo. The mesh-morphing approach used here can be used as a versatile tool to map the missing fabric information, as well as any other micro-structural information to the patient models. We expect that this approach can lead to more accurate results in particular in cases where bone anisotropy plays an important role, such as in osteoporotic patients and around implants.

Acknowledgements

Funding from the European Union for the osteoporotic virtual physiological human project (VPHOP FP7-ICT2008-223865) is gratefully acknowledged.

Conflict of interest statement

Bert van Rietbergen is a consultant for Scanco Medical AG.

Chapter 5

Inter-individual Variability of Bone Density and Morphology Distribution in the Proximal Femur and T12 Vertebra

The concepts of this chapter are based on: Javad Hazrati Marangalou, Keita Ito, Fulvia Taddei and Bert van Rietbergen. Inter-individual variability of bone density and morphology distribution in the proximal femur and T12 vertebra. submitted.

Inter-individual Variability of Bone Density and Morphology Distribution in the Proximal Femur and T12 Vertebra

[a]*Javad Hazrati Marangalou,* [a]*Keita Ito,* [b]*Fulvia Taddei,* [a]*Bert van Rietbergen*

[a]*Orthopaedic Biomechanics, Biomedical Engineering Department, Eindhoven University of Technology, Eindhoven, The Netherlands*

[b]*Laboratorio di Tecnologia Medica, Istituti Ortopedici Rizzoli, Bologna, Italy*

Abstract

Bone geometry, density and microstructure can vary widely between subjects. Knowledge about this variation in a population is of interest in particular for the design of orthopaedic implants and interventions. The goal of this study is to investigate the local variability of bone density and microstructural parameters between subjects using a novel inter-subject image registration approach. Human proximal femora of 29 and T12 vertebrae of 20 individuals were scanned on a micro-CT system. A pre-defined iso-anatomic mesh template was morphed to each micro-CT scan. For each element bone volume fraction and other morphological parameters (Tb.Th, Tb.N, Tb.Sp, SMI, DA) were determined and assigned to the element. A coefficient of variation (CV) was calculated for each parameter at each element location of the 29 femora and 20 T12 vertebrae. Contour plots of the CV distribution revealed very detailed information about the inter-individual variation in bone density and morphology. It is also shown that analyzing large sub-volumes, as commonly done in previous studies, would miss much of this variation. Detailed quantitative information of bone morphological parameters for each sample in the femur and the T12 database and their inter-individual variability are available from the mesh templates as supplementary data (http://w3.bmt.tue.nl/nl/fe_database/). We expect that these results can help to optimize implants and orthopaedic procedures by taking local bone morphological parameter variations into account.

Introduction

Bone geometry, density and microstructure can vary widely between subjects. Such differences can be related to genetic factors, lifestyle factors, and affections of the skeleton (e.g. osteoporosis). Knowledge about this variation in a population is of interest in particular for the design of orthopaedic implants and interventions. In a pre-clinical stage, such implants and interventions now are usually designed and tested using finite element (FE) computer models (Huiskes et al., 1992; Polikeit et al., 2003; Prendergast, 1997; Rohlmann et al., 1983; Villarraga et al., 2005; Weinans et al., 2000). In such models, bone geometry and density distribution are usually derived from a CT-scan of a representative bone (Dopico-González et al., 2010; Little et al., 2007; Radcliffe and Taylor, 2007; Reggiani et al., 2007). Empirical laws are then used to calculate the bone mechanical properties from bone density and/or other microstructural parameters such as bone fabric. For a thorough pre-clinical evaluation of implants and interventions, however, the models used should be able to represent the range in bone shape, density and microstructure that can be expected in a patient population (Dopico-González et al., 2010; Weinans et al., 2000). Presently, however, no such detailed 3D information is available.

Variations in bone shape have been described by whole-bone morphological parameters, such as bone cross-sectional area, moment of inertia, femoral neck angle etc. and, more recently, by using model-indexing methods for bones at several sites (Chintalapani et al., 2007; Querol et al., 2006; Rajamani et al., 2004; Zachow et al., 2005). With this latter technique, the bone geometry is represented by a number of parameters that each represents a specific feature. It has been demonstrated that even a limited set of parameters can accurately describe the complex external geometry of a bone (Grassi et al., 2011; Zachow et al., 2005). This information can then be used to create computer models to represent a range of bone geometries. In many cases, however, variation in bone size and shape can be (at least partly) compensated by designing different implant sizes and shapes. As such, variation in geometry and size that can be expected in a population is already accounted for.

Little information, however, is available for the spatial variation in bone density that can be expected in a population. Whereas excellent data is available about areal bone density as measured for projected areas using DXA scanning, this information does not provide much insight in the actual 3D distribution of the bone density. Even less information is available about the spatial distribution of bone microstructural parameters. In earlier studies, variation in such parameters was quantified by measuring these from samples taken from the same anatomical location. To quantify these parameters, different methods were used, such as histological methods (Banse et al., 2002; Chappard et al., 1999; Ciarelli et al., 2000; Hordon et al., 2000; Müller et al., 1998), MRI (Link et al., 2003; Wehrli et al., 1998), CT (Carballido-Gamio et al., 2013; Lang et al., 1998; Stiehl et al., 2007) and micro-CT (Banse et al., 2001;

Ciarelli et al., 2000; Hulme et al., 2007; Lai et al., 2005; Mueller et al., 2009; Nazarian et al., 2007; Sode et al., 2010; Sran et al., 2007; Turunen et al., 2013) measurements. Such measurements, however, are averaged values for the specimen and their value depends on the method used, the homogeneity of the bone they were taken from, the size of the specimen, and their exact location. Because of all these issues, data of different studies is hard to compare. Moreover, since only limited locations were sampled, no data is available about the variation in spatial distribution of the parameters other than in terms of general anatomical locations.

Recently, inter-subject image registration tools were developed that can be used to integrate 3D CT images into a statistical atlas of bone density distribution (Carballido-Gamio et al., 2013; Grassi et al., 2011). In a recent study, using such techniques in combination with CT scans of the femur of a large cohort of women, it was demonstrated that this approach can provide a detailed overview of the femoral bone density distribution and differences therein due to aging (Carballido-Gamio et al., 2013). In that study, however, the variability in the density distributions between subjects was not quantified. Moreover, results were limited to the density distribution and to the femur.

In the present study, we aim at using a similar technique to quantify the inter-individual variation in bone density and bone microstructural parameters within a population. Since bone microstructural parameters cannot be measured from clinical CT scans, the registration technique used here takes micro-CT images as the basis for bone density and structural analysis (Hazrati Marangalou et al., 2013). Using a mesh-morphing approach, the bone is first subdivided in a large number of small sub-volumes that are positioned at well-defined anatomical locations within the bone as defined by a mesh-template (Grassi et al., 2011). Micro-CT based morphological analysis is then used to quantify bone density and microstructure for each location defined by the template. By using the same mesh template for different bones, a straightforward inter-individual comparison of parameter distributions becomes possible.

Specific goal of this study was to apply this approach to a set of cadaver femora and vertebrae from an elderly population to provide very detailed quantitative information about the variability in bone density and microstructure between subjects. In order to compare this data with the literature, results were also quantified for larger sub-regions defined by anatomical planes or anatomical regions.

Materials and methods

Samples

A total of 29 human cadaver femora were collected. The mean age of the donors was 76.7±10.0 years (range 61-95 years), 13 donors were female and 16 donors were male. In

addition, 20 T12 vertebrae were collected from other donors. The mean age of these donors was 78.0±8.1 years (range 64-92 years); 10 donors were female and 10 donors were male. The dataset used for the femora was the same as used in chapter 4 but four femora were excluded here because the available proximal length was smaller than that of the others. In all cases, it was made sure that the donors had no known bone or metastatic disorders.

Micro-CT Scanning

The proximal portion of the femora were scanned in a HR-pQCT system (XtremeCT, Scanco Medical AG, Brüttisellen, Switzerland) as described earlier in chapter 4 (Hazrati Marangalou et al., 2013). In summary: the most proximal 90 mm of the bones was scanned using an isotropic voxel size of 82 µm. Images were processed using the standard settings recommended by the manufacturer. This included the application of a Laplace-Hamming filter (Laplace-epsilon=0.5, Hamming-cutoff frequency=0.4) and segmentation using the default threshold setting.

The T12 vertebrae were also scanned in a micro-computed tomography system (micro-CT 80, Scanco Medical AG, Brüttisellen, Switzerland) using an isotropic voxel size of 37 µm. Image processing included the application of a modest Gauss filter (sigma=0.6, support=1 voxels) and segmentation using a global threshold of 11% of the maximum gray-value.

Compartments of cortical and cancellous bone were identified using masks. A first mask comprising the whole vertebra/femur was made based on the periosteal contour. In order to separate the cortical shell, original images were filtered using a strong Gauss filter (sigma=5, support=5 voxels) and segmented using a threshold of 15% of the maximum gray-value, leaving only the cortical bone. This image was used to identify the cortical shell in the original mask. In addition, the most periosteal 1 mm region of the original mask was also identified as part of the (sub)cortical compartment. The remainder of the mask was considered the cancellous compartment (Hazrati Marangalou et al., 2012).

Bone morphology analysis

Two pre-defined mesh templates, one for the femur and one for the T12 vertebra, were developed earlier (Grassi et al., 2011). Both mesh templates were based on the average shape extracted from a CT database of a large number of bones. The mesh template contained 85,184 tetrahedral elements with a typical size of 2 mm for the proximal femora and 51,119 elements with a typical size of 1 mm for the T12 vertebrae excluding posterior processes.

In the present study, these templates were morphed to each micro-CT scan by identifying a number of anatomical landmarks on the bone surface. For the femur a minimum of 8 landmarks were used, for the vertebrae a minimum of 22 landmarks. After morphing, each

element within the mesh template is at a specific anatomical location which makes it possible to refer to a specific anatomical location by the element number.

The homogenization procedure was described earlier as well in chapters 2 & 4 and is summarized here. Using an in-house algorithm, percentages of cortical and cancellous bone were determined for each element in the mesh. For each element that was at least partly within the cancellous bone, a spherical region around the element centroid with a radius of 2 mm was defined. Bone microstructural parameters were analyzed using the image processing software (IPL V5.16, Scanco Medical AG, Brüttisellen, Switzerland) for the part of that spherical region within the cancellous compartment. Parameters investigated were: bone volume fraction (BV/TV), trabecular thickness (Tb.Th) trabecular number (Tb.N), trabecular spacing (Tb.Sp), structural model index (SMI) and degree of anisotropy (DA). Tb.Th, Tb.Sp and Tb.N were determined based on direct measurements using the distance transformation method rather than plate model assumptions. Measured morphological parameters (Tb.Th, Tb.N, Tb.Sp, SMI, DA) were then assigned to the elements. For elements that were in the cortical compartment a cortical volume fraction was defined as the volume of the bone voxels within the element boundaries over the total volume of the element. For elements that comprised both compartments, a mixture rule was used for the volume fraction whereas the morphology parameters of the cancellous compartment were used to identify the cancellous morphology. Figure 1 depicts the bone morphology analysis procedure.

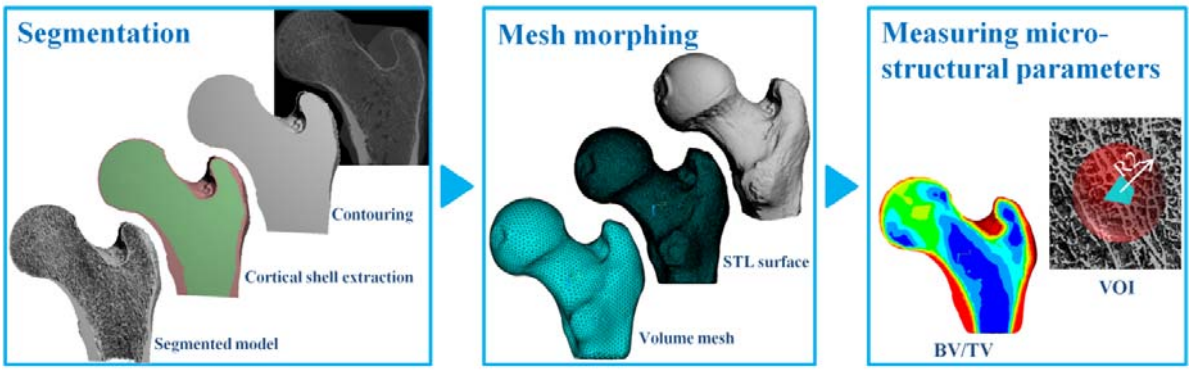

Figure 1. Bone morphology analysis procedure (taken from Hazrati Marangalou et al., 2013).

Inter-individual variability analysis

A coefficient of variation (CV) was calculated for each parameter at each element location of the 29 femora and 20 T12 vertebrae. This coefficient of variation reflects the variation of a parameter value between subjects for the specific location represented by the element. The spatial distribution of the morphology parameter for the whole population then can be visualized by making contour plots of the mesh template in which the parameter average value or its CV is plotted as an element property.

The variability between subjects was further summarized by calculating the root-mean-square (RMS) average of the CV and expressed as a percentage (RMS-CV), similar to the measure used in reproducibility studies (Eq. 1). For the femur dataset, the RMS-CV was calculated for the whole proximal femur and five sub-regions including the femoral neck, femoral head, greater trochanter, Ward's triangle and smaller trochanter regions. For the vertebrae, the RMS-CV was also calculated for the whole vertebrae, for the 8 octants separated by the sagittal, coronal and transverse planes and for the vertebrae central region defined as a 10 mm cube around the center of vertebra (Figure 2).

$$RMS\text{-}CV = \sqrt{\sum_{i=1}^{n} \frac{(CV_i)^2}{n}} \tag{1}$$

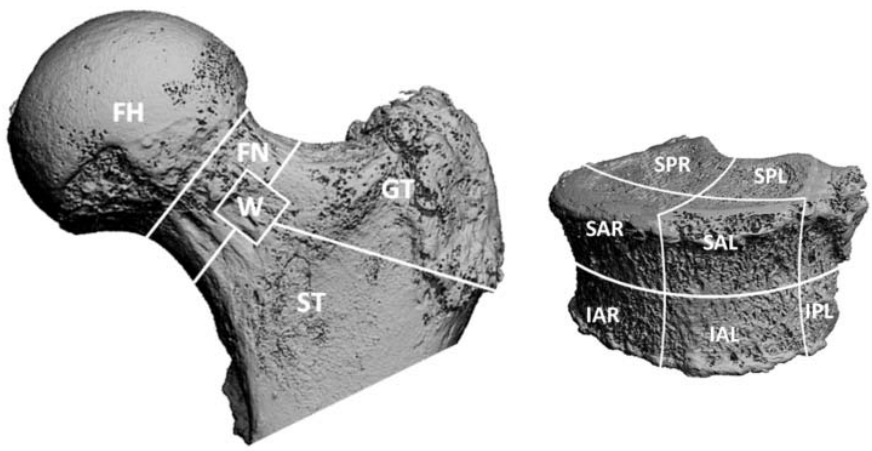

Figure 2. Left: Proximal femur; this diagram shows the subdivision of the proximal femur conventionally used for DXA and CT scans: femoral head (FH), femoral neck (FN), Ward's region (W), greater trochanter (GT) and smaller trochanter (ST). Right: T12 vertebra were divided into 8 sub-regions by anatomical planes; S (Superior), I (Inferior), A (Anterior), P (Posterior), L (Left) and R (Right). In addition a central region was defined (not shown).

Results

Inter-individual variability analysis for the femur

Contour plot of the average bone morphological parameters such as BV/TV, Tb.Th, Tb.N, Tb.Sp, DA and SMI and their coefficient of variation (CV) within the group of 29 individuals are shown in Figure 3.

For BV/TV (Figure 3a) low variations (< 30%) were found in regions where bone volume fraction is high such as in the cortex and femoral head center while high inter-individual

variations (> 75%) were found for regions where bone volume fraction is generally low such as Ward's triangle, the shaft and the greater trochanter. For DA (Figure 3b) high values were found in high density regions near the cortex while low values are found in the femoral neck and greater trochanter region. A high inter-individual variation of DA (CV> 30%) was found near the cortical regions while in most other regions the variation is rather modest (CV< 20%). Contour plots of the SMI distribution (Figure 3c) show high values, implying rod-like structures, in the trochanter region and femoral neck. Low values, indicating plate-like structures, are found in the femoral head center. Due to the low, or even negative (indicating concave structures) average SMI values in the femoral head, the inter-individual variation in these regions is high. Contour plots of Tb.Th (Figure 3d) revealed thicker trabeculae in the femoral head center and thinner trabeculae in the femoral neck and Ward's triangle. The highest inter-individual variation (CV> 70%) was found for regions with thinner trabeculae (e.g. Ward's triangle) while throughout the femoral head the inter-individual variation is modest and rather constant CV (< 25%). Contour plots of Tb.Sp (Figure 3e) are the inverse of that of Tb.Th: with high values found in low density regions like Ward's triangle and low values in the femoral head. Its inter-individual variation was low in the femoral head, but rather high in the trochanter and shaft region. The contour plots of Tb.N (Figure 3f) were very similar to that of Tb.Th. In particular the inter-individual variation of Tb.N and Tb.Th were very similar. The averaged bone morphological parameters for different anatomical locations are summarized in Table 1.

The inter-individual variability of bone morphological parameters was further evaluated by the RMS-CV values for each parameter, for the whole femur as well as for different sub-regions (Table 2). In general, the variability of DA is low whereas that of BV/TV is high. Except for the variability of SMI within the femoral head, the variability for all investigated bone morphological parameters followed the same trend for all sub-regions. The inter-individual variation generally was lower in the femoral head than in other sub-regions. For most investigated morphological parameters, the highest inter-individual variation occurred in Ward's triangle. The high variability found in the femoral head for SMI originates from the fact that close to-zero or negative average values occurred in this region.

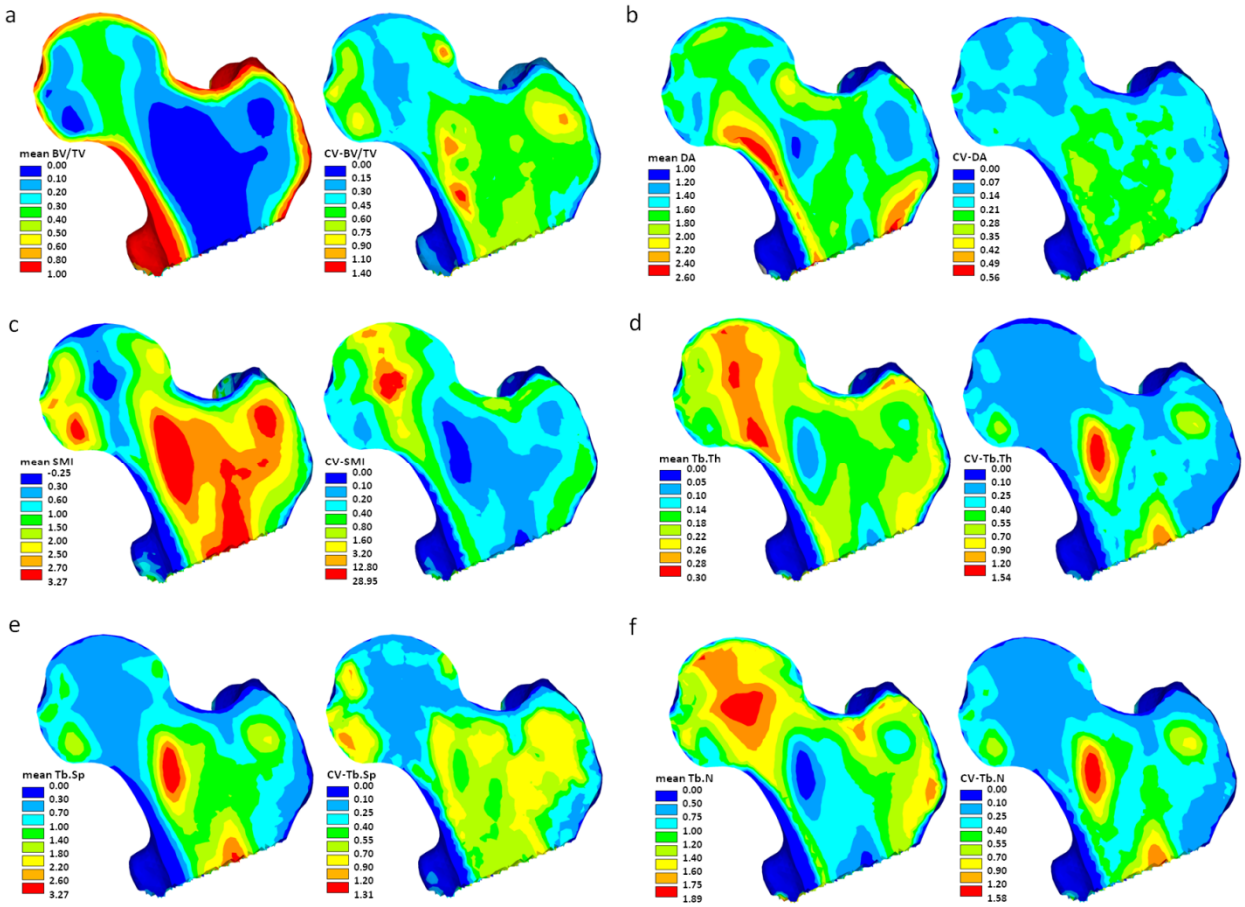

Figure 3. Contour plot of average bone morphological parameters and their inter-individual variation distribution within 29 individuals; BV/TV (a), DA (b), SMI (c), Tb.Th (d), Tb.Sp (e) and Tb.N (f).

Table 1. Averaged bone morphological parameters for the whole femur, femoral head and neck, Ward's triangle, greater trochanter and smaller trochanter (n=29).

	Whole femur	Femoral head	Femoral neck	Ward's triangle	Greater trochanter	Smaller trochanter
BV/TV	0.19±0.03 (0.12-0.25)	0.24±0.05 (0.13-0.35)	0.19±0.04 (0.11-0.27)	0.1±0.02 (0.05-0.18)	0.17±0.04 (0.09-0.24)	0.14±0.03 (0.08-0.19)
Tb.Th	0.21±0.02 (0.16-0.3)	0.22±0.02 (0.18-0.3)	0.21±0.02 (0.14-0.32)	0.16±0.03 (0.09-0.24)	0.2±0.03 (0.13-0.31)	0.19±0.02 (0.15-0.27)
Tb.N	1.31±0.18 (0.91-1.65)	1.5±0.2 (1.13-1.93)	1.27±0.23 (0.84-1.85)	0.88±0.23 (0.39-1.32)	1.33±0.23 (0.83-1.65)	1.09±0.16 (0.71-1.35)
Tb.Sp	0.92±0.22 (0.69-1.47)	0.71±0.15 (0.48-1.19)	0.94±0.29 (0.62-1.77)	1.6±0.52 (0.76-2.88)	0.94±0.32 (0.62-1.75)	1.15±0.3 (0.82-1.88)
DA	1.72±0.1 (1.57-2)	1.65±0.1 (1.48-1.94)	1.93±0.18 (1.65-2.51)	1.61±0.1 (1.41-1.79)	1.6±0.08 (1.45-1.84)	1.82±0.14 (1.53-2.16)
SMI	1.89±0.32 (1.32-2.4)	1.49±0.5 (0.57-2.37)	1.85±0.29 (1.41-2.43)	2.51±0.21 (1.94-2.87)	2.23±0.31 (1.59-2.72)	2.19±0.26 (1.65-2.57)

Table 2. Root-mean-square average of the element coefficient of variation (RMS-CV) for all

investigated parameters (bold values indicate the maximum found for a parameter).

	Whole femur	Femoral head	Femoral neck	Ward's triangle	Greater trochanter	Smaller trochanter
BV/TV	0.4996	0.4393	0.4887	**0.6433**	0.5800	0.6090
Tb.Th	0.3298	0.2043	0.3198	**0.6968**	0.3314	0.4031
Tb.N	0.3622	0.2302	0.3563	**0.7375**	0.3594	0.4393
Tb.Sp	0.5294	0.4111	0.5103	0.5957	**0.6284**	0.5644
DA	0.1931	0.1434	0.1954	**0.2339**	0.1828	0.2287
SMI	8.7925	**14.4530**	0.5177	0.2333	0.4476	0.3801

Inter-individual variability analysis for T12

Contour plots of the average bone morphological parameters and their inter-individual variability within the group of 20 individuals are shown in Figure 4 for the T12 vertebrae. For BV/TV (Figure 4a) low densities are found in the central region. The inter-individual variability in this region is high (typically up to 100%) but less than that of the higher density regions near the endplates and processes (CV<180%). For DA (Figure 4b) the highest values occur in the central-anterior regions, while lower values are found for the posterior regions where bone tends to be isotropic. The inter-individual variation was higher near the cortex (CV> 20%) and rather low (< 20%) in central regions. Contour plots of SMI (Figure 4c) revealed high SMI values in the central region, indicating a rod-like structure, while the lower SMI values are found in the peripheral region. Similar to BV/TV and DA, the inter-individual variation was lower in the central region. For SMI, the higher variability is found in the posterior region. Maximum Tb.Th is found near the cortex (Figure 4d) while thinner trabeculae are found in the region between the cortex and the central region. Trabeculae of intermediate thickness (around 0.12 mm in thickness) are located in the central-superior region. The inter-individual variability for trabecular thickness show a converse relationship with Tb.Th itself: wherever Tb.Th is low, its variability gets higher values and vice versa. The distribution found for Tb.Sp resembles that of SMI, with high values in the center and lower values in the periphery (Figure 4e). Its inter-individual variability was low in the center and higher in the posterior region. As with the femur, for Tb.N, a distribution (Figure 4f) similar to that of Tb.Th was found, with highest values found at the periphery, and lowest values in the region between the cortex and the central region. As with SMI and Tb.Th the higher inter-individual variability is found in the posterior region. Averaged BV/TV and other morphological parameters were evaluated for the full cancellous region and for the eight sub regions (Table 3). As can be seen, the amount of variation found when analyzing relatively large sub-regions, such as the octants analyzed here, is much smaller than the amount of variation found when using the 4 mm spherical regions of Figure 4.

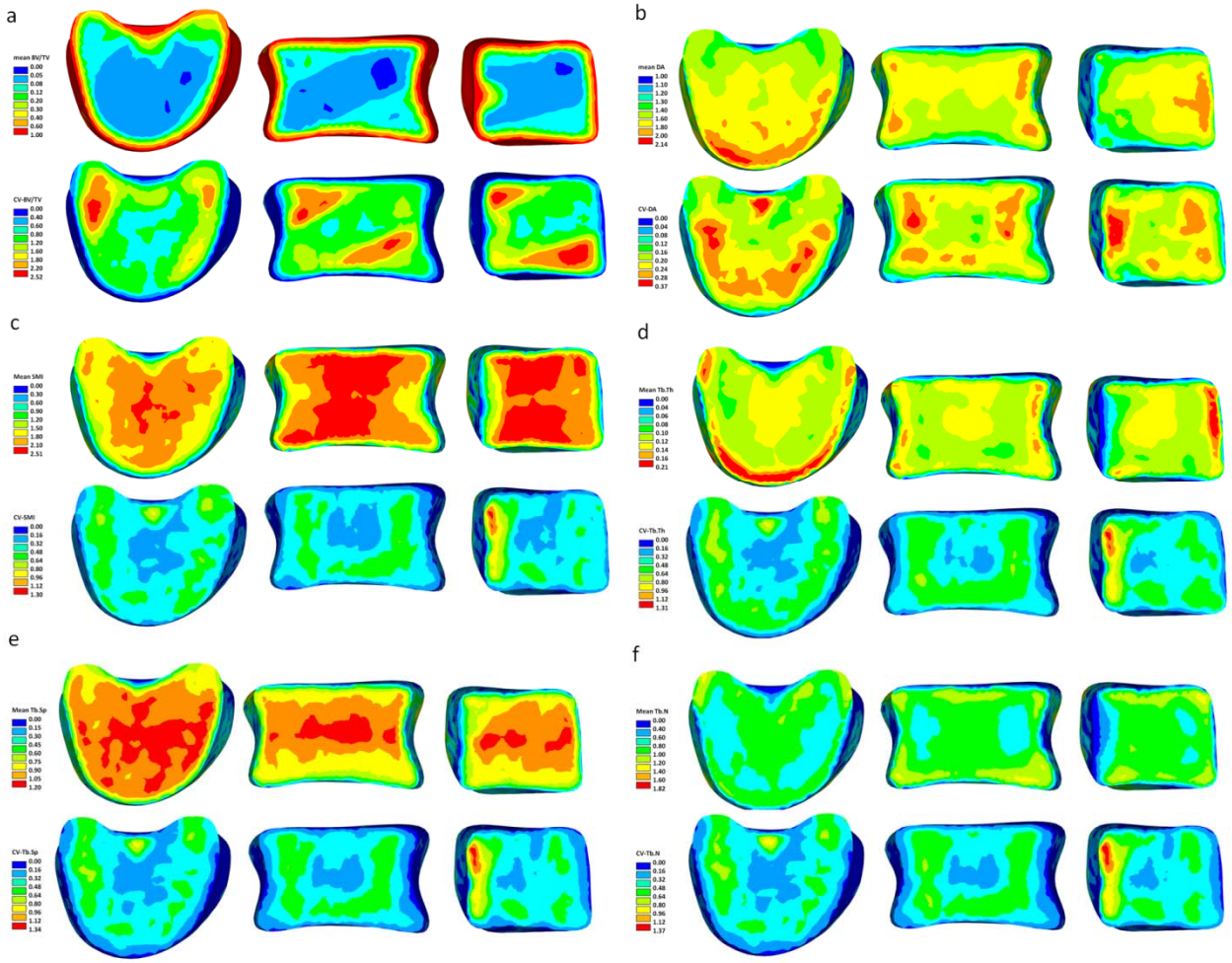

Figure 4. Contour plots of average bone morphological parameters and their coefficient of variation distribution within 20 individuals for T12 vertebrae; BV/TV (a), DA (b), SMI (c), Tb.Th (d), Tb.Sp (e) and Tb.N (f). From left to right: transverse, coronal and sagittal section views.

As for the femur, the inter-individual variability of bone morphological parameters was further evaluated by calculating RMS-CV values for each parameter, for the whole T12 vertebrae and the different sub-regions (Table 4). For the whole vertebral body, the inter-individual variability of DA (20%) is the lowest, whereas that of BV/TV is the highest (121%). The RMS-CV values for the different sub-regions, were similar to those of the whole bone, indicating that the distribution is rather homogeneous.

Table 3. Averaged bone morphological parameters for the whole T12 vertebral body (WT12), the vertebral center, and the eight octants (n=20), where S: Superior, I: inferior, P: posterior, A: anterior, L: left, R: right.

	WT12	Center	IAL	IAR	IPL	IPR	SAL	SAR	SPL	SPR
BV/TV	0.11±0.06 (0.06-0.32)	0.05±0.04 (0.01-0.23)	0.12±0.08 (0.06-0.42)	0.12±0.05 (0.05-0.32)	0.13±0.08 (0.06-0.41)	0.12±0.06 (0.07-0.38)	0.1±0.04 (0.06-0.24)	0.11±0.05 (0.07-0.29)	0.1±0.05 (0.06-0.32)	0.11±0.07 (0.05-0.32)
TbTh	0.12±0.03 (0.08-0.23)	0.11±0.03 (0.03-0.21)	0.12±0.04 (0.03-0.22)	0.12±0.04 (0.02-0.23)	0.12±0.03 (0.06-0.24)	0.12±0.03 (0.08-0.23)	0.13±0.03 (0.08-0.22)	0.13±0.03 (0.09-0.22)	0.12±0.03 (0.07-0.23)	0.11±0.03 (0.06-0.22)
TbN	1±0.24 (0.62-1.74)	0.88±0.25 (0.27-1.5)	1.03±0.29 (0.3-1.62)	1±0.31 (0.25-1.76)	1.14±0.3 (0.58-2.09)	1.13±0.29 (0.71-2.09)	0.93±0.24 (0.51-1.39)	0.96±0.26 (0.65-1.61)	0.96±0.24 (0.54-1.69)	0.97±0.27 (0.52-1.78)
TBSp	0.89±0.12 (0.63-1.06)	0.99±0.2 (0.34-1.24)	0.87±0.18 (0.37-1.09)	0.88±0.17 (0.31-1.08)	0.81±0.13 (0.51-0.98)	0.84±0.12 (0.51-1.03)	0.96±0.12 (0.73-1.2)	0.95±0.13 (0.67-1.15)	0.92±0.13 (0.64-1.11)	0.89±0.15 (0.54-1.13)
DA	1.59±0.12 (1.27-1.83)	1.66±0.2 (1.24-1.98)	1.66±0.17 (1.3-2.07)	1.69±0.2 (1.32-2.07)	1.51±0.15 (1.22-1.81)	1.53±0.14 (1.26-1.82)	1.75±0.17 (1.35-2.07)	1.73±0.18 (1.31-2.06)	1.55±0.12 (1.24-1.72)	1.53±0.12 (1.25-1.75)
SMI	1.93±0.24 (1.19-2.28)	2.16±0.41 (0.78-2.73)	2.03±0.44 (0.79-2.52)	1.95±0.43 (0.63-2.43)	1.91±0.37 (0.87-2.43)	1.93±0.34 (0.97-2.34)	1.85±0.25 (1.37-2.19)	1.91±0.22 (1.22-2.23)	1.94±0.26 (1.2-2.27)	1.95±0.31 (1.2-2.36)

Table 4. Root-mean-square average of the element coefficient of variation (RMS-CV) for all investigated parameters within the whole vertebra (WT12), the vertebral center, and the eight octants, where S: Superior, I: inferior, P: posterior, A: anterior, L: left, R: right (bold values indicate the maximum found for a parameter).

	WT12	Center	IAL	IAR	IPL	IPR	SAL	SAR	SPL	SPR
BV/TV	1.2170	1.0847	**1.4847**	1.0369	1.2485	1.0262	1.0274	1.1617	1.1904	1.3824
Tb.Th	0.4852	0.4223	0.4957	**0.5209**	0.4707	0.4399	0.4671	0.4877	0.4915	0.4998
Tb.N	0.4612	0.3951	0.4207	0.4307	0.4471	0.4216	0.4328	0.4474	0.4790	**0.5029**
Tb.Sp	0.4343	0.3890	0.4139	0.4158	0.4060	0.3717	0.4215	0.4211	0.4555	**0.4718**
DA	0.2011	0.2119	0.2095	0.2092	0.1831	0.1757	0.2162	**0.2184**	0.1993	0.2031
SMI	0.4717	0.3701	0.4267	0.4476	0.4733	0.4608	0.4717	0.4741	0.4805	**0.4829**

Discussion

In this study, we used a novel approach to quantify the average distribution and the inter-individual variation of bone density and other morphological parameters for a population. Two anatomical sites, the proximal femur and T12 vertebra were investigated. The present paper describes the results merely in qualitative terms, but detailed quantitative information is available from the mesh templates that are part of this publication as supplementary data (http://w3.bmt.tue.nl/nl/fe_database/). These templates represent averaged bone geometry (for the femur and T12) with the distribution and inter-individual variation of all parameters described in this publication mapped to the elements. Using a mesh-morphing tool, this information can also be mapped to other bone geometries.

The inter-individual variation found in this study for the femur corresponds well to data obtained in earlier studies (Ascenzi et al., 2011; Bousson et al., 2006; Ciarelli et al., 2000; Cui et al., 2008). Cui et al. (2008) investigated regional variability using core samples extracted from different regions of the proximal femur (n=11, age: 60-79 years). We found similar values for all morphological parameters in the femoral head, neck and greater trochanter. However, in our study we found a lower coefficient of variation for morphological parameters within the different regions particularly in the femoral neck, even though our age-range and number of specimens were larger. This might be due to the fact that using the mesh morphing technique we are able to better select the same anatomical regions than is possible by using radiographs or other techniques.

For the femur, we typically found a high inter-individual variation in Ward's triangle. This is partly due to the way we quantified the inter-individual variation by the coefficient of variation (CV), which implies that high values can result if the average value is very small. Thus for several morphological parameters that relate to the amount of bone (BV/TV, Tb.Th, Tb.N), high CV values are found in regions of low density, such as Ward's triangle. The high

variation in Ward's triangle, however, can also indicate that the location of this region differs between subjects. Depending on the goal of the study one could consider making Ward's triangle location an anatomical landmark. Doing so could reduce the inter-individual variation in the density in that region, at cost of having to identify an extra anatomical landmark, increased deformation of the mesh template and, possibly, increased distortion of elements.

For the T12 vertebrae, the BV/TV measurements in this study are in agreement with previous studies (Banse et al., 2001; Hulme et al., 2007; Nepper-Rasmussen and Mosekilde, 1989) as well. Values found for BV/TV are in good agreement with those reported by Hulme, et al. (2007) for T9-L5 vertebrae. Our BV/TV values are some 30% less though than those reported by Banse, et al. (2001), but this difference likely relates to the differences in imaging and analysis techniques used. Nevertheless our finding of higher posterior than anterior side BV/TV was in agreement with their study. Also in agreement with other studies we found higher BV/TV values in the inferior anterior region than in the superior region, which implies that the inferior endplate is stronger and explains the preferential failure of superior endplates (Grant et al., 2002; Hulme et al., 2007).

The mesh-morphing approach is an important factor for the accuracy of the results. This accuracy of the mesh-morphing is determined by the precision by which the anatomical landmarks are indicated and by the accuracy of the mesh morphing algorithm itself. Inaccuracies in the mesh morphing approach will result in an overestimation of the inter-individual variation. With the homogenization technique used in the present study, however, morphological parameters are always measured over a 4 mm spherical region. Hence, a positioning error much less than that size will not affect the values too much. Using a similar mesh-morphing technique, a positioning error of 0.19 mm on average was found (Grassi et al., 2011), such that we do not expect this to lead to large errors. In the cortical bone, where homogenization was performed over the element volume which is typically 1 mm in size, errors can be larger. The largest inaccuracies are expected for elements at the cancellous/cortical interface for three reasons. First, even a small deviation of the element position can cause a drastic variation of its fraction located in the cortical and cancellous region. Second, the cancellous region for elements partly in the cortical bone can be much smaller than the 4 mm sphere, making these results unreliable. Third, since the mesh template does not have a separate element distribution for the cortical and cancellous regions, variation in cortical thickness will also results in high inter-individual variability for parameters measured near the endosteal contour. It would be possible to solve these issues by making a mesh template that separates the cortical and cancellous compartments, but since the cortical bone regions can be very thin, this would complicate the meshing procedure and possibly require the use of very small elements. Since all accuracy errors mentioned above will result

in an overestimation of the inter-individual variation, the results presented here can be seen as an upper-bound to this variability.

A number of other points need to be discussed as well. First, the number of bones analyzed in this study is still rather limited: only 29 femora and 20 T12 vertebrae were available. Nevertheless, it represents an elderly population, which is the target group for orthopaedic interventions such as bone implants (e.g. hip and intervertebral disc) and intervention treatment (e.g. vertebroplasty). As a result of the limited size, however, it was not possible to subdivide it in age groups, such that we cannot compare our results directly to an earlier study that uses registration technique for the femur (Carballido-Gamio et al., 2013). Second, it is possible that the amount of inter-individual variation is dependent on the size of the sphere used for calculating the homogenized properties. In this study we used a 4 mm sphere based on the notion that, in order to define valid continuum level properties, measurements over a minimum length scale on the order of 4 mm are required. In an earlier study we demonstrated that the density and other parameters' distributions are not much dependent on the size of this sphere, although larger spheres will obviously 'blur' the distributions. However, since larger spheres will average over larger volumes, it is possible that the variation will be less.

Our results indicate considerable variability in bone morphology between subjects for the neck and trochanter regions in femur dataset. Since hip implants typically are anchored in these regions, applying realistic variations to material properties in these regions is important to accurately evaluate implant behavior with FE models. For implants that are anchored primarily in the femoral head, e.g. resurfacing implants, accounting for such variations might be less essential. The results can also help to optimize implants and orthopaedic procedures like T12 augmentation processes such as kyphoplasty and vertebroplasty and identifying anchoring regions for implants or screws in which bone quality is generally good. In conclusion, using the current method we are able to measure bone morphological parameters locally, in a very detailed way and to quantify inter-individual variability in a large population with fair accuracy.

Acknowledgments

Funding from the European Union for the osteoporotic virtual physiological human project (VPHOP FP7-ICT2008-223865) is gratefully acknowledged.

Conflict of interest statement

Bert van Rietbergen is a consultant for Scanco Medical AG.

Chapter 6

Vertebral Strength Can Be Accurately Predicted From Bone Microstructural Parameters

The concepts of this chapter are based on: Javad Hazrati Marangalou, Felix Eckstein, Volker Kuhn, Keita Ito, Matteo Cataldi, Fulvia Taddei, Bert van Rietbergen. Vertebral Strength Can Be Accurately Predicted from Bone Microstructural Parameters. submitted.

Vertebral Strength Can Be Accurately Predicted From Bone Microstructural Parameters

[a]*Javad Hazrati Marangalou,* [b]*Felix Eckstein,* [c]*Volker Kuhn,* [a]*Keita Ito,* [d]*Matteo Cataldi,* [d]*Fulvia Taddei,* [a]*Bert van Rietbergen*

[a]*Orthopaedic Biomechanics, Department of Biomedical Engineering, Eindhoven University of Technology, Eindhoven, The Netherlands*

[b]*Institute of Anatomy & Musculoskeletal Research, Paracelsus Private Medical University, Salzburg, Austria*

[c]*Medizinische Universität Innsbruck, Insbruck, Austria*

[d]*Laboratorio di Tecnologia Medica, Istituti Ortopedici Rizzoli, Bologna, Italy*

Abstract

Whole vertebrae areal and volumetric BMD measurements are not ideal predictors of vertebral osteoporotic fractures. Recent studies have shown that sampling bone microstructural parameters in smaller regions may permit better predictions. In such studies, however, the sampling location is described only in general anatomical terms. Here, we introduce a technique that enables the quantification of bone volume fraction and microstructural parameters at precisely defined anatomical locations. Specific goals of this study were: to investigate at what anatomical location within the vertebrae local bone volume fraction best predicts vertebral-body strength, whether this prediction can be improved by adding microstructural parameters and to explore if this approach could better predict vertebral-body strength than whole bone volume fraction and finite element (FE) analyses.

Eighteen T12 vertebrae were scanned in a micro-CT system and FE meshes were made using a mesh-morphing tool. For each element bone microstructural parameters were measured and correlated with vertebral compressive strength as measured experimentally. Whole bone volume fraction and FE-predicted vertebral strength were also compared to the experimental measurements.

The results show that local volume fraction at the optimal location can explain up to 90% of the variation in vertebral-body strength. Adding local microstructural parameters can raise this to 98%. Whole bone volume fraction could explain only 64% and FE analyses 76% of the variation in bone strength.

A local assessment of volume fraction at the optimal location can substantially improve the prediction of bone strength. Local assessment of other microstructural parameters can further improve this prediction.

Introduction

Osteoporosis is characterized by low bone mass and micro-architectural deterioration of bone tissue and represents a major public health problem due to the high prevalence and complications associated with fragility fractures (Grigoryan et al., 2003; Legrand et al., 2000; Riggs and Melton Iii, 1995). It has been demonstrated that the clinical diagnostic standard approach based on site specific BMD measurements using dual energy X-ray absorptiometry (DXA) is not an optimal predictor of vertebral osteoporotic fractures, and more than 50% of these fractures occur in patients with a DXA T-score greater than the diagnostic criterion (-2.5 SD). It has been stated that this poor performance could be related to the fact that DXA provides an areal density measure, and that it does not provide any information about the bone micro-architecture (Kanis, 2002; Lochmüller et al., 2003). Three-dimensional imaging techniques, such as CT enable the measurement of the volumetric density and, more recently, even some microstructural features of vertebrae in-vivo (Duan et al., 1999; Mulder et al., 2012; Peel and Eastell, 1994; Seeman et al., 2001). Several studies have demonstrated, however, that the predictive value of QCT derived volumetric density for vertebral fractures generally is not much better than that of areal measures of density (Lang et al., 1999; Tabensky et al., 1996) and the same has been shown in experimental studies on vertebral strength (Lochmüller et al., 2003; Lochmüller et al., 2002).

Such volumetric density measures generally comprise the whole vertebrae. It has been proposed that assessment of the weakest parts of the cancellous bone may lead to better prediction of fracture risk (Banse et al., 2001). Indeed, earlier studies demonstrated that sampling bone density and microstructural parameters in smaller regions can provide better predictions of vertebral strength (Gong et al., 2006; Parkinson et al., 2012; Stauber and Müller, 2006). The number of samples analyzed per vertebrae, however, was usually rather limited and, depending on the techniques used (experimental, computational), dictated by minimum size requirements for meaningful analysis of a bone sample. Further, the location of the samples was usually described only in terms of the anatomical planes, which makes it difficult to reproduce the exact anatomical location of the specimen, in particular for small samples. It is also unclear how sensitive the results are for small deviations from the sampling location. Although such studies could give general guidelines about the importance of different vertebral regions to predict vertebral strength, the results of these studies are hard to compare due to differences in experimental design, parameters investigated, techniques used and sampling locations. However, the fact that most of these studies demonstrated that predictions can be improved by focusing the analysis on a specific region, begs the question if

results can be further improved by finding an optimal location and size of the sampling region and if so, how these findings can be potentially translated to the clinic.

In order to answer that question, we hereby introduce a computational technique that enables the quantification of bone volume fraction and microstructural parameters at any precisely defined anatomical location in the bone. The approach relies on a combination of two essential tools: The first is a morphing tool that can morph a 3D finite element (FE) mesh template to a CT-image of a bone after identification of a limited number of anatomical landmarks. After morphing, each element is positioned at a well defined anatomical location in the bone. The second is a tool to measure bone volume fraction and microstructural parameters at the location of each element, hence at each anatomical location. The combined approach thus makes it possible to directly compare bone volume fraction and microstructure between bones at any given location. By correlating local values measured at a specific anatomical position for a large number of bones with whole bone strength, it then becomes possible to find which anatomical location best predicts whole vertebral-body strength. Since any particular anatomical location can be easily identified with the help of the mesh template and morphing tool, also for bone in-vivo, such an approach could be used to improve bone strength predictions in patients, particularly in clinical studies.

In the present study we explore this approach for thoracic (T12) vertebrae. The specific goals of the study were a) to investigate at what anatomical location within the vertebrae local bone volume fraction best predicts whole vertebral-body strength, b) to study whether the prediction can be further improved by measuring microstructural parameters and c) to explore if this approach could better predict bone strength than whole-bone volume fraction and non-linear finite element (FE) analysis.

Material and methods

Material

Eighteen vertebral segments comprising T11-L1 were obtained from an earlier study (Lochmüller et al., 2008). The donors were free of bone disease other than osteoporosis, as determined by histopathological examination of pelvic bone samples, and the vertebrae had no metastatic or other apparent disorder on radiography; they were stored in buffered formalin solution. Mean age was 78.0 ± 8.07 years (range 64-92 years); ten donors were female and eight donors were male. The donors had dedicated their body by testament to the Institute of Anatomy in Munich during life for the purpose of teaching and research.

Imaging and mechanical testing

The central T12 vertebrae of each segment was scanned in a micro-computed tomography system (micro-CT 80, Scanco Medical AG, Brüttisellen, Switzerland) at a nominal isotropic

resolution of 37 µm using a 2048x2048 in plane image matrix. The scanner energy was 70 kV (114 µA). Images were filtered using a modest Gauss filter (sigma = 0.6, support = 1 voxels) and segmented using a global threshold of 11% of the maximum gray-value. Compartments of cortical and cancellous bone were identified using masks. A first mask comprising the whole vertebrae was made based on the periosteal contour. In order to separate the thin cortical shell, original images were filtered using a strong Gauss filter (sigma = 5, support = 5 voxels) and segmented using a threshold of 15% of the maximum gray-value, leaving only the cortical bone. This image was used to identify the cortical shell in the original mask. In addition, the most periosteal 1 mm region of the original mask was identified as part of the (sub)cortical compartment. The remainder of the mask was considered the cancellous compartment.

After imaging, the vertebral segments were tested to failure in an axial compressive loading configuration as a functional spinal unit (T11 to L1) with intact ligaments and intervertebral discs, but without posterior elements, using an uniaxial material testing machine (Zwick 1445, Ulm, Germany) and a 10 kN load cell. The strength was determined at a rate of 6.5 mm/s, by identifying the first peak that is followed by a drop of > 10% from the load–displacement curve. To ensure fracture, the segments were compressed to 25% of their original height (Lochmüller et al., 2003; Lochmüller et al., 2002; Lochmüller et al., 2008).

Creation of vertebrae meshes

A mesh template for T12 vertebrae was created based on a mesh convergence study. The mesh template contained 51,119 second order tetrahedron elements with a typical size of 1 mm. To morph this template to a CT scan of a vertebra, a total of 22 specific anatomical landmarks at the bone periosteal surface were identified. To do so, a triangularized description of the periosteal surface of each vertebra was created from the CT-scan using a marching cubes algorithm and converted to STL format (IPL V5.16, Scanco Medical AG). Using a dedicated morphing tool (Ansys, Inc., United States), the anatomical landmarks then were identified at the bone surface based on which the mesh template was automatically morphed to the CT scan. Using this procedure, it was ensured that each element of the mesh template corresponded to a specific anatomical location in all samples (Grassi et al., 2011).

Bone volume fraction and microstructural analysis

Using an algorithm developed in-house, it was determined what fraction of the volume of each element in the mesh template was in the cancellous compartment and what fraction in the cortical compartment. If the element was at least partly in the cancellous bone compartment, a spherical region with a diameter of 4 mm was defined around the element centroid, for which the volume fraction and microstructural parameters were determined (Harrigan et al., 1988). Microstructural analyses for the part of this spherical region that was

within the cancellous bone compartment were performed using image processing software provided with the micro-CT system (IPL V5.16, Scanco Medical AG). The parameters included the calculation of bone volume fraction (BV/TV), trabecular thickness (Tb.Th) trabecular number (Tb.N), trabecular spacing (Tb.Sp), structural model index (SMI) and degree of anisotropy (DA). Tb.Th, Tb.Sp and Tb.N were determined based on direct measurement using a distance transformation method. The measured microstructural parameters were then assigned to the element located at the centroid of the sphere. Since the elements were around 1 mm in size, considerable overlap exists in the regions analyzed for neighboring elements.

For elements that were at least partly in the (sub)cortical compartment, a cortical bone volume fraction was defined as the volume of cortical bone within the element divided by the element volume that was within the cortical compartment as defined earlier. For elements that comprised both the cancellous and cortical compartments, the final BV/TV was based on a rule of mixtures for the cortical and cancellous bone parts whereas the microstructural parameters were based on the cancellous bone only.

Figure 1 depicts the mesh generation and bone microstructural analysis procedures.

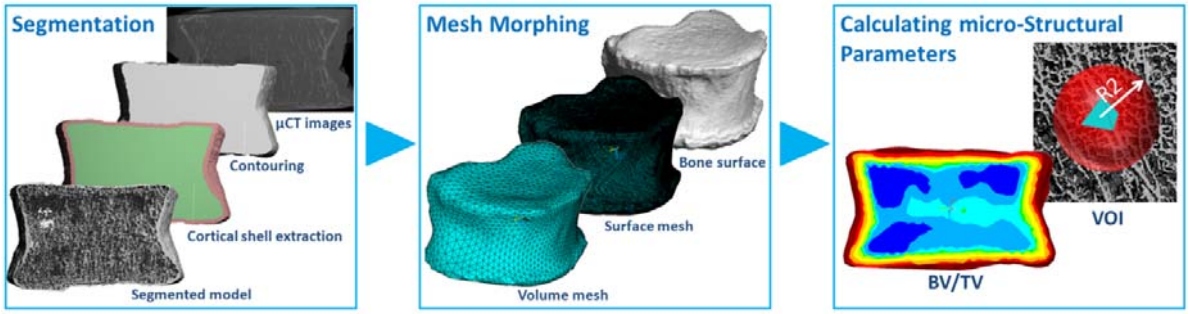

Figure 1. Mesh morphing and bone microstructural analysis procedure.

In addition to the local volume fraction and microstructural measurements, the whole bone volume fraction was calculated from the micro-CT images as the total bone tissue volume divide by the total volume of the vertebrae. Further, the cancellous/cortical bone volume fraction was calculated as the total bone tissue volume divided by the total volume of the cancellous/cortical compartment.

Finite Element analyses

In a next step, the meshed vertebrae were used for FE analysis. Based on the element volume fraction measurements described earlier, isotropic material properties were defined for each element. Elastic-plastic-damage constitutive behavior (Charlebois et al., 2010) was prescribed to simulate failure and post-failure behavior of the vertebrae under compression loading. Nonlinear FE analyses were carried out using ANSYS (Ansys Inc., United States). The

boundary conditions applied were chosen to mimic the experimental setting. Nodes at the inferior endplate were fixed in all directions while a displacement in the axial direction was applied to nodes at superior endplate. A total compressive displacement of 3 mm was applied in 100 load increments, and for each step the total reaction force was calculated. The force displacement curve peak was taken as the vertebral strength.

Statistical analysis and visualisation

To investigate which parameter and which anatomical location best predict bone strength, values for the bone volume fraction and microstructural parameters were collected for each element in the mesh template. These 18 numbers then were correlated to the whole vertebral-body strength values of the 18 vertebrae as measured in the experiment, to explore which element location and parameter correlates best to bone strength. Results were quantified by an element coefficient of determination (R^2). Using the mesh template as the geometry, contour plots of this element coefficient of determination enabled visualization of the regions that best correlate to the measured whole bone strength. In a first analysis, only BV/TV was considered as a predictor for bone strength. In a second analysis, a multiple regression analysis was performed that combined all measured parameters for a specific element to predict bone strength. Note that, since we were looking for a single best location, we did not aim at combining different parameters obtained from multiple locations.

To provide further insight in the average distribution of BV/TV and its local variation, the average value of each element parameter (i.e. when averaged over the 18 specimens) was calculated as well as its coefficient of variation (CV). To investigate if local value could better predict bone strength than whole bone volume fraction, the whole bone volume fraction and cancellous/cortical bone volume fraction of the 18 vertebrae were correlated to the whole bone strength values of the 18 vertebrae as well. Similarly, to investigate if local value could better predict bone strength than FE-analysis; the strength predicted from the non-linear FE-analyses was correlated to the whole bone strength values of the 18 vertebrae.

Fisher z transformation was used to test whether the correlations obtained for each method significantly differ from each other.

Results

The central regions of the vertebrae best predict the bone strength, with coefficients of determination in the range of 0.60 to 0.90 (Figure 2). To better visualize the regions that best predict bone strength, the contour plots were thresholded such that only element with a coefficient of determination that exceeded 0.75 or 0.90 were shown (Figure 2b and c). These plots confirmed that the central region is the best predictor for bone strength, and also revealed that the central location that was the best predictor (element #46205 in the mesh template) explained >90% of the variation in whole vertebral-body strength. Figure 2d-e

depicts the average BV/TV and its coefficient of variation within the population. By combining these plots with Fig. 2a, it can be seen that the best predictive region is a region with a rather consistent low bone volume fraction.

When analyzing the predictive value of the individual microstructural parameters, it was found that Tb.N better correlated with vertebral strength than other microstructural parameters (max R^2=0.88). For this parameter, the regions that best predicted strength were found mainly near the endplates (Figure 3a.)

The other microstructural parameters, Tb.Th, Tb.Sp, SMI and DA correlated much less with vertebral strength (R^2<0.83). DA was the poorest predictor of the microstructural parameters analyzed (R^2<0.61).

Results of the multi-linear regression analysis revealed that combining BV/TV with microstructural parameters measured at that element can improve the prediction (Table 1). The combination of BV/TV and Tb.N could increase the coefficient of determination to 0.92. In this case also, the central regions best predict vertebral strength (Figure 3b). The highest coefficient of determination (R^2=0.98) was obtained when taking all six microstructural parameters into account.

Table 1. Determination coefficient relating bone microstructural parameters and vertebral strength.

Bone microstructural parameter	Location (element no.)*	Max. determination coefficient for measured vertebral strength	Mean and SD parameter values for element with max. R-squared value
BV/TV	46205	0.90	0.0658 ± 0.0498
Tb.N	21102	0.88	1.2498 ± 0.3236
Tb.Th	6550	0.81	0.1311 ± 0.0369
Tb.Sp	21102	0.77	0.8688 ± 0.1777
SMI	48012	0.83	2.0575 ± 0.9795
DA	4041	0.61	1.7377 ± 0.4311
α_1BV/TV+α_2Tb.N	21102	0.92	N/A
α_1BV/TV+α_2Tb.N+α_3Tb.Th	48274	0.92	N/A
α_1BV/TV+α_2Tb.N+α_3Tb.Th+α_4Tb.Sp	47073	0.94	N/A
α_1BV/TV+α_2Tb.N+α_3Tb.Th+α_4Tb.Sp+α_5SMI	9683	0.95	N/A
α_1BV/TV+α_2Tb.N+α_3Tb.Th+α_4Tb.Sp+α_5SMI+α_6DA	18336	0.98	N/A

* refers to the location in the mesh template which is included as supplementary data.

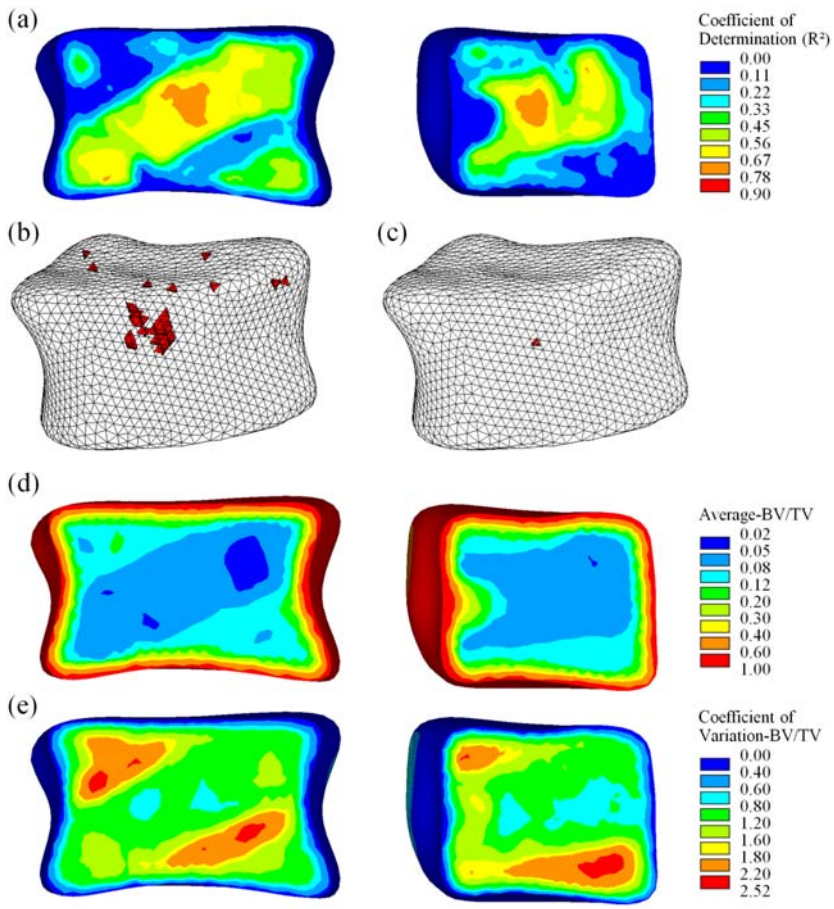

Figure 2. (a) Contour plot of coefficient of determination between whole vertebral strength and BV/TV; elements with R-squared value (b) above 0.75 and (c) above 0.90; (d) Contour plots of average BV/TV and (e) its CV within the population (left: frontal section, right: sagittal section).

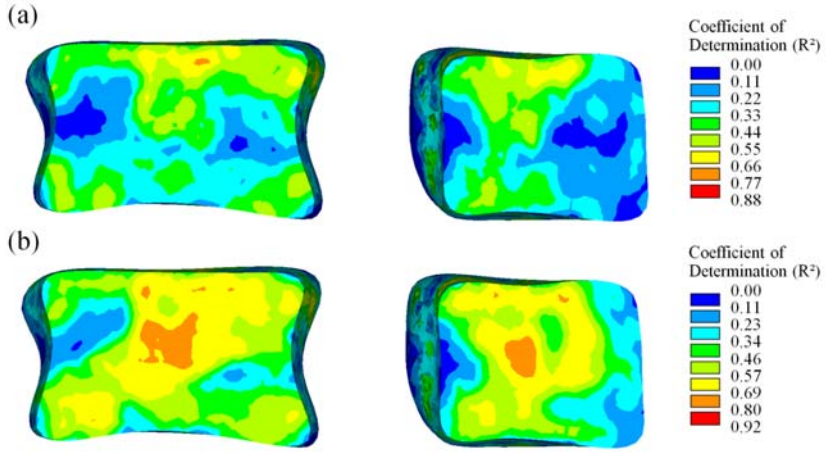

Figure 3. Contour plots of coefficient of determination between whole vertebral strength and (a) Tb.N and (b) $\alpha_1 BV/TV + \alpha_2 Tb.N$ (left: frontal section, right: sagittal section).

For the multi-linear regression model that combined all parameters, thresholding the coefficient of determination at 90% revealed a somewhat scattered plot of elements that exceeded that threshold, mainly in the central regions. When further increasing the threshold up to 98%, one element located at the superior-posterior region (element #18336 in the mesh template). Measuring these 6 microstructural parameters at this particular location thus could explain over 98% of the variation in vertebral strength (Figure 4).

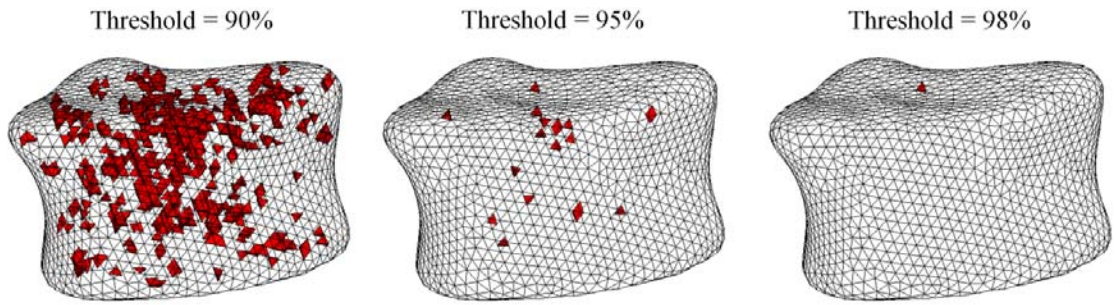

Figure 4. Different threshold levels were applied in order to identify the best predictive regions of whole vertebrae strength taking all microstructural parameters in multi-linear regression analysis.

Non-linear FE analyses of the vertebrae revealed typical failure behavior (Figure 5). The simulated force displacement curves demonstrated that some of the samples show elastic-perfectly plastic behavior at the apparent level whereas for others some softening occurs (Figure 5a). Closer analysis of the results demonstrated the presence of bands in which the failure concentrates, in agreement with results described by others (Charlebois et al., 2010; Imai et al., 2006; Kopperdahl et al., 1999) (Figure 5b).

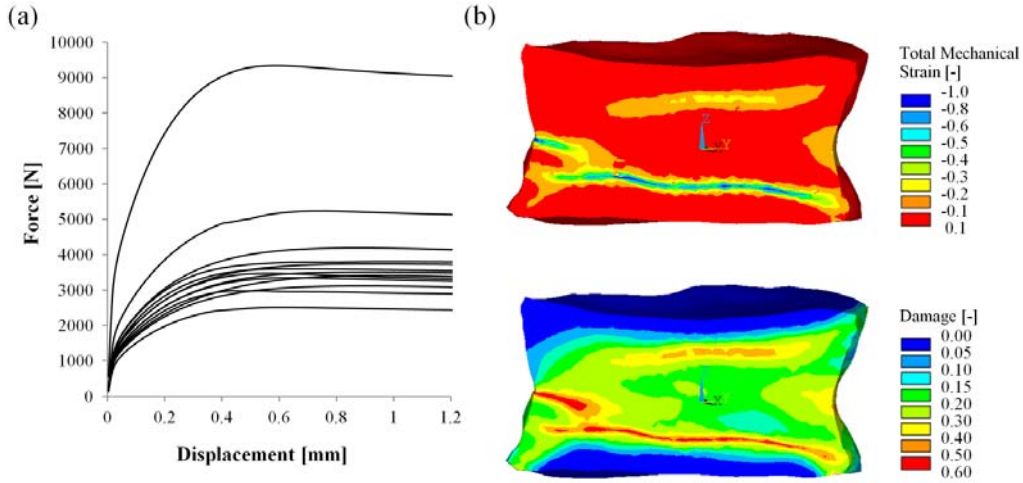

Figure 5. (a) Force-displacement curve obtained from whole vertebral compression FE analyses (n=18); (b) total mechanical strain and damage distribution in the vertebral body under compression test for a typical sample.

In contrast to the local measurement, whole bone, cancellous and cortical bone volume fractions could explain only 64%, 68% and 57% of the variation in measured bone strength respectively. Figure 6a-c depicts the correlation between these volume fractions and the vertebral strength values measured in the experiments. When correlating the FE-predicted and measured whole-bone strengths, a coefficient of determination R^2=0.76 was found (Figure 6d).

Fisher z transformation tests revealed that the correlation values for the local BV/TV-based prediction (R^2=0.90) and for the FE-based prediction (R^2=0.76) are not significantly different (p-value=0.064). However, the correlation for the local BV/TV-based prediction was significantly better than that obtained for the whole-bone BV/TV-based prediction (R^2=0.64; p-value=0.005).

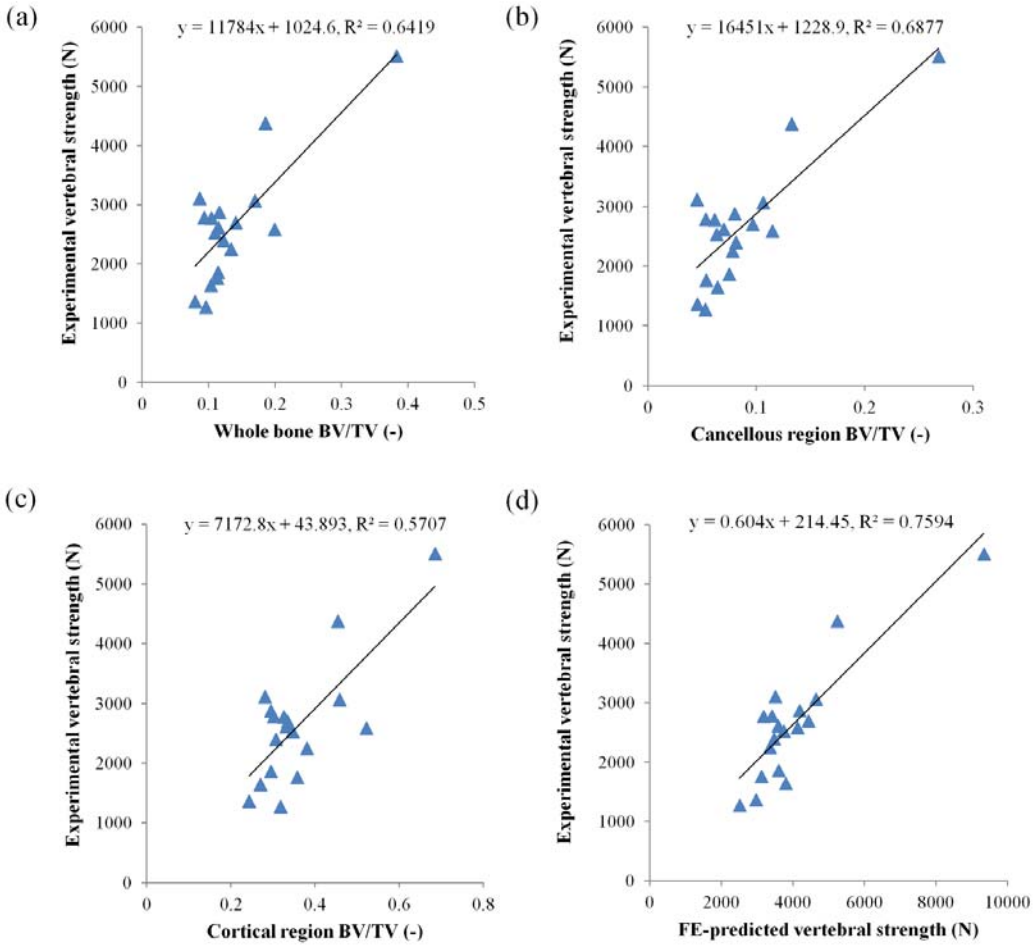

Figure 6. Vertebral strength predictions with (a) whole bone volume fraction, (b) cancellous bone volume fraction, (c) cortical bone volume fraction and (d) nonlinear FE analyses.

Discussion

The results of this study demonstrate that accurate predictions of vertebral bone strengths can be made based on volume fraction and structural measurements at a specific anatomical location. Even when measuring local volume fraction only, predictions of whole bone strength were better than predictions based on whole bone density and at least as accurate as predictions from whole-bone nonlinear FE-analyses.

A key methodological innovation is the use of a combination of morphing and local microstructure measurement tools. We demonstrated that in this way it is possible to measure volume fraction and microstructural parameters at well-defined anatomical positions within vertebrae. Since, after mesh morphing, each element is at a specific anatomical position, it becomes possible to specify the location by the element number. As long as the same mesh template is used, the same procedure can be applied to patient CT-data, thus making it possible to perform local measurement in-vivo with much lower acquisition time and radiation dose, and at the same anatomical locations as used in the present study. This technique can also warrant reproducible measurement at baseline and follow-up in a clinical study.

The first goal of this study was to investigate at what anatomical location within the vertebrae local bone volume fraction best predicts whole bone strength. The coefficient of determination found (R^2=0.90) was surprisingly high and higher than the predictive value of whole bone volume fraction or values found by others (Cheng et al., 1997b; Ebbesen et al., 1999; Edmondston et al., 1994b; Hulme et al., 2007; Moro et al., 1995). The average bone volume fraction and the CV at this location (average BV/TV=0.07 and CV=0.80) were in the midrange, suggesting that this is not a very weak spot or a spot at which bone volume fraction undergoes drastic changes that would correlate with bone strength. Results of the FE-analysis revealed that also the local loading conditions during compression were in the mid-range while the model did not predict fracture for this element in most cases. This is in agreement with results of micro-FE analyses recently presented by others that also suggested that failure does not accumulate at the vertebral center but rather near the endplates (Fields et al., 2012). These combined results suggest that the particular location is a good predictor mainly because of the consistent correlation between BV/TV and bone strength, and not because it is the weakest link during fracture.

A second goal was to investigate if the prediction can be further improved by measuring microstructural parameters. As expected, adding more parameters improved the prediction. Adding more parameters, however, also resulted in the selection of different anatomical regions. For instance, adding Tb.N and Tb.Th and Tb.Sp to BV/TV in multi-linear regression analysis results in a high determination coefficient within elements far from the vertebra

central region. Interestingly, these selected elements are mostly scattered at locations where the FE-model predicts high damage to occur (compare Figure 4 and Figure 5). This suggests that adding more microstructural parameters to the regression analysis leads to the identification of the weakest links, while BV/TV alone is not sensitive enough to do so and thus identifies a region where bone density varies most consistently with bone strength.

A third goal was to investigate if this approach could better predict bone strength than whole bone volume fraction and non-linear whole-bone finite element analysis with volume fraction-dependent local stiffness and strength assignment. Our results demonstrate that this is the case. Whole bone volume fraction and cancellous bone volume fraction could predict only 64% and 68% of the variation in bone strength respectively, whereas local volume fraction could explain over 90%. Strength obtained from FE analyses predicted 76% of the variation in bone strength, which is also less than the local measures. The correlation between FE and experimental results found here is in accordance with previous studies (Buckley et al., 2007; Crawford et al., 2003; Dall'ara et al., 2010; Imai et al., 2006; Matsumoto et al., 2009); Dall'Ara et al. (2010) found a determination coefficient of 0.79 between FE-predicted vertebral strength and experimental values. It should be emphasized that the locations that we identified as the best predictor for vertebral strength represent the microstructure of the bone in a 4 mm spherical region around the element centroid. It is not possible to make these regions smaller, since that would violate the continuum assumption necessary to calculate meaningful bone volume fraction and microstructural parameters (Harrigan et al., 1988). Increasing the size of the sphere would be possible, but would obviously lead to a reduction of the effective resolution of the anatomical location determination. To investigate if the results are dependent on the size of the sphere, we did some sensitivity analyses in which we varied the sphere radius from 4 to 8 mm. It was found that the actual chosen size has a very small effect on the calculated bone volume fraction and other microstructural parameters.

As mentioned earlier, the coefficient of determination found when correlating the local density at the vertebral centre and vertebral strength (R^2=0.90) was surprisingly high. In order to further investigate the predictive value of this relationship, an additional analysis was done in which the 18 vertebrae used in this study were divided into two groups of 10 and 8 vertebrae. The group of 10 vertebrae was used to find the best predictive region (element) in the same way as done earlier for the full data set. The coefficient of determination when correlating local density and vertebral strength for these 10 vertebrae (R^2=0.97) was even higher than for the full data set, but the best predicting element (#46401) was very close to the one found earlier. The regression constants obtained from this analysis then was used to predict the strength of the other 8 vertebrae. In this case, the coefficient of determination was less (R^2=0.77) and almost the same as that found for the FE-predictions.

Although we did not explicitly investigate the sensitivity of the approach used here for errors in the mesh morphing procedure, this error was addressed implicitly. Since the mesh morphing tool was used 18 times, for all vertebrae used in this study, large deviations from the intended anatomical position would lead to variance in the parameters obtained at that position that is unrelated to bone strength. If that variance is high, the location thus will likely not be a suitable predictor for bone strength. Conversely, it is possible that locations that are good predictors for bone strength are locations that are relatively insensitive to such errors in the positioning.

There are several limitations of this study: We used micro-CT images to measure bone microstructural parameters in this study. From standard clinical CT scans, however, only bone density measurements can be made. Nevertheless, recent studies using high-resolution flat panel systems have demonstrated that at least some microstructural parameters can be measured in-vivo (Bredella et al., 2008; Cheung et al., 2009; Gupta et al., 2006; Mulder et al., 2012; Walsh et al., 2010). In particular, these studies demonstrated that Tb.N can be measured rather adequate in-vivo. Interestingly, the combination of BV/TV and Tb.N was found to be one of the combinations that could considerably improve the prediction of vertebral strength, indicating that this could be a promising parameter to include.

Second, our FE-model modeled bone as an isotropic material, even though the material model used could account for anisotropy by measuring a fabric tensor (Hazrati Marangalou et al., 2012). We have chosen not to do so here to make the FE-results comparable with the nowadays clinical practice and to make sure that the FE-model contains the same information as the regression model based on volume fraction only. It is well possible though that including anisotropy could enhance the predictions of the FE-analysis (Pahr and Zysset, 2009).

Third, the specimens were stored in formalin before testing. It has been shown that this can affect the mechanical properties of the bone (Edmondston et al., 1994a; Wilke et al., 1996). As with the previous comment, we here assume that this error would be consistent for all vertebrae and thus not affect the correlation too much.

In conclusion, the results suggest that the local density measurement techniques investigated here better predicts whole vertebral-body strength than current methods based on whole-bone density. Since its translation to a clinical situation is straightforward, we expect that it will better predict whole vertebral-body strength in patients as well. Clinical studies, however, will need to confirm whether these techniques will also lead to a better prediction of vertebral fractures than DXA or QCT derived measures.

Acknowledgements

Funding from the European Union for the osteoporotic virtual physiological human project (VPHOP FP7-ICT2008-223865) is gratefully acknowledged.

Conflict of interest statement

Bert van Rietbergen is a consultant for Scanco Medical AG.

Chapter 7

General Discussion

The overall goal of the work described in this thesis was to enhance finite element models of bones by implementing information about the bone microstructure. Since the bone microstructure cannot be imaged for bone in-vivo, an explicit modeling of the bone microstructure as done with micro-finite element modeling was not possible, and continuum models need to be used. Information about the bone microstructure then can be implemented only by making these continuum-level material properties somehow dependent on bone microstructure as characterized by morphological parameters. At the start of this project, we thus asked ourselves a number of questions. First, what material model should we use, and what morphological parameter(s) should it account for? Second how do we get information about the bone microstructure if we can't measure this for bone in-vivo? And third, are the results of such enhanced models really better than those of the isotropic models?

To answer the first question we considered a few empirical relationships proposed in the literature. Although these relationships usually are validated relative to experimental work earlier, a comparative evaluation of different models would have required us to redo much of this experimental work. Apart from the fact that this would have involved a lot of additional work, we also realized that such experimental tests have many limitations. Whole bone experimental tests are usually restricted to bone surface strain measurements and the measurement of whole bone stiffness and strength. Based on these measurements, it is not possible to validate the stress or strain distribution within the cancellous bone region which is one of the important determinants for bone mechanical properties. More detailed information about the mechanical behavior of cancellous bone can be obtained from mechanical tests on cancellous bone core samples, but such tests are generally limited to uniaxial compression/tension tests which are prone to error in particular for porous materials such as cancellous bone. We therefore developed a novel computational approach to validate the empirical relationships that makes use of homogenized micro-FE results (chapter 2). Using this approach we could demonstrate that continuum models implementing the material model that we selected (Zysset and Curnier, 1995) would produce a stress distribution very similar to that of the homogenized micro-FE results. In this study we only investigated the linear-elastic response, but it would be possible as well to homogenize plastic/damage response from non-linear micro-FE results. The development of such non-linear micro-FE analyses, however, is still an active field of research and, though such analyses now are possible (Fields et al., 2012), they would be very expensive from a computational point of view.

Whereas this approach of testing empirical relationships relative to homogenized micro-FE results likely is more accurate and sensitive than any comparison with experimental results, it also has some limitations. Since it uses results of micro-FE models as a reference, the accuracy of this approach is directly dependent on the accuracy of the micro-FE models. Although these have been well validated in many studies, factors such as image resolution and

the fact that bone tissue is usually modeled as homogeneous with a constant modulus can introduce errors.

Having selected the material model, the microstructural property that should be measured was known: bone fabric. This brought us to the second question: how can we measure fabric if the resolution of in-vivo images is not good enough to resolve the trabecular architecture?

We developed two approaches that could answer this question, as described in chapters 3 and 4. With the first approach, we used the principle that, for load adapted bone, the bone fabric tensor and the stress tensor should be aligned, hence, the local fabric tensor can be estimated from the stress tensor. With the second approach, a database (DB) of high-resolution models is used in combination with a mesh morphing approach to map the fabric information from one of the database models to a patient image. It was demonstrated in chapters 3 and 4 that both approaches can produce fabric tensors that are close to the true fabric tensors. Whereas both approaches thus were successfully implemented and tested, the pros and cons of both approaches warrant some additional discussion.

The major limitation of the DB approach was already discussed in chapter 3 and is the fact that a large DB is needed. Presently, only a limited number of bones is available, and only for 2 sites: the femur and T12 vertebra. Extending the DB size will require high-resolution imaging and analysis of additional cadaver bones, which is time consuming. At present, scanning a single vertebra takes a few hours, whereas the homogenization procedure takes a few days. Although scanning and processing time likely can be considerably reduced in the near future by using faster micro-CT scanners and new computers, the amount of work involved still inhibits the development of large databases for many sites.

A particular strong point of the DB approach is that it is a very versatile method that possibly can be enhanced in many different ways, of which we mention a few here. First, for the models investigated here, not only bone fabric was measured, but many other bone microstructural parameters (Tb.Th, Tb.Sp, SMI, etc.). To the best of our knowledge, no material laws exist at present that can use this information though. Since this information now is available, it might be interesting to develop material laws that can account for more than just bone density and fabric. This information could also be used to further enhance models that describe continuum-level fluid-structure interaction, e.g. for simulations of cement flow in bone in-vivo. These models usually require some bone microstructural parameters such as Tb.Sp, DA and etc. (Widmer and Ferguson, 2012). To test such material and flow relationships, the techniques developed in chapter 2 could be a valuable tool.

Second, in the present study, we selected the database bone by comparing the density distributions of the patient bone with the DB models. Many other criteria would have been reasonable as well. As already mentioned in chapter 3, it would be possible to also account for

bone size and shape parameters or to include other morphological parameters in the selection procedure. A very different approach, not mentioned before, however, could be to do this comparison not for the whole bone, but per location. E.g. it would be possible to take the fabric at position *x* from model *i*, and the fabric at position *y* from model *j*, because at location *x* the density best agrees with model *i* and at position *y* with model *j*. An advantage of this approach would be that by combining the information of different models, the DB effectively would be extended by a very large number of 'mixed models'. Presently, however, we do not know if this approach would further enhance the results.

Third, the present study still relies on the use of empirical relationships to derive bone elastic and strength properties, but the database approach, in theory, could also provide these mechanical properties directly. It would be possible, for example, to solve micro-FE problems for each element in the DB models. By defining a region of interest centered at each element, similar as done in this thesis to calculate morphological properties, it would be possible to calculate the full anisotropic bone elastic properties as well as the multi-axial yield and failure surfaces. By pre-calculating these for each element, these can be mapped directly to the patient bone. The amount of work involved for the pre-calculation of these properties, however, is tremendous.

Fourth, it is possible to extend the DB by creating 'virtual' bone models. Such models can be obtained, e.g. from bone remodeling simulations, that simulate the effects of osteoporosis, drug treatment, physical activity etc. Some of such analyses were already performed as part of the VPHOP project. Although such analyses could lead to non-physiological bone density and microstructure distributions, this might not be a major problem for including these in the DB. DB models with an unrealistic density distribution will never be selected and, eventually could be removed from the DB.

For the other approach, estimating fabric from the stress, the major limitation is that it assumes that bone is fully load adapted. From other work it is known that this is not the case (Christen et al., 2013). This is likely because bone also serves other functions, such as a reservoir for calcium. Another limitation is that the approach will only produce accurate results if the full loading history that it is remodeled to is applied to calculate the time-averaged stress tensor. In practice, such loading histories are not known, although as also mentioned in chapter 3, they can be estimated from the density distribution (Campoli et al., 2012). A final limitation is that this approach obviously is limited to estimating the fabric tensor; other morphological parameters cannot be estimated.

But this approach also has some strong points. First, it does not require a DB to be developed, and thus might be the only possible tool for most sites. Second, it can also predict a fabric tensor for the cortical bone, which is not possible with the DB approach, since that would

require high resolution images that can resolve the haversian system and possibly also the canalicular network. The fabric tensor generated by the estimation approach can be considered as an 'effective' fabric tensor that might not accurately reflect the microscopic morphological features, but might well reflect the features relevant for the mechanical anisotropy.

Using these approaches, we were also able to answer the third question (are the results of such enhanced models really better than those of isotropic models?). Generally speaking, results of models that implement anisotropic mechanical properties based on estimated or DB-derived fabric and density were in closer agreement to those of models based on measured fabric and density than the results of isotropic models that take only density into account. However, when looking at stress/strain distributions, differences were rather small, and by 'tweaking' constants, the isotropic models can produce force-displacement curves very close to those of anisotropic models. Nevertheless, as also suggested in chapter 3, the use of anisotropic models is worthwhile in case of modeling the mechanical behavior of implants, where loads are applied in a directions that differs considerably from the normal loading directions. In particular in this case local stress and strain concentrations might play an important role, and accounting for material anisotropy might be an important requirement for the calculation of these local conditions.

Whereas we thus found answers to the questions originally posed when we started this work, the successful development of the bone database inspired us to address new questions. Further analysis of the DB entries of femurs and vertebrae revealed that, at some locations there is a large variation in local bone morphological parameters between individuals. The obvious question then is: what is the inter-individual variation between subjects and how do these depend on location (chapter 5)?

A large variability in bone morphology between subjects was found for the neck and trochanter regions in femurs, and near the endplates of vertebrae. These regions are important anchoring sites for implants (e.g. hip implants and disc implants) and this variation thus might be an important determinant for the success rate of such implants. We therefore expect that the very detailed results presented here can help to optimize implants and orthopaedic procedures by identifying anchoring regions for implants or screws in which bone quality is generally good. The results obtained here also gave raise to further questions: what is the cause for these large local variations between subjects? Are these differences related to gender/ethnicity/age etc.? Addressing such questions, however, would require a considerable extension of the database and therefore could not be answered now.

At many sites the differences in density and morphology between individuals was much larger than the difference in whole bone BMD. This finding made us ask a second additional

question: would it be possible to improve the prediction of bone strength if it is based on the measurement of bone density or morphology at a specific location, rather than on whole bone density as done with DXA. Results in chapter 6 demonstrated that this is indeed the case. Bone density measured at a specific location in the center of vertebrae can explain over 90% of the variation in vertebral strength. Interestingly, FE analyses revealed that these locations were not identified as the weakest spot, at least not for the compressive loading conditions applied here. It is possible though, that the application of more diverse and complex loading conditions would provide new information about the mechanical importance of these regions.

Adding more morphological parameters could further enhance the prediction. The measurement of such additional morphological parameters is not possible in-vivo. However, it might be possible to use the same approach as we used in other studies: use a DB to derive these morphological parameters.

In summary, in this research project, we were able to provide answers to several intriguing questions related to the diagnosis of bone strength. To do so, we introduced a new approach to validate morphology-elasticity relationships, alternative approaches to build patient specific anisotropic FE models, a new computational tool to quantify local bone morphological parameters at the element level and a new stochastic relationship to predict bone strength directly from bone morphological parameters. Apart from answering the questions that we posed, we expect that these tools can help to better explore bone tissue and to continue the journey started centuries ago to understand bone tissue.

Summary

Continuum finite element (FE) analysis has become a standard computational tool for the analysis of bone mechanical behavior in orthopaedic biomechanics. Such models are used, e.g. for the pre-clinical evaluation of orthopaedic implants and treatments and for the evaluation of bone strength in osteoporotic patients. These models are usually based on clinical CT scans and thus can account for the patient-specific geometry and density distribution. In most models, however, the bone material properties are modeled in a rather simplified manner. First, the elastic and failure behavior is usually modeled as isotropic, even though it is known that the underlying microstructure can result in highly anisotropic material behavior, in particular for cancellous bone. Second, the failure behavior is often described as elastic-plastic only, which cannot well describe the damage accumulation, localization and softening behavior as is typically seen, e.g. in overloaded vertebrae. More enhanced material models to describe anisotropic and failure behavior of bone do exist, but their clinical application is limited by the fact that these require a reliable homogenization of the underlying bone microstructure, in particular its density and directionality ('fabric'). The latter, however, cannot be measured from clinical CT images.

To make it possible to use such microstructure-enhanced material models for patient FE-analysis, we here develop alternative approaches to obtain homogenized bone density and microstructural information, which can be used even when only clinical CT images are available. We further test if the use of non-linear continuum FE models that implement such microstructure-enhanced material models can improve the prediction of bone mechanical properties and strength compared to FE-models that use simpler material models and compared to statistical models that relate bone strength directly to density or microstructure measurements.

The first question we addressed is how we can identify the accuracy of FE-models that implement different material behavior. In the past, experimental tests using strain gauges have been used to validate results of FE-analysis. However, such measurements are limited to the bone surface and thus cannot be used to validate the stress or strain distribution within the cancellous bone region. In a first study, we therefore introduce a novel computational approach that uses results of micro-FE models, which can represent the bone trabecular architecture in detail, as a reference. By comparing the homogenized micro-FE stress results to stress results obtained from continuum FE models that implement isotropic and anisotropic properties, it is possible to identify the errors related to the use of empirical relationships that translate bone density and microstructure to stiffness. First results demonstrated that the Zysset-Curnier fabric-elasticity relationship can well replicate the stress distribution and

whole bone stiffness as obtained from the homogenized micro-FE results, and that models implementing anisotropic properties can provide more accurate results than isotropic models.

The second question we addressed is how we can obtain bone fabric information, which is needed for such anisotropic fabric-elasticity relationships, if we are not able to measure this from clinical CT scans. Two approaches were proposed and tested. The first approach is based on the notion that the bone micro-architecture is adapted to the continuum-level stress state. As a result of this adaptation, the principal directions of the fabric and stress tensors will align. We here explore this concept in the inverse way: to derive the fabric tensor from the stress tensor as obtained from continuum FE-analysis for physiological loading conditions. In this inverse analysis, the material properties in the FE-model are iteratively changed from isotropic to anisotropic, based on the predicted fabric tensor, until convergence is reached. The fabric thus estimated is compared to real fabric measurements obtained from micro-CT measurements for validation. We found that this approach generally leads to acceptable estimates of the fabric tensor orientation, although at some locations large deviations between the estimated and measured fabric tensor exist. Also, the degree of anisotropy was not predicted well. In spite of this, the stress calculation based on the model with estimated and measured fabric tensors compared very well, suggesting that such errors in fabric estimation do not affect the stress calculation too much.

The second approach explores the concept of using a database of high-resolution bone models to derive the fabric information that is missing in clinical images. For this purpose, databases of human proximal femurs and T12 vertebrae were generated from micro-CT scans and continuum FE models were generated from the images using a pre-defined mesh template and an iso-anatomic mesh morphing procedure. With this procedure, each element within the mesh template is at a specific anatomical location which enabled us to identify density and microstructural properties at these anatomical locations for all samples. This makes it possible to map microstructural parameters that cannot be measured for patients from a best matching model in the database. By combining the patient-specific density information measured from the CT scan with fabric information from the database, the microstructure-enhanced anisotropic material models can be used for non-linear failure analysis of a patient's bone. We demonstrated that such models with database-derived fabric predict similar mechanical stresses, stiffness and strength as models based on the actually measured bone fabric. We therefore expect that this approach can lead to more accurate results in particular for cases where bone anisotropy plays an important role, such as in osteoporotic patients and around implants.

Using the database and mapping approach described above it was also possible to create a map of the average subject density for each element in the mesh template, as well as of its variation between subjects. Similar maps could be made for all microstructural parameters.

These maps demonstrated that the variation at some location is high, whereas at other location always a very similar parameter value was found. This led us to the next question that we addressed: would it be possible to predict bone strength from bone density or other parameter measured locally at a very specific 'critical site' directly using a statistical model? To investigate this, we correlated bone density and structural parameters as determined for each element in the mesh template to whole bone strength data obtained from compression tests performed on the same bones. The results show that local volume fraction when measured at the optimal location can explain up to 90% of the variation in vertebral strength (n=18). Adding more morphological parameters in a multi-regression analysis between bone morphological parameters and vertebral strength can raise this value to 98%. These predictions were even better than those obtained from non-linear continuum FE-analysis. Although such local density/morphology based predictions will not provide nearly as much information as FE-analyses, they might be a viable alternative in case only bone strength predictions are required.

References

Ascenzi, M.G., Hetzer, N., Lomovtsev, A., Rude, R., Nattiv, A., Favia, A., 2011. Variation of trabecular architecture in proximal femur of postmenopausal women. Journal of Biomechanics 44, 248-256.

Ashman, R.B., Jae Young, R., 1988. Elastic modulus of trabecular bone material. Journal of Biomechanics 21, 177-181.

Ashman, R.B., Rho, J.Y., Turner, C.H., 1989. Anatomical variation of orthotropic elastic moduli of the proximal human tibia. Journal of Biomechanics 22, 895-900.

Banse, X., Devogelaer, J.P., Grynpas, M., 2002. Patient-specific microarchitecture of vertebral cancellous bone: a peripheral quantitative computed tomographic and histological study. Bone 30, 829-835.

Banse, X., Devogelaer, J.P., Munting, E., Delloye, C., Cornu, O., Grynpas, M., 2001. Inhomogeneity of human vertebral cancellous bone: systematic density and structure patterns inside the vertebral body. Bone 28, 563-571.

Bergmann G., Graichen F., Rohlmann A., A. Bender, B. Heinlein, G.N. Duda, M.O. Heller, Morlock, M.M., 2010. Realistic loads for testing hip implants Bio-Medical Materials and Engineering 20, 65-75.

Biewener, A.A., 1992. Biomechanics--structures and systems: a practical approach. Oxford University Press, USA.

Bousson, V., Le Le Bras, A., Roqueplan, F., Kang, Y., Mitton, D., Kolta, S., Bergot, C., Skalli, W., Vicaut, E., Kalender, W., Engelke, K., Laredo, J.D., 2006. Volumetric quantitative computed tomography of the proximal femur: relationships linking geometric and densitometric variables to bone strength. Role for compact bone. Osteoporosis International 17, 855-864.

Boutroy, S., Bouxsein, M.L., Munoz, F., Delmas, P.D., 2005. In Vivo Assessment of Trabecular Bone Microarchitecture by High-Resolution Peripheral Quantitative Computed Tomography. Journal of Clinical Endocrinology & Metabolism 90, 6508-6515.

Bredella, M.A., Misra, M., Miller, K.K., Madisch, I., Sarwar, A., Cheung, A., Klibanski, A., Gupta, R., 2008. Distal Radius in Adolescent Girls with Anorexia Nervosa: Trabecular Structure Analysis with High-Resolution Flat-Panel Volume CT1. Radiology 249, 938-946.

Brekelmans, W.A.M., Poort, H.W., Slooff, T.J.J.H., 1972. A New Method to Analyse the Mechanical Behaviour of Skeletal Parts. Acta Orthopaedica 43, 301-317.

Buckley, J.M., Loo, K., Motherway, J., 2007. Comparison of quantitative computed tomography-based measures in predicting vertebral compressive strength. Bone 40, 767-774.

Burghardt, A., Link, T., Majumdar, S., 2011. High-resolution Computed Tomography for Clinical Imaging of Bone Microarchitecture. Clin Orthop Relat Res 469, 2179-2193.

Burrows, M., Liu, D., McKay, H., 2010. High-resolution peripheral QCT imaging of bone micro-structure in adolescents. Osteoporosis International 21, 515-520.

Campoli, G., Weinans, H., Zadpoor, A.A., 2012. Computational load estimation of the femur. Journal of the Mechanical Behavior of Biomedical Materials 10, 108-119.

Carballido-Gamio, J., Harnish, R., Saeed, I., Streeper, T., Sigurdsson, S., Amin, S., Atkinson, E.J., Therneau, T.M., Siggeirsdottir, K., Cheng, X., Melton, L.J., Keyak, J., Gudnason, V., Khosla, S., Harris, T.B., Lang, T.F., 2013. Proximal femoral density distribution and structure in relation to age and hip fracture risk in women. Journal of Bone and Mineral Research 28, 537-546.

Carter, D.R., Hayes, W.C., 1976. Bone compressive strength: the influence of density and strain rate. Science 194, 1174-1176.

Carter, D.R., Hayes, W.C., 1977. The compressive behavior of bone as a two-phase porous structure. J Bone Joint Surg Am 59, 954-962.

Chappard, D., Legrand, E., Pascaretti, C., Baslé, M.F., Audran, M., 1999. Comparison of eight histomorphometric methods for measuring trabecular bone architecture by image analysis on histological sections. Microscopy Research and Technique 45, 303-312.

Charlebois, M., Jirasek, M., Zysset, P.K., 2010. A nonlocal constitutive model for trabecular bone softening in compression. Biomech Model Mechanobiol 9, 597-611.

Cheng, X.G., Lowet, G., Boonen, S., Nicholson, P.H.F., Brys, P., Nijs, J., Dequeker, J., 1997a. Assessment of the strength of proximal femur in vitro: Relationship to femoral bone mineral density and femoral geometry. Bone 20, 213-218.

Cheng, X.G., Nicholson, P.H.F., Boonen, S., Lowet, G., Brys, P., Aerssens, J., van der Perre, G., Dequeker, J., 1997b. Prediction of Vertebral Strength In Vitro by Spinal Bone Densitometry and Calcaneal Ultrasound. Journal of Bone and Mineral Research 12, 1721-1728.

Cheung, A., Bredella, M., Al Khalaf, M.m., Grasruck, M., Leidecker, C., Gupta, R., 2009. Reproducibility of trabecular structure analysis using flat-panel volume computed tomography. Skeletal Radiology 38, 1003-1008.

Chevalier, Y., Pahr, D., Zysset, P.K., 2008. Anatomy- and morphology-based smooth finite element models of the vertebral body. Journal of Biomechanics 41, S252-S252.

Chevalier, Y., Quek, E., Borah, B., Gross, G., Stewart, J., Lang, T., Zysset, P., 2010. Biomechanical effects of teriparatide in women with osteoporosis treated previously with alendronate and risedronate: results from quantitative computed tomography-based finite element analysis of the vertebral body. Bone 46, 41-48.

Chintalapani, G., Ellingsen, L., Sadowsky, O., Prince, J., Taylor, R., 2007. Statistical Atlases of Bone Anatomy: Construction, Iterative Improvement and Validation, in: Ayache, N., Ourselin, S., Maeder, A. (Eds.), Medical Image Computing and Computer-Assisted Intervention – MICCAI 2007. Springer Berlin Heidelberg, pp. 499-506.

Christen, P., Ito, K., Santos, A.A.d., Müller, R., van Rietbergen, B., 2013. Validation of a bone loading estimation algorithm for patient-specific bone remodelling simulations. Journal of Biomechanics 46, 941-948.

Christen, P., van Rietbergen, B., Lambers, F., Müller, R., Ito, K., 2012. Bone morphology allows estimation of loading history in a murine model of bone adaptation. Biomech Model Mechanobiol 11, 483-492.

Ciarelli, T.E., Fyhrie, D.P., Schaffler, M.B., Goldstein, S.A., 2000. Variations in Three-Dimensional Cancellous Bone Architecture of the Proximal Femur in Female Hip Fractures and in Controls. Journal of Bone and Mineral Research 15, 32-40.

Courtney, A.C., Wachtel, E.F., Myers, E.R., Hayes, W.C., 1994. Effects of loading rate on strength of the proximal femur. Calcif Tissue Int 55, 53-58.

Courtney, A.C., Wachtel, E.F., Myers, E.R., Hayes, W.C., 1995. Age-related reductions in the strength of the femur tested in a fall-loading configuration. J Bone Joint Surg Am 77, 387-395.

Cowin, S.C., 1985. The relationship between the elasticity tensor and the fabric tensor. Mechanics of Materials 4, 137-147.

Cowin, S.C., Mehrabadi, M.M., 1989. Identification of the elastic symmetry of bone and other materials. Journal of Biomechanics 22, 503-515.

Cowin, S.C., Turner, C.H., 1992. On the relationship between the orthotropic Young's moduli and fabric. Journal of Biomechanics 25, 1493-1494.

Crawford, R.P., Cann, C.E., Keaveny, T.M., 2003. Finite element models predict in vitro vertebral body compressive strength better than quantitative computed tomography. Bone 33, 744-750.

Cui, W.Q., Won, Y.Y., Baek, M.H., Lee, D.H., Chung, Y.S., Hur, J.H., Ma, Y.Z., 2008. Age- and region-dependent changes in three-dimensional microstructural properties of proximal femoral trabeculae. Osteoporosis International 19, 1579-1587.

Currey, J., 2002. Bones: structure and mechanics. Princeton University Press.

Currey, J., 2009. Measurement of the Mechanical Properties of Bone: A Recent History. Clin Orthop Relat Res 467, 1948-1954.

Currey, J., 2012. The structure and mechanics of bone. J Mater Sci 47, 41-54.

Dall'ara, E., Schmidt, R., Pahr, D., Varga, P., Chevalier, Y., Patsch, J., Kainberger, F., Zysset, P., 2010. A nonlinear finite element model validation study based on a novel experimental technique for inducing anterior wedge-shape fractures in human vertebral bodies in vitro. J Biomech.

Dalle Carbonare, L., Giannini, S., 2004. Bone microarchitecture as an important determinant of bone strength. Journal of endocrinological investigation 27, 99-105.

Dopico-González, C., New, A.M., Browne, M., 2010. Probabilistic finite element analysis of the uncemented hip replacement—effect of femur characteristics and implant design geometry. Journal of Biomechanics 43, 512-520.

Duan, Y., Parfitt, A.M., Seeman, E., 1999. Vertebral Bone Mass, Size, and Volumetric Density in Women with Spinal Fractures. Journal of Bone and Mineral Research 14, 1796-1802.

Ebbesen, E.N., Thomsen, J.S., Beck-Nielsen, H., Nepper-Rasmussen, H.J., Mosekilde, L., 1999. Lumbar vertebral body compressive strength evaluated by dual-energy X-ray absorptiometry, quantitative computed tomography, and ashing. Bone 25, 713-724.

Eckstein, F., Kuhn, V., Lochmüller, E.-M., 2004. Strength Prediction of the Distal Radius by Bone Densitometry—Evaluation Using Biomechanical Tests. Annals of Biomedical Engineering 32, 487-503.

Edmondston, S.J., Singer, K.P., Day, R.E., Breidahl, P.D., Price, R.I., 1994a. Formalin fixation effects on vertebral bone density and failure mechanics: an in-vitro study of human and sheep vertebrae. Clinical Biomechanics 9, 175-179.

Edmondston, S.J., Singer, K.P., Day, R.E., Breidahl, P.D., Price, R.I., 1994b. In-vitro relationships between vertebral body density, size, and compressive strength the elderly thoracolumbar spine. Clinical Biomechanics 9, 180-186.

Farahmand, B., Michaëlsson, K., Ahlbom, A., Ljunghall, S., Baron, J., 2005. Survival after hip fracture. Osteoporosis International 16, 1583-1590.

Fields, A.J., Nawathe, S., Eswaran, S.K., Jekir, M.G., Adams, M.F., Papadopoulos, P., Keaveny, T.M., 2012. Vertebral fragility and structural redundancy. Journal of Bone and Mineral Research 27, 2152-2158.

Forsén, L., Søgaard, A.J., Meyer, H.E., Edna, T.H., Kopjar, B., 1999. Survival after Hip Fracture: Short- and Long-Term Excess Mortality According to Age and Gender. Osteoporosis International 10, 73-78.

Fyhrie, D.P., Carter, D.R., 1986. A unifying principle relating stress to trabecular bone morphology. Journal of Orthopaedic Research 4, 304-317.

Gass, M., Dawson-Hughes, B., 2006. Preventing Osteoporosis-Related Fractures: An Overview. The American Journal of Medicine 119, S3-S11.

Gong, H., Zhang, M., Qin, L., Lee, K.K.H., Guo, X., Shi, S.Q., 2006. Regional variations in microstructural properties of vertebral trabeculae with structural groups. Spine 31, 24-32.

Grant, J.P., Oxland, T.R., Dvorak, M.F., Fisher, C.G., 2002. The effects of bone density and disc degeneration on the structural property distributions in the lower lumbar vertebral endplates. Journal of Orthopaedic Research 20, 1115-1120.

Grassi, L., Hraiech, N., Schileo, E., Ansaloni, M., Rochette, M., Viceconti, M., 2011. Evaluation of the generality and accuracy of a new mesh morphing procedure for the human femur. Medical Engineering & Physics 33, 112-120.

Grigoryan, M., Guermazi, A., Roemer, F., Delmas, P., Genant, H., 2003. Recognizing and reporting osteoporotic vertebral fractures. European Spine Journal 12, S104-S112.

Grisso, J.A., Kelsey, J.L., Strom, B.L., Ghiu, G.Y., Maislin, G., O'Brien, L.A., Hoffman, S., Kaplan, F., 1991. Risk factors for falls as a cause of hip fracture in women. New England Journal of Medicine 324, 1326-1331.

Gross, T., Pahr, D., Zysset, P., 2013. Morphology–elasticity relationships using decreasing fabric information of human trabecular bone from three major anatomical locations. Biomech Model Mechanobiol 12, 793-800.

Gullberg, B., Johnell, O., Kanis, J.A., 1997. World-wide Projections for Hip Fracture. Osteoporosis International 7, 407-413.

Guo, X.E., Kim, C.H., 2002. Mechanical consequence of trabecular bone loss and its treatment: a three-dimensional model simulation. Bone 30, 404-411.

Gupta, R., Grasruck, M., Suess, C., Bartling, S., Schmidt, B., Stierstorfer, K., Popescu, S., Brady, T., Flohr, T., 2006. Ultra-high resolution flat-panel volume CT: fundamental principles, design architecture, and system characterization. European Radiology 16, 1191-1205.

Haïat, G., Padilla, F., Barkmann, R., Gluer, C.C., Laugier, P., 2006. Numerical simulation of the dependence of quantitative ultrasonic parameters on trabecular bone microarchitecture and elastic constants. Ultrasonics 44, Supplement, e289-e294.

Haïat, G., Padilla, F., Svrcekova, M., Chevalier, Y., Pahr, D., Peyrin, F., Laugier, P., Zysset, P., 2009. Relationship between ultrasonic parameters and apparent trabecular bone elastic modulus: A numerical approach. Journal of Biomechanics 42, 2033-2039.

Harrigan, T.P., Jasty, M., Mann, R.W., Harris, W.H., 1988. Limitations of the continuum assumption in cancellous bone. Journal of Biomechanics 21, 269-275.

Harrigan, T.P., Mann, R.W., 1984. Characterization of microstructural anisotropy in orthotropic materials using a second rank tensor. J Mater Sci 19, 761-767.

Hazrati Marangalou, J., Ito, K., Cataldi, M., Taddei, F., van Rietbergen, B., 2013. A novel approach to estimate trabecular bone anisotropy using a database approach. Journal of Biomechanics.

Hazrati Marangalou, J., Ito, K., van Rietbergen, B., 2012. A new approach to determine the accuracy of morphology–elasticity relationships in continuum FE analyses of human proximal femur. Journal of Biomechanics 45, 2884-2892.

Hedlund, R., Lindgren, U., 1987. Trauma type, age, and gender as determinants of hip fracture. Journal of Orthopaedic Research 5, 242-246.

Helgason, B., Perilli, E., Schileo, E., Taddei, F., Brynjólfsson, S., Viceconti, M., 2008. Mathematical relationships between bone density and mechanical properties: A literature review. Clinical Biomechanics 23, 135-146.

Heller, M.O., Bergmann, G., Kassi, J.P., Claes, L., Haas, N.P., Duda, G.N., 2005. Determination of muscle loading at the hip joint for use in pre-clinical testing. Journal of Biomechanics 38, 1155-1163.

Hengsberger, S., Kulik, A., Zysset, P., 2002. Nanoindentation discriminates the elastic properties of individual human bone lamellae under dry and physiological conditions. Bone 30, 178-184.

Hordon, L.D., Raisi, M., Aaron, J.E., Paxton, S.K., Beneton, M., Kanis, J.A., 2000. Trabecular architecture in women and men of similar bone mass with and without vertebral fracture: I. two-dimensional histology. Bone 27, 271-276.

Huiskes, R., 1993. Mechanical failure in total hip arthroplasty with cement. Current Orthopaedics 7, 239-247.

Huiskes, R., Chao, E.Y.S., 1983. A survey of finite element analysis in orthopedic biomechanics: The first decade. Journal of Biomechanics 16, 385-409.

Huiskes, R., Janssen, J., Slooff, T., 1981. A detailed comparison of experimental and theoretical stress-analyses of a human femur. Mechanical properties of Bone 45, 211-234.

Huiskes, R., Weinans, H.H., Rietbergen, B.v., 1992. The relationship between stress shielding and bone resorption around total hip stems and the effects of flexible materials. Clinical Orthopaedics and Related Research, 124-134.

Hulme, P.A., Boyd, S.K., Ferguson, S.J., 2007. Regional variation in vertebral bone morphology and its contribution to vertebral fracture strength. Bone 41, 946-957.

Imai, K., Ohnishi, I., Bessho, M., Nakamura, K., 2006. Nonlinear Finite Element Model Predicts Vertebral Bone Strength and Fracture Site. Spine 31.

Johnell, O., 1997. The socioeconomic burden of fractures: Today and in the 21st century. The American Journal of Medicine 103, S20-S26.

Johnell, O., Kanis, J., 2005. Epidemiology of osteoporotic fractures. Osteoporosis International 16, S3-S7.

Johnell, O., Kanis, J.A., Odén, A., Sernbo, I., Redlund-Johnell, I., Petterson, C., Laet, C., Jönsson, B., 2004. Mortality after osteoporotic fractures. Osteoporosis International 15, 38-42.

Kabel, J., Odgaard, A., van Rietbergen, B., Huiskes, R., 1999a. Connectivity and the elastic properties of cancellous bone. Bone 24, 115-120.

Kabel, J., van Rietbergen, B., Odgaard, A., Huiskes, R., 1999b. Constitutive relationships of fabric, density, and elastic properties in cancellous bone architecture. Bone 25, 481-486.

Kanis, J., Borgstrom, F., Laet, C., Johansson, H., Johnell, O., Jonsson, B., Oden, A., Zethraeus, N., Pfleger, B., Khaltaev, N., 2005. Assessment of fracture risk. Osteoporosis International 16, 581-589.

Kanis, J.A., 1994. Assessment of fracture risk and its application to screening for postmenopausal osteoporosis: Synopsis of a WHO report. Osteoporosis International 4, 368-381.

Kanis, J.A., 2002. Diagnosis of osteoporosis and assessment of fracture risk. The Lancet 359, 1929-1936.

Keaveny, T.M., Morgan, E.F., Yeh, O.C., 2009. Bone mechanics. Biomechanics of the Human Body, McGraw-Hill.

Keller, T.S., 1994. Predicting the compressive mechanical behavior of bone. Journal of Biomechanics 27, 1159-1168.

Keyak, J.H., 2001. Improved prediction of proximal femoral fracture load using nonlinear finite element models. Medical Engineering & Physics 23, 165-173.

Keyak, J.H., Fourkas, M.G., Meagher, J.M., Skinner, H.B., 1993. Validation of an automated method of three-dimensional finite element modelling of bone. Journal of Biomedical Engineering 15, 505-509.

Keyak, J.H., Lee, I.Y., Skinner, H.B., 1994. Correlations between orthogonal mechanical properties and density of trabecular bone: Use of different densitometric measures. Journal of Biomedical Materials Research 28, 1329-1336.

Keyak, J.H., Rossi, S.A., Jones, K.A., Skinner, H.B., 1997. Prediction of femoral fracture load using automated finite element modeling. Journal of Biomechanics 31, 125-133.

Kopperdahl, D.L., Roberts, A.D., Keaveny, T.M., 1999. Localized Damage in Vertebral Bone Is Most Detrimental in Regions of High Strain Energy Density. Journal of biomechanical engineering 121, 622-628.

Lai, Y.M., Qin, L., Yeung, H.Y., Lee, K.K.H., Chan, K.M., 2005. Regional differences in trabecular BMD and micro-architecture of weight-bearing bone under habitual gait loading—A pQCT and microCT study in human cadavers. Bone 37, 274-282.

Lang, T., Augat, P., Majumdar, S., Ouyang, X., Genant, H.K., 1998. Noninvasive Assessment of Bone Density and Structure Using Computed Tomography and Magnetic Resonance. Bone 22, 149S-153S.

Lang, T.F., Li, J., Harris, S.T., Genant, H.K., 1999. Assessment of Vertebral Bone Mineral Density Using Volumetric Quantitative CT. Journal of Computer Assisted Tomography 23.

Legrand, E., Chappard, D., Pascaretti, C., Duquenne, M., Krebs, S., Rohmer, V., Basle, M.-F., Audran, M., 2000. Trabecular Bone Microarchitecture, Bone Mineral Density, and Vertebral Fractures in Male Osteoporosis. Journal of Bone and Mineral Research 15, 13-19.

Lepore, F., Brun, C., Yi-Yu, C., Ming-Chang, C., Dutton, R.A., Hayashi, K.M., Luders, E., Lopez, O.L., Aizenstein, H.J., Toga, A.W., Becker, J.T., Thompson, P.M., 2008. Generalized Tensor-Based Morphometry of HIV/AIDS Using Multivariate Statistics on Deformation Tensors. Medical Imaging, IEEE Transactions on 27, 129-141.

Liebschner, M.A.K., Kopperdahl, D.L., Rosenberg, W.S., Keaveny, T.M., 2003. Finite Element Modeling of the Human Thoracolumbar Spine. Spine 28, 559-565.

Link, T.M., Vieth, V., Langenberg, R., Meier, N., Lotter, A., Newitt, D., Majumdar, S., 2003. Structure Analysis of High Resolution Magnetic Resonance Imaging of the Proximal Femur: In Vitro Correlation with Biomechanical Strength and BMD. Calcified Tissue International 72, 156-165.

Little, J.P., Taddei, F., Viceconti, M., Murray, D.W., Gill, H.S., 2007. Changes in femur stress after hip resurfacing arthroplasty: Response to physiological loads. Clinical Biomechanics 22, 440-448.

Liu, X.S., Zhang, X.H., Sekhon, K.K., Adams, M.F., McMahon, D.J., Bilezikian, J.P., Shane, E., Guo, X.E., 2010. High-resolution peripheral quantitative computed tomography can assess

microstructural and mechanical properties of human distal tibial bone. Journal of Bone and Mineral Research 25, 746-756.

Lochmüller, E.-M., Müller, R., Kuhn, V., Lill, C.A., Eckstein, F., 2003. Can Novel Clinical Densitometric Techniques Replace or Improve DXA in Predicting Bone Strength in Osteoporosis at the Hip and Other Skeletal Sites? Journal of Bone and Mineral Research 18, 906-912.

Lochmüller, E.M., Bürklein, D., Kuhn, V., Glaser, C., Müller, R., Glüer, C.C., Eckstein, F., 2002. Mechanical strength of the thoracolumbar spine in the elderly: prediction from in situ dual-energy X-ray absorptiometry, quantitative computed tomography (QCT), upper and lower limb peripheral QCT, and quantitative ultrasound. Bone 31, 77-84.

Lochmüller, E.M., Krefting, N., Bürklein, D., Eckstein, F., 2001. Effect of Fixation, Soft-Tissues, and Scan Projection on Bone Mineral Measurements with Dual Energy X-ray Absorptiometry (DXA). Calcified Tissue International 68, 140-145.

Lochmüller, E.M., Miller, P., Bürklein, D., Wehr, U., Rambeck, W., Eckstein, F., 2000. In Situ Femoral Dual-Energy X-ray Absorptiometry Related to Ash Weight, Bone Size and Density, and its Relationship with Mechanical Failure Loads of the Proximal Femur. Osteoporosis International 11, 361-367.

Lochmüller, E.M., Pöschl, K., Würstlin, L., Matsuura, M., Müller, R., Link, T.M., Eckstein, F., 2008. Does thoracic or lumbar spine bone architecture predict vertebral failure strength more accurately than density? Osteoporosis International 19, 537-545.

Lotz, J.C., Gerhart, T.N., Hayes, W.C., 1991. Mechanical properties of metaphyseal bone in the proximal femur. Journal of Biomechanics 24, 317-329.

MacNeil, J.A., Boyd, S.K., 2008. Bone strength at the distal radius can be estimated from high-resolution peripheral quantitative computed tomography and the finite element method. Bone 42, 1203-1213.

Malandrino, A., Fritsch, A., Lahayne, O., Kropik, K., Redl, H., Noailly, J., Lacroix, D., Hellmich, C., 2012. Anisotropic tissue elasticity in human lumbar vertebra, by means of a coupled ultrasound-micromechanics approach. Materials Letters 78, 154-158.

Matsumoto, T., Ohnishi, I., Bessho, M., Imai, K., Ohashi, S., Nakamura, K., 2009. Prediction of Vertebral Strength Under Loading Conditions Occurring in Activities of Daily Living Using a Computed Tomography-Based Nonlinear Finite Element Method. Spine 34.

Matsuura, M., Eckstein, F., Lochmuller, E.M., Zysset, P.K., 2008. The role of fabric in the quasi-static compressive mechanical properties of human trabecular bone from various anatomical locations. Biomech Model Mechanobiol 7, 27-42.

Meyer, H.v., 1867. Die architektur der spongiosa. Arch Anat Physiol Wiss Med 34, 615-628.

Morgan, E.F., Bayraktar, H.H., Keaveny, T.M., 2003. Trabecular bone modulus-density relationships depend on anatomic site. Journal of Biomechanics 36, 897-904.

Morgan, E.F., Yeh, O.C., Chang, W.C., Keaveny, T.M., 2001. Nonlinear behavior of trabecular bone at small strains. Journal of biomechanical engineering 123, 1-9.

Moro, M., Hecker, A.T., Bouxsein, M.L., Myers, E.R., 1995. Failure load of thoracic vertebrae correlates with lumbar bone mineral density measured by DXA. Calcified Tissue International 56, 206-209.

Mueller, T.L., van Lenthe, G.H., Stauber, M., Gratzke, C., Eckstein, F., Müller, R., 2009. Regional, age and gender differences in architectural measures of bone quality and their correlation to bone mechanical competence in the human radius of an elderly population. Bone 45, 882-891.

Mulder, L., van Rietbergen, B., Noordhoek, N.J., Ito, K., Determination of vertebral and femoral trabecular morphology and stiffness using a flat-panel C-arm-based CT approach. Bone 50, 200-208.

Mulder, L., van Rietbergen, B., Noordhoek, N.J., Ito, K., 2012. Determination of vertebral and femoral trabecular morphology and stiffness using a flat-panel C-arm-based CT approach. Bone 50, 200-208.

Müller, R., Van Campenhout, H., Van Damme, B., Van der Perre, G., Dequeker, J., Hildebrand, T., Rüegsegger, P., 1998. Morphometric Analysis of Human Bone Biopsies: A Quantitative Structural Comparison of Histological Sections and Micro-Computed Tomography. Bone 23, 59-66.

Nagel, E., 1951. Mechanistic Explanation and Organismic Biology. Philosophy and Phenomenological Research 11, 327-338.

Nair, A.K., Gautieri, A., Chang, S.-W., Buehler, M.J., 2013. Molecular mechanics of mineralized collagen fibrils in bone. Nat Commun 4, 1724.

Nazarian, A., Muller, J., Zurakowski, D., Müller, R., Snyder, B.D., 2007. Densitometric, morphometric and mechanical distributions in the human proximal femur. Journal of Biomechanics 40, 2573-2579.

Nepper-Rasmussen, J., Mosekilde, L., 1989. Local Differences in Mineral Content in Vertebral Trabecular Bone Measured by Dual-Energy Computed Tomography. Acta Radiologica 30, 369-371.

Odgaard, A., 1997. Three-dimensional methods for quantification of cancellous bone architecture. Bone 20, 315-328.

Odgaard, A., Kabel, J., van Rietbergen, B., Dalstra, M., Huiskes, R., 1997. Fabric and elastic principal directions of cancellous bone are closely related. Journal of Biomechanics 30, 487-495.

Pahr, D.H., Zysset, P.K., 2009. A comparison of enhanced continuum FE with micro FE models of human vertebral bodies. Journal of Biomechanics 42, 455-462.

Parkinson, I.H., Badiei, A., Stauber, M., Codrington, J., Müller, R., Fazzalari, N.L., 2012. Vertebral body bone strength: The contribution of individual trabecular element morphology. Osteoporosis International 23, 1957-1965.

Peel, N.F.A., Eastell, R., 1994. Diagnostic value of estimated volumetric bone mineral density of the lumbar spine in osteoporosis. Journal of Bone and Mineral Research 9, 317-320.

Pettersen, S.H., Wik, T.S., Skallerud, B., 2009. Subject specific finite element analysis of stress shielding around a cementless femoral stem. Clinical Biomechanics 24, 196-202.

Pithioux, M., Lasaygues, P., Chabrand, P., 2002. An alternative ultrasonic method for measuring the elastic properties of cortical bone. Journal of Biomechanics 35, 961-968.

Polikeit, A., Nolte, L.P., Ferguson, S.J., 2003. The Effect of Cement Augmentation on the Load Transfer in an Osteoporotic Functional Spinal Unit: Finite-Element Analysis. Spine 28.

Prendergast, P.J., 1997. Finite element models in tissue mechanics and orthopaedic implant design. Clinical Biomechanics 12, 343-366.

Prentice, A., Parsons, T.J., Cole, T.J., 1994. Uncritical use of bone mineral density in absorptiometry may lead to size-related artifacts in the identification of bone mineral determinants. The American Journal of Clinical Nutrition 60, 837-842.

Querol, L., Büchler, P., Rueckert, D., Nolte, L., Ballester, M.G., 2006. Statistical Finite Element Model for Bone Shape and Biomechanical Properties, in: Larsen, R., Nielsen, M., Sporring, J. (Eds.), Medical Image Computing and Computer-Assisted Intervention – MICCAI 2006. Springer Berlin Heidelberg, pp. 405-411.

Radcliffe, I.A.J., Taylor, M., 2007. Investigation into the affect of cementing techniques on load transfer in the resurfaced femoral head: A multi-femur finite element analysis. Clinical Biomechanics 22, 422-430.

Rajamani, K.T., Joshi, S.C., Styner, M.A., Year Bone model morphing for enhanced surgical visualization. In Biomedical Imaging: Nano to Macro, 2004. IEEE International Symposium on.

Rauber, A., 1876. Elasticität und Festigkeit der Knochen: anatomisch-physiologische Studie. Engelmann.

Reggiani, B., Cristofolini, L., Varini, E., Viceconti, M., 2007. Predicting the subject-specific primary stability of cementless implants during pre-operative planning: Preliminary validation of subject-specific finite-element models. Journal of Biomechanics 40, 2552-2558.

Reilly, D.T., Burstein, A.H., 1975. The elastic and ultimate properties of compact bone tissue. Journal of Biomechanics 8, 393-405.

Rho, J.Y., Ashman, R.B., Turner, C.H., 1993. Young's modulus of trabecular and cortical bone material: Ultrasonic and microtensile measurements. Journal of Biomechanics 26, 111-119.

Rho, J.Y., Kuhn-Spearing, L., Zioupos, P., 1998. Mechanical properties and the hierarchical structure of bone. Medical Engineering & Physics 20, 92-102.

Rho, J.Y., Zioupos, P., Currey, J.D., Pharr, G.M., 2002. Microstructural elasticity and regional heterogeneity in human femoral bone of various ages examined by nano-indentation. Journal of Biomechanics 35, 189-198.

Rice, J.C., Cowin, S.C., Bowman, J.A., 1988. On the dependence of the elasticity and strength of cancellous bone on apparent density. Journal of Biomechanics 21, 155-168.

Richmond, B.G., Wright, B.W., Grosse, I., Dechow, P.C., Ross, C.F., Spencer, M.A., Strait, D.S., 2005. Finite element analysis in functional morphology. The Anatomical Record Part A: Discoveries in Molecular, Cellular, and Evolutionary Biology 283A, 259-274.

Riggs, B.L., Melton Iii, L.J., 1995. The worldwide problem of osteoporosis: Insights afforded by epidemiology. Bone 17, S505-S511.

Rincon-Kohli, L., Zysset, P.K., 2009. Multi-axial mechanical properties of human trabecular bone. Biomech Model Mechanobiol 8, 195-208.

Roesler, H., 1987. The history of some fundamental concepts in bone biomechanics. Journal of Biomechanics 20, 1025-1034.

Rohlmann, A., Mössner, U., Bergmann, G., Kölbel, R., 1983. Finite-element-analysis and experimental investigation in a femur with hip endoprosthesis. Journal of Biomechanics 16, 727-742.

Roux, W., 1881. Der züchtende Kampf der Theile, oder die 'Theilauslese'im Organismus (The struggle of the components within organisms). Wilhelm Englemann: Leipzig.

Saha, P.K., Wehrli, F.W., 2004. A robust method for measuring trabecular bone orientation anisotropy at in vivo resolution using tensor scale. Pattern Recognition 37, 1935-1944.

Schwartzman, A., Dougherty, R.F., Taylor, J.E., 2010. Group Comparison of Eigenvalues and Eigenvectors of Diffusion Tensors. Journal of the American Statistical Association 105, 588-599.

Seeman, E., Duan, Y., Fong, C., Edmonds, J., 2001. Fracture Site-Specific Deficits in Bone Size and Volumetric Density in Men with Spine or Hip Fractures. Journal of Bone and Mineral Research 16, 120-127.

Siris Es, C.Y.A.T.A., et al., 2004. Bone mineral density thresholds for pharmacological intervention to prevent fractures. Archives of Internal Medicine 164, 1108-1112.

Sode, M., Burghardt, A.J., Kazakia, G.J., Link, T.M., Majumdar, S., 2010. Regional variations of gender-specific and age-related differences in trabecular bone structure of the distal radius and tibia. Bone 46, 1652-1660.

Sran, M.M., Boyd, S.K., Cooper, D.M.L., Khan, K.M., Zernicke, R.F., Oxland, T.R., 2007. Regional trabecular morphology assessed by micro-CT is correlated with failure of aged thoracic vertebrae under a posteroanterior load and may determine the site of fracture. Bone 40, 751-757.

Stauber, M., Müller, R., 2006. Age-related changes in trabecular bone microstructures: Global and local morphometry. Osteoporosis International 17, 616-626.

Stiehl, J., Jacobson, D., Carrera, G., 2007. Morphological analysis of the proximal femur using quantitative computed tomography. International Orthopaedics 31, 287-292.

Svendsen, O.L., Hassager, C., Skødt, V., Christiansen, C., 1995. Impact of soft tissue on in vivo accuracy of bone mineral measurements in the spine, hip, and forearm: A human cadaver study. Journal of Bone and Mineral Research 10, 868-873.

Tabensky, A.D., Deluca, V., Briganti, E., Seeman, E., Williams, J., 1996. Bone mass, areal, and volumetric bone density are equally accurate, sensitive, and specific surrogates of the breaking strength of the vertebral body: An in vitro study. Journal of Bone and Mineral Research 11, 1981-1988.

Tabor, Z., 2007. Estimating structural properties of trabecular bone from gray-level low-resolution images. Medical Engineering & Physics 29, 110-119.

Tabor, Z., Petryniak, R., Latała, Z., Konopka, T., 2013. The potential of multi-slice computed tomography based quantification of the structural anisotropy of vertebral trabecular bone. Medical Engineering & Physics 35, 7-15.

Tabor, Z., Rokita, E., 2007. Quantifying anisotropy of trabecular bone from gray-level images. Bone 40, 966-972.

Taddei, F., Cristofolini, L., Martelli, S., Gill, H.S., Viceconti, M., 2006. Subject-specific finite element models of long bones: An in vitro evaluation of the overall accuracy. Journal of Biomechanics 39, 2457-2467.

Taddei, F., Schileo, E., Helgason, B., Cristofolini, L., Viceconti, M., 2007. The material mapping strategy influences the accuracy of CT-based finite element models of bones: An evaluation against experimental measurements. Medical Engineering & Physics 29, 973-979.

Tawara, D., Sakamoto, J., Murakami, H., Kawahara, N., Oda, J., Tomita, K., 2010. Mechanical evaluation by patient-specific finite element analyses demonstrates therapeutic effects for osteoporotic vertebrae. Journal of the Mechanical Behavior of Biomedical Materials 3, 31-40.

Taylor, W.R., Roland, E., Ploeg, H., Hertig, D., Klabunde, R., Warner, M.D., Hobatho, M.C., Rakotomanana, L., Clift, S.E., 2002. Determination of orthotropic bone elastic constants using FEA and modal analysis. Journal of Biomechanics 35, 767-773.

Trabelsi, N., Yosibash, Z., Wutte, C., Augat, P., Eberle, S., 2011. Patient-specific finite element analysis of the human femurâ€"A double-blinded biomechanical validation. Journal of Biomechanics 44, 1666-1672.

Treece, G.M., Gee, A.H., Mayhew, P.M., Poole, K.E.S., 2010. High resolution cortical bone thickness measurement from clinical CT data. Medical Image Analysis 14, 276-290.

Turner, C.H., 1992. On Wolff's law of trabecular architecture. Journal of Biomechanics 25, 1-9.

Turner, C.H., Cowin, S.C., Rho, J.Y., Ashman, R.B., Rice, J.C., 1990. The fabric dependence of the orthotropic elastic constants of cancellous bone. Journal of Biomechanics 23, 549-561.

Turunen, M.J., Prantner, V., Jurvelin, J.S., Kröger, H., Isaksson, H., 2013. Composition and microarchitecture of human trabecular bone change with age and differ between anatomical locations. Bone 54, 118-125.

Van Lenthe, G.H., Muller, R., 2008. CT-based visualization and quantification of bone microstructure in vivo. IBMS BoneKEy 5, 410-425.

Van Rietbergen, B., Huiskes, R., Eckstein, F., Rüegsegger, P., 2003. Trabecular Bone Tissue Strains in the Healthy and Osteoporotic Human Femur. Journal of Bone and Mineral Research 18, 1781-1788.

Van Rietbergen, B., Odgaard, A., Kabel, J., Huiskes, R., 1996. Direct mechanics assessment of elastic symmetries and properties of trabecular bone architecture. Journal of Biomechanics 29, 1653-1657.

Vander Sloten, J., Van der Perre, G., 1989. Trabecular structure compared to stress trajectories in the proximal femur and the calcaneus. Journal of Biomedical Engineering 11, 203-208.

Varga, P., Dall'Ara, E., Pahr, D., Pretterklieber, M., Zysset, P., 2011. Validation of an HR-pQCT-based homogenized finite element approach using mechanical testing of ultra-distal radius sections. Biomech Model Mechanobiol 10, 431-444.

Verhulp, E., van Rietbergen, B., Huiskes, R., 2006. Comparison of micro-level and continuum-level voxel models of the proximal femur. Journal of Biomechanics 39, 2951-2957.

Verhulp, E., van Rietbergen, B., Huiskes, R., 2008. Load distribution in the healthy and osteoporotic human proximal femur during a fall to the side. Bone 42, 30-35.

Villarraga, M.L., Bellezza, A.J., Harrigan, T.P., Cripton, P.A., Kurtz, S.M., Edidin, A.A., 2005. The Biomechanical Effects of Kyphoplasty on Treated and Adjacent Nontreated Vertebral Bodies. Journal of Spinal Disorders & Techniques 18.

Walsh, C.J., Phan, C.M., Misra, M., Bredella, M.A., Miller, K.K., Fazeli, P.K., Bayraktar, H.H., Klibanski, A., Gupta, R., Women with Anorexia Nervosa: Finite Element and Trabecular Structure Analysis by Using Flat-Panel Volume CT. Radiology 257, 167-174.

Walsh, C.J., Phan, C.M., Misra, M., Bredella, M.A., Miller, K.K., Fazeli, P.K., Bayraktar, H.H., Klibanski, A., Gupta, R., 2010. Women with Anorexia Nervosa: Finite Element and Trabecular Structure Analysis by Using Flat-Panel Volume CT. Radiology 257, 167-174.

Wehrli, F.W., Hwang, S.N., Ma, J., Song, H.K., Ford, J.C., Haddad, J.G., 1998. Cancellous bone volume and structure in the forearm: noninvasive assessment with MR microimaging and image processing. Radiology 206, 347-357.

Weinans, H., R. Sumner, D., Igloria, R., Natarajan, R.N., 2000. Sensitivity of periprosthetic stress-shielding to load and the bone density-modulus relationship in subject-specific finite element models. Journal of Biomechanics 33, 809-817.

Whitcher, B., Wisco, J.J., Hadjikhani, N., Tuch, D.S., 2007. Statistical group comparison of diffusion tensors via multivariate hypothesis testing. Magnetic Resonance in Medicine 57, 1065-1074.

Widmer, R.P., Ferguson, S.J., 2012. On the interrelationship of permeability and structural parameters of vertebral trabecular bone: a parametric computational study. Computer Methods in Biomechanics and Biomedical Engineering, 1-15.

Wilke, H.-J., Krischak, S., Claes, L.E., 1996. Formalin fixation strongly influences biomechanical properties of the spine. Journal of Biomechanics 29, 1629-1631.

Wirtz, D.C., Schiffers, N., Pandorf, T., Radermacher, K., Weichert, D., Forst, R., 2000. Critical evaluation of known bone material properties to realize anisotropic FE-simulation of the proximal femur. Journal of Biomechanics 33, 1325-1330.

Wolff, J., 1892. Das Gesetz der Transformation der Knochen. Berlin: Hirchwild; Wolff, J. The Law of Bone Remodeling, translated by P. Maquet and R. Furlong, 1986. Berlin: Springer.

Xu, J., Rho, J.Y., Mishra, S.R., Fan, Z., 2003. Atomic force microscopy and nanoindentation characterization of human lamellar bone prepared by microtome sectioning and mechanical polishing technique. Journal of Biomedical Materials Research Part A 67A, 719-726.

Yan, K., Engelke, K., Kalender, W.A., 2003. A new accurate and precise 3-D segmentation method for skeletal structures in volumetric CT data. Medical Imaging, IEEE Transactions on 22, 586-598.

Yang, G., Kabel, J., Van Rietbergen, B., Odgaard, A., Huiskes, R., Cown, S., 1998. The Anisotropic Hooke's Law for Cancellous Bone and Wood. Journal of Elasticity 53, 125-146.

Yoon, H.S., Lawrence Katz, J., 1976. Ultrasonic wave propagation in human cortical bone—II. Measurements of elastic properties and microhardness. Journal of Biomechanics 9, 459-464.

Yosibash, Z., Padan, R., Joskowicz, L., Milgrom, C., 2007. A CT-Based High-Order Finite Element Analysis of the Human Proximal Femur Compared to In-vitro Experiments. Journal of biomechanical engineering 129, 297-309.

Zachow, S., Lamecker, H., Elsholtz, B., Stiller, M., 2005. Reconstruction of mandibular dysplasia using a statistical 3D shape model. International Congress Series 1281, 1238-1243.

Zannoni, C., Mantovani, R., Viceconti, M., 1999. Material properties assignment to finite element models of bone structures: a new method. Medical Engineering & Physics 20, 735-740.

Zysset, P.K., 2003. A review of morphology-elasticity relationships in human trabecular bone: theories and experiments. J Biomech 36, 1469-1485.

Zysset, P.K., Curnier, A., 1995. An alternative model for anisotropic elasticity based on fabric tensors. Mechanics of Materials 21, 243-250.

Zysset, P.K., Goulet, R.W., Hollister, S.J., 1998. A global relationship between trabecular bone morphology and homogenized elastic properties. J Biomech Eng 120, 640-646.

Acknowledgements

I would like to thank all the people who made this thesis possible.

First of all, I would like to express my deepest gratitude to my supervisor, Bert van Rietbergen not only for giving me the opportunity to work on this exciting project, but also for his generous support and continuous encouragement. You were always an inspiring, insightful teacher to me.

My special thanks also go to my promoter, Keita Ito for his willingness to provide all kinds of support and encouragement. You always had a great insight in my research which helped me a lot to improve my research and my thinking as a researcher.

I sincerely thank the members of my doctoral committee, prof.dr. Marco Viceconti, prof.dr. Philippe Zysset, prof.dr. Harry van Lenthe and prof.dr. Marc Geers for accepting to be in the committee, interest in my thesis and approving it.

I would also like to acknowledge all my colleagues in VPHOP project, particularly, my collaborators in IOR; Fulvia, Matteo, Lorenzo and Ilaria for sharing ideas, fruitful discussions, reviewing and commenting on my publications as co-authors.

Special thanks to my colleagues in Eindhoven; Patrik, Janneke, René, Reza, Pooya, Michele, Lars, Esther, Andrés, Irene, Véronique, Bart, Roman, Lorenza, Juan and Marc for providing a pleasant working environment and the good time we had together. I gladly thank Sanam, Mojtaba, Taha, Amin, Amir and my Iranian friends in Eindhoven for having a great time and enjoyable social life.

Finally and most importantly, I would like to take the opportunity to thank my parents Abdollah and Nadereh, to whom I am deeply indebted for their endless love, support and encouragement. I love to thank my sister Maryam and my brothers Jafar and Amin for their love and support.

Javad

Curriculum vitae

Javad Hazrati Marangalou was born on 11 May 1984 in Urmia, Iran. He finished his secondary studies in Math & Physics Sciences in June 2002. In September 2002, he moved to the neighboring city of Tabriz to start his bachelor in Mechanical Engineering at the I.A. University of Tabriz. After finishing his bachelor in 2006, in the same year he started his Master of Science at the department of Mechanical Engineering of the Sahand University of Technology. During his MSc. studies, he was introduced to the field of orthodontic biomechanics by his supervisor Behnam Mirzakouchaki. His MSc. thesis involved the simulation of orthodontic tooth movement based on bone remodeling theories. During this period in the orthodontics lab he was also involved in a few interesting additional projects such as designing patient specific maxillofacial implants. Having finished his master studies in 2008, it was time to start his PhD studies in Biomechanics. He decided to move abroad and went to the Orthopaedic Biomechanics group at the Eindhoven University of Technology where he did his PhD work under supervision of Bert van Rietbergen and Keita Ito. The present thesis presents the results of this work.

PhD. publications

Javad Hazrati Marangalou, Felix Eckstein, Volker Kuhn, Keita Ito, Matteo Cataldi, Fulvia Taddei, Bert van Rietbergen. "Vertebral strength can be accurately predicted from bone micro-structural parameters" submitted.

Javad Hazrati Marangalou, Keita Ito, Bert van Rietbergen. "A novel approach to estimate trabecular bone anisotropy from continuum-level stress tensors" submitted.

Javad Hazrati Marangalou, Keita Ito, Matteo Cataldi, Fulvia Taddei, Bert van Rietbergen. "A novel approach to estimate trabecular bone anisotropy using a database approach" Journal of Biomechanics, in press.

Javad Hazrati Marangalou, Keita Ito, Matteo Cataldi, Fulvia Taddei, Bert van Rietbergen. "Inter-individual variability of bone density and morphology distribution in the proximal femur and T12 vertebra" submitted.

Javad Hazrati Marangalou, Keita Ito, Bert van Rietbergen. "A New Approach to Determine the Accuracy of Morphology-Elasticity Relationships in Continuum FE Analyses of Human Proximal Femur" Journal of Biomechanics, 45(16): 2884-2892.

Refereed proceedings

Javad Hazrati Marangalou, Bert van Rietbergen and Keita Ito. "Patient-specific fracture risk assessment in osteoporosis" AOR2013, Shenzhen, Hong Kong.

Javad Hazrati Marangalou, Keita Ito, Bert van Rietbergen. "Contribution of bone morphological parameters to vertebral fracture strength within different vertebral regions" ORS, San Antonio, USA, 2013.

Javad Hazrati Marangalou, Keita Ito, Bert van Rietbergen. "A novel approach to estimate trabecular bone anisotropy using a database approach" ORS, San Antonio, USA, 2013.

Javad Hazrati Marangalou, Keita Ito, Bert van Rietbergen. "A novel approach to estimate trabecular bone anisotropy using a database approach" pre-ORS, San Antonio, USA, 2013.

Javad Hazrati Marangalou, Keita Ito, Fulvia Taddei, Bert van Rietbergen. "A new method to implement anisotropy in clinical continuum-FE analyses of the proximal femur" ICCB, Leuven, Belgium, 2013.

Alina Levchuk, Sandro Badilatti, Duncan Webster, Bert van Rietbergen, Javad Hazrati Marangalou, Keita Ito, Ralph Müller. "in silico medicine approach to predict changes in human vertebrae due to osteoporosis and treatment" BMT, Graz, Austria, 2013.

Judith Roost, Benedikt Helgason, René Widmer, Luca Cristofolini, Javad Hazrati Marangalou, Bert van Rietbergen, Keita Ito, Stephen J. Ferguson. "Validation of FE models for simulating the mechanical response of human vertebrae before and after vertebroplasty" SSBE, Switzerland, 2012.

Javad Hazrati Marangalou, Keita Ito, Bert van Rietbergen. "Inter-individual variability of bone density and morphology distribution in the proximal femur and vertebrae" ECCOMAS, Vienna, Austria, 2012.

Javad Hazrati Marangalou, Keita Ito, Bert van Rietbergen. "A Novel Approach to Validate Elasticity-density Relationships in Continuum-FE Analysis of Bone" Journal of Biomechanics, Volume 45, Supplement 1. 18th Congress of European Society of Biomechanics (ESB), Lisbon, Portugal, 2012.

Javad Hazrati Marangalou, Keita Ito, Bert van Rietbergen. "A Novel Approach to Estimate Trabecular Bone Anisotropy using Fabric Tensors Derived from Stress Tensors" IASTED, Innsbruck, Austria, 2012.

Javad Hazrati Marangalou, Keita Ito, Bert van Rietbergen. "A Novel Approach to Estimate Trabecular Bone Anisotropy using Fabric Tensors Derived from Stress Tensors" pre-ORS, San Francisco, USA, 2012.

Javad Hazrati Marangalou, Keita Ito, Bert van Rietbergen. "A Novel Approach to Validate Elasticity-density Relationships in Continuum-FE Analysis of Proximal Femur" pre-ORS, San Francisco, USA, 2012.

Javad Hazrati Marangalou, Bert van Rietbergen, Lorenzo Grassi, Fulvia Taddei, Keita Ito. "Inter-Individual Variability of Bone Density and Morphology Distribution in the Proximal Femur" ORS, San Francisco, USA, 2012.

Javad Hazrati Marangalou, Bert van Rietbergen, Keita Ito. "Accounting for Bone Anisotropy Improves the Calculated Stress Distributions in FE-Models of the Human Proximal Femur" 3rd Dutch Biomedical Engineering Conference, Egmond aan Zee, Netherlands, 2011.